# INVESTIGATION OF END-STOP MOTION CONSTRAINT FOR A WAVE ENERGY CONVERTER

Morgan Dirk Flinchum

Dissertação de Mestrado apresentada ao Programa de Pós-graduação em Engenharia Oceânica, COPPE, da Universidade Federal do Rio de Janeiro, como parte dos requisitos necessários à obtenção do título de Mestre em Engenharia Oceânica.

Orientador: Segen Farid Estefen

Rio de Janeiro

Outubro de 2018

INVESTIGATION OF END-STOP MOTION CONSTRAINT
FOR A WAVE ENERGY CONVERTER

Morgan Dirk Flinchum

DISSERTAÇÃO SUBMETIDA AO CORPO DOCENTE DO INSTITUTO ALBERTO LUIZ COIMBRA DE PÓS-GRADUAÇÃO E PESQUISA DE ENGENHARIA (COPPE) DA UNIVERSIDADE FEDERAL DO RIO DE JANEIRO COMO PARTE DOS REQUISITOS NECESSÁRIOS PARA A OBTENÇÃO DO GRAU DE MESTRE EM CIÊNCIAS EM ENGENHARIA OCEÂNICA.

Examinada por:

_____

Prof. Segen Farid Estefen, Ph.D.

_____

Prof. Carlos Antônio Levi da Conceição, Ph.D.

_____

Prof. Luiz Paulo de Freitas Assad, D.Sc.

RIO DE JANEIRO, RJ - BRASIL
OUTUBRO DE 2018

Flinchum, Morgan Dirk

Investigation of end-stop motion constraint for a wave energy converter/ Morgan Dirk Flinchum. – Rio de Janeiro: UFRJ/COPPE, 2018.

XXI, 173 p.: il.; 29,7 cm.

Orientador: Segen Farid Estefen

Dissertação (mestrado) – UFRJ/ COPPE/ Programa de Engenharia Oceânica, 2018.

Referências Bibliográficas: 149-155.

1. Energia das ondas. 2. Amortecimento. 3. Mola. 4. Atrito. 5. Interfaces. 6. Biomimética I. Estefen, Segen Farid. II. Universidade Federal do Rio de Janeiro, COPPE, Programa de Engenharia Oceânica. III. Título.

I would like to dedicate this dissertation in loving memory to my grandfather Kenneth Wright Damerow, a continuous inspiration in every way, who showed me that age nor generation impede bonding and mutual admiration, and propelled my pursuit of engineering.

1921-2018

# Acknowledgements

To my parents, Abby and Russell Flinchum. I know I do not make it easy for them. This work and everything that has led up to it are the result of their tireless love, support, and encouragement.

To my dear siblings and best friends McKenzie, Dylan, and Gunnar Flinchum; thank you for being such a great support structure throughout this research process and always.

To my advisor Prof. Segen Farid Estefen, for accepting me as his student and guiding me, with patience and wisdom, over multiple hurdles and challenges during this research journey.

To Milad Shadman for being a teacher, guide, and incredible friend. Thank you for supporting me in every way since day one, and for providing the foundation and direction that made this dissertation possible.

To Jose Luis Parragas for helping extensively with Abaqus-CAE finite element analysis, helping me be organized, and generally carrying a portion of the burden.

To Freddy Murillo for guiding me in dynamical analysis, providing knowledge and encouragement, and teaching me to trust my intuition as a mechanical engineer and researcher.

To CAPES for the M.Sc. scholarship.

Without you all, this dissertation would not have been possible.

# Further Acknowledgements

To Pedro Rodrigues for being a great friend, patient and kind, always going above and beyond to help me achieve my vision, with tireless concern and care for my well-being during the course of my studies.

To Mariana Velozo for her patience, understanding, love, and diligent care during the research process, and doing everything in her power for the achievement of this work.

To Irvin Alberto for practical and friendly support, getting me over rough spots during the research process.

To Fernando (Rovas) Roversi for helping translate the abstract, guiding the presentation strategy, and being overall an exemplarily supportive and reliable friend.

To Mario Grune for helping me with crucial final formatting, and always being present as a friend and colleague, and for showing me the best of Rio.

To Paula Velozo; thank you for your kindness and hospitality, for opening your home to me and providing a healthy working environment and process.

To Avo Velozo for providing countless meals and care for my daily needs, and those of many others, through pure kindness and concern, routinely, with grace and humility.

To Simone and Jose Rodrigues for being a second set of parents in Brazil, providing peace of mind for whatever I might need, and inviting me into their family with utmost benevolence.

To Lucianita, Marise, and Eloisa for helping me navigate time frames and deadlines most graciously.

To all of the LTS (laboratorio de tecnologia submarina) technicians and staff for their support and kindness.

To Hudson, Carol, students at UFRJ as well as the team and coaches formerly and currently at Vasco Karate, and Sensei Antonio and Sensei Rodolfo for welcoming me into your respective

sports programs and clubs, allowing me to continue developing myself in a most familiar and enjoyable context.

To Sensei Sebastian Rodriguez Valle for believing in me, and inspiring me to follow my dreams. You are sorely missed.

To my students and associates at Body By Karate RJ, thank you for your enthusiasm, valuing my original ideas, and providing meaningful recreation.

To the many new friends and kind strangers I met as a consequence of this research program, from all corners of Brazil, South America, and Earth.

The emotional, practical, and social contribution of these special people greatly facilitated the completion of this work.

*"We do not inherit the earth from our ancestors;*

*we borrow it from our children."*

Traditional sentiment of native peoples from the Americas and beyond (unknown origin)

Environmental activists and sympathizers of the 20th& 21stcenturies (1960s – present)

Environmentalists and stewards of the planet yet to be born (eternal)

*"Connection and energy*

*make the world go 'round."*

Self-penned (September 15, 12018)

Resumo da Dissertação apresentada à COPPE/UFRJ como parte dos requisitos necessários para a obtenção do grau de Mestre em Ciências (M.Sc.)

# INVESTIGAÇÃO DE UM LIMITADOR DE FIM DE CURSO PARA UM CONVERSOR DE ENERGIA DAS ONDAS

Morgan Dirk Flinchum

Outubro/2018

Orientador: Segen Farid Estefen

Programa: Engenharia Oceânica

Esta dissertação desenvolve um protocolo para projetos de sistemas de restrição de movimentos associado a um limitador de fim de curso em conversores de energia das ondas. Inicialmente, é aplicado um modelo numérico hidrodinâmico para análise de cargas em um conversor de energia das ondas (WEC). Em seguida, é apresentado um conjunto definitivo de critérios de seleção, para análise de um sistema de molas helicoidais compressivas, para atenuar as forças provocadas pelos movimentos extremos da boia. Um projeto preliminar é modelado com análises de elementos finitos e comparado com os resultados analíticos. Novos tipos de modelos dinâmicos são idealizados para amortecimento do impacto, baseados em molas e no fenômeno de atrito superficial anisotrópico, aplicando o conceito observado na pele ventral de cobras. As forças de atrito e compressivas foram correlacionadas por meio de princípios de mecânica clássica. Finalmente, uma análise adimensional é utilizada para gerar a parametrização do projeto, para comparar diretamente as micro e macro influências entre esses modelos distintos, resultando em novos conhecimentos sobre as relações físicas nas interfaces de contato e uma formulação adimensional de impedância mecânica.

Abstract of Dissertation presented to COPPE/UFRJ as a partial fulfillment of the requirements for the degree of Master of Science (M.Sc.)

INVESTIGATION OF END-STOP MOTION CONSTRAINT
FOR A WAVE ENERGY CONVERTER

Morgan Dirk Flinchum
October/2018

Advisor: Segen Farid Estefen

Department: Ocean Engineering

This work develops a design protocol for wave energy converter motion constraint, end-stop systems. It applies the protocol by first using a numerical hydrodynamic wave energy converter (WEC) model to obtain preliminary design loads. Following a definitive set of selection criteria, comprehensive design of a system of load-bearing, helical springs is produced. A preliminary design is modeled with finite element analysis, and compared to analytical results. New dynamical collision models are conceived for impact damping systems based on spring-mass and anisotropic surface friction phenomena, by applying the concept observed on the snake ventral skin. Friction and compressive forces are correlated by classical mechanics. Finally, dimensional analysis is applied to yield design parameterization to directly compare the micro and macro influences within these distinct models, resulting in new knowledge on the physical relationships within contact interfaces and a dimensionless mechanical impedance formulation.

# Contents

# List of figures

# List of tables

# Chapter 1

# 1. Introduction

## 1.1 Overview

Direct kinetic energy extraction from renewable sources has proven no easy task, engineering or otherwise, yet progress has been made in recent years. As industry plateaus are surpassed, with both specific technologies and the renewable energy industry as a whole becoming more competitive against the far-from-sustainable status quo, a new reality is conceivable. However, this progress comes accompanied by new challenges, and the budding wave energy subindustry faces its own.

One such challenge in wave energy is actuation limitations, prompting the need for motion constraint on wave energy converters (WECs) in practical application. Consequently, *end-stops* are finding their way into the system architecture of wave energy conversion devices by necessity.

PTO (power take-off) systems have inherent limitations, and improvements in WEC optimization and control present the need for actuation limits to attenuate vigorous, excitation responses that can also result in *slamming*, or other destructive dynamics. These constraint problems may be addressable by end-stops. However, the sophistication of these crucial system components is in its infancy.

There is little to no literature on practical solutions or design protocols for the end-stop motion constraint dilemma, that many wave energy converters face, and some WEC designs have been developed specifically to avoid an end-stop altogether, without fully understanding the implications of its implementation. How impractical is the end-stop anyways? What can be expected of its incorporation in the preliminary design phase? What are some possible, practical solutions worth deeper investigation and development?

This paper serves to open a broader dialogue on the subject, and simultaneously provide means to the best fit motion constraint solution for a particular, heaving point absorber WEC. It also proposes a design methodology and simplifies dynamical modeling to its truest base components, for the most efficient, universal, outlook, available. The contents of this preliminary work should instigate further research to produce a most effective, universal solution.

It is the opinion of this author that wave energy deserves a place as one of the top three, renewable energy sources, not eventually, but in an ideal, near future. Well-designed, safe, and controlled point absorbers can help pave this path. And the end-stop is a small, but crucial piece of this puzzle.

## 1.2 Ocean renewable energy potential

A number of viable renewable energy technologies exist for generation of useable power from the ocean by various means. Potential, kinetic, thermal, and chemical energy of seawater can be used to produce electricity, thermal energy, or potable water [1]. These technologies are in different stages of development, but none are considered commercialized of yet. Compared with other renewable power sources, ocean energy is the most immature, with the possible exception of tidal barrages which exploit established hydroelectric power turbine technology. Figure 1-1 compares the budding ocean energy industry with other emergent renewable energy classes, with respect to technological development and system commercialization at a global scale.

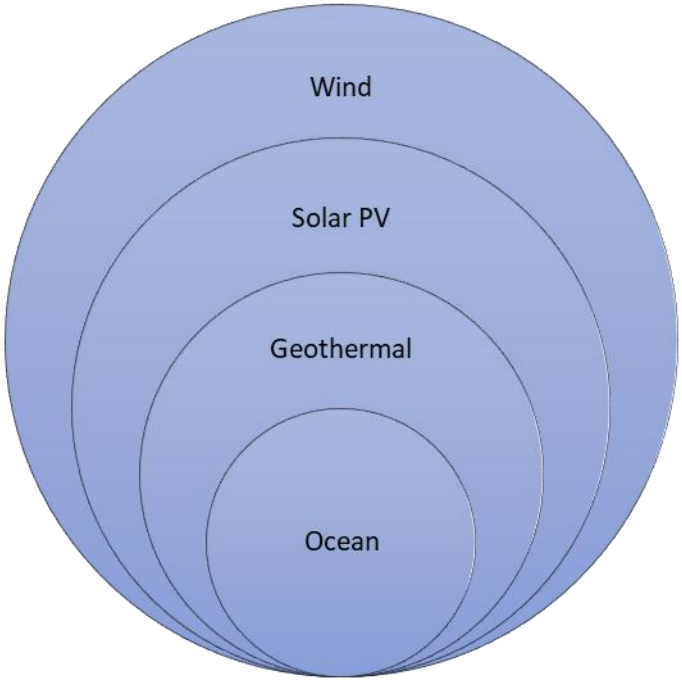


**Figure 1-1 - Qualitative Comparison of technological development and global commercialization status of emerging renewable energy generation classes.**

It is interesting to note correlations between the most mature wind and least mature ocean energy industries within the emerging class of renewable energy technologies shown in figure 1-1. Both technologies exhibit direct mechanical power production. Furthermore, ocean wave energy is the direct result of natural mechanical energy transfer from the wind resource to the water. Industry trends in wind power are leading to more offshore projects. This is due to the fact that larger wind turbines produce more power and the limiting factor in terrestrial installation is turbine transportation to installation sites. The limited size of roads and trucks to transport larger turbine blades and component parts are increasingly replaced by barges and seaside manufacturing plants.

Geothermal and solar PV (photovoltaic) technologies both eclipse the variety of ocean energy technologies in current development status. Each produce grid and privatized power with increasingly insurable reliability in respective resource rich, or subsidized cost, regions or nations throughout the world. While ocean energy is directly accessible to nearly every sovereign economy on the planet, no formidable ocean power technology presents market viability or reliable insurability and a variety of technologies continue to be tested in their respective research and development stages.

The fact that the ocean covers 70% of the planet's surface indicates that great potential development could accompany general technological advancement in the coming decades, especially in materials and controls engineering. The optimism is resonated in Ocean Energy System's (OES) report [2], where ocean energy technologies are ranked by type with respect to their potential worldwide capacity.

Notable strategies include ocean thermal energy conversion (OTEC), wave energy, salinity gradient, tidal, and ocean current power.

OTEC is derived from temperature differentials between solar energy stored as heat in upper ocean layers and the colder seawater present at depths below 1000 m [5].

Wave energy is direct mechanical energy extraction from ocean free surface oscillations induced by wind over time.

Salinity gradient power is produced osmotically where fresh water at river mouths meets saline ocean water [5].

The ocean tidal fluctuations produced by lunar gravitation occur periodically and astronomically predictably, producing tidal currents as well as a gravitational potential energy extraction opportunity. Some bays and inlets observe large vertical or lateral tide fluctuations that can be contained and subsequently run through turbines to produce power, like hydroelectric dams. Tidal phenomena also generate currents that can be actively run though turbines without entrapping large quantities of seawater.

Ocean currents generally occur near the surface and are measurably consistent in trajectory and speed, accessible for ‘permanent’ turbine placement. The Atlantic gulf stream off the coast of Florida is a prominent projected current power source under R&D investigation.

A major benefit of tidal barrage and ocean current sources is that turbines can be modified from developed, hydroelectric turbine models. These technologies are well established, facilitating adaptations for offshore or nearshore installation, leaving the primary technological problem areas to other system components and grid connection. Ocean tides are relatively consistent and predictable with a growing bank of oceanographic data. Ocean current energy extraction is in the development phase with less predictability, but promises high energy extraction potential if powerful currents such as the gulf stream can be harnessed. Bottleneck challenges are high installation cost and studies on environmental impact.

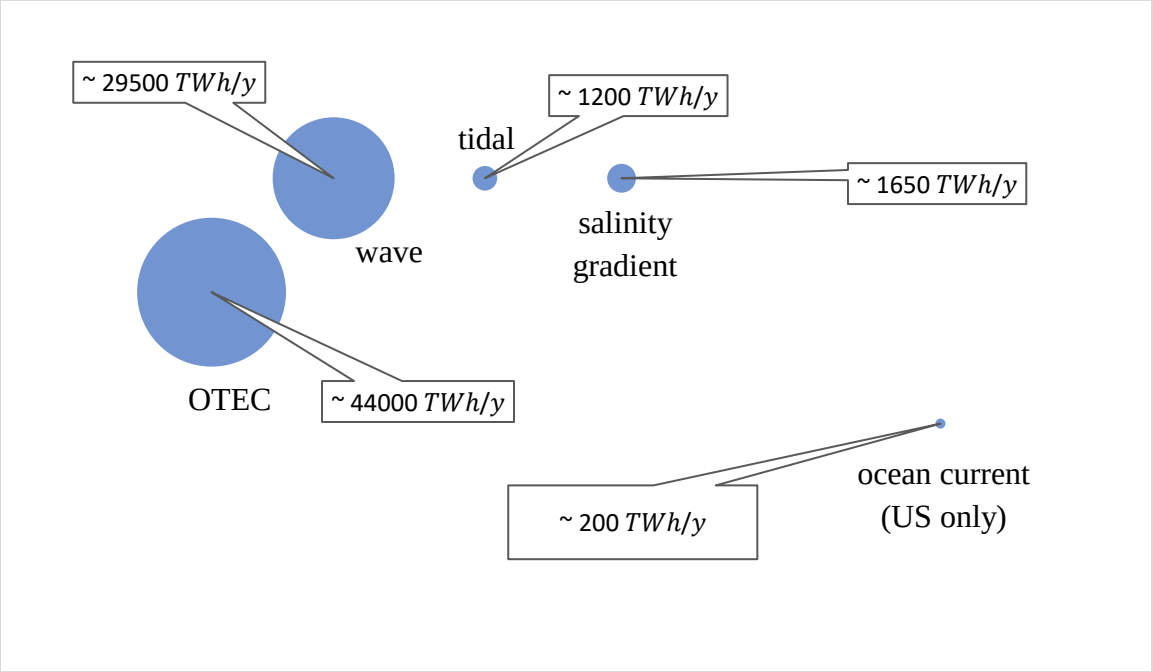


**Figure 1-2 - Graphical comparison of ocean energy resource percentages by type. From highest to lowest theoretical resource potential - shown: OTEC (ocean thermal energy conversion), wave energy, tidal barrage and currents, salinity gradient, ocean current off the U.S. coastline. [2][5][6]**

With regard to global resource potential, theoretical potential is the highest known potential, and considers only natural and climatic resource restrictions. The global ocean resource theoretical power potential estimates, reported by the OES (Ocean Energy Systems) and IEA (Energy Technology Network) organizations [2] are represented graphically in figure 2-2 and are broken down as follows: Ocean thermal$\sim 44000\ TWh/y$, wave $\sim 29500\ TWh/y$, tidal $\sim 1200\ TWh/y$, salinity gradient $\sim 1650\ TWh/y$, ocean current along the U.S. coast $\sim 200\ TWh/y$ [6][2].

Ocean energy has been proposed to solve problems other than curb the worldwide nonrenewable electrical power consumption. One of these potentials is ocean power used for onsite water desalination to produce potable water. Another is HVAC (heating, ventilation, and air conditioning) systems, which some seaside resorts have recently begun trialing [2].

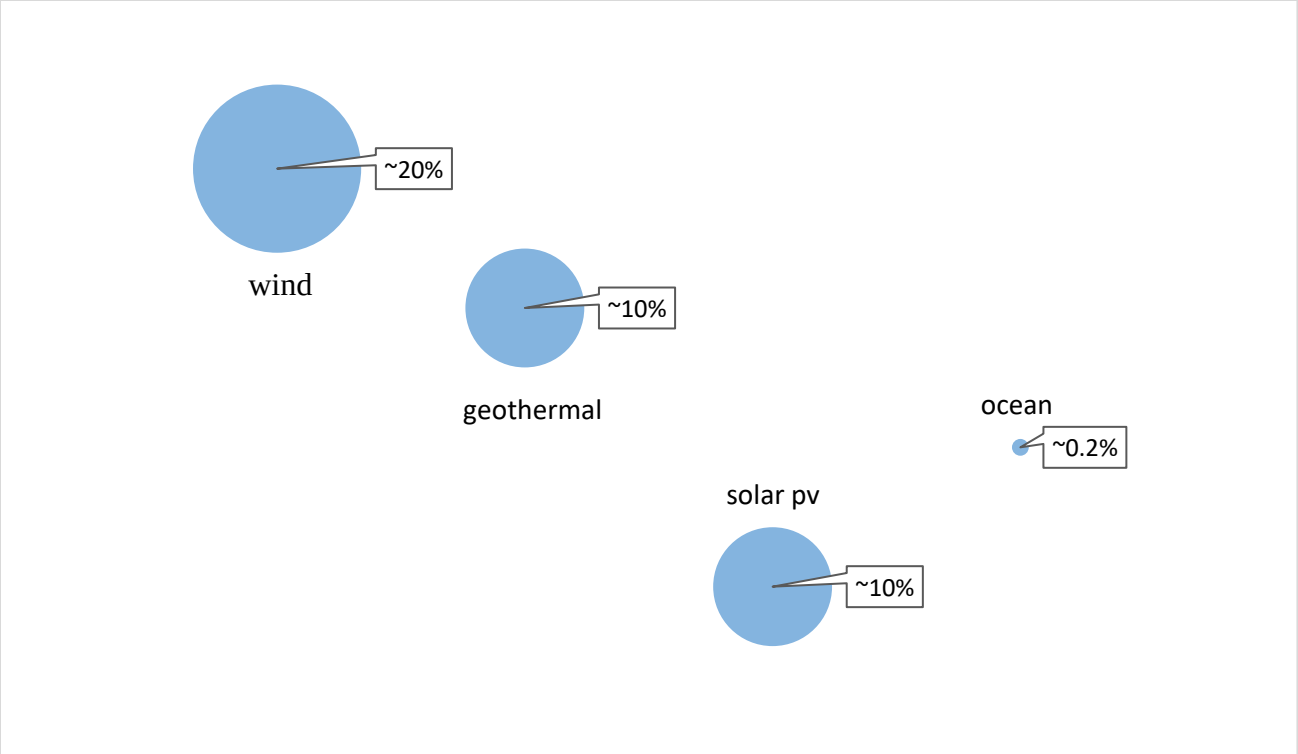


**Figure 1-3 - Graphical comparison of the relative shares of emerging renewable energy sources in the global primary energy supply in 2008 [1] (large scale hydroelectric and biomass plants are omitted from the comparison).**

In 2014, solar PV and wind energy increased their contributed power generation by 40 GW and 51 GW, respectively [2]. 1.5 GW of the increased wind generated power were provided by new offshore installations. At large, the renewable energy market has seen 30-40% growth rate in recent years. Ocean energy seems to be developing slower than previously predicted over the last decade and a half. Models predict possible, future rates of rapid growth, mimicking that which offshore wind experienced in the last 2 decades, but only between 2030 and 2050 [2]. There is a lot of uncertainty pertaining to the rates of development of ocean energy and its specific technologies, especially relative to other renewable energies. Nevertheless, the fact that technological development and industry growth of the major ocean power sources will continue to accelerate seems to be the universal consensus.

### 1.2.1 Wave energy status

Wave energy makes up roughly 12% of projected ocean renewable energy technical potential (calculated based on [3][4][5], divergent from the nearly 39% theoretical potential observed in figure 2-2). As mentioned in the previous section, the combined theoretical wave energy resource is estimated around $\sim 29500\ TWh/y$ by OES [2], accounting for a fraction of the current global energy consumption. However, the characteristics of the ocean wave resource are exceptional due to their consistency and energy density, compared with other renewable sources. Waves propagate with consistency throughout the ocean, day and night. This differs from the wind and solar resources which exhibit more sporadic but predictable energy source modulation. The fact that the seawater medium also has a higher mass density than air for example, relays a higher kinetic energy content at velocity. The limiting factor of industry development seems to be with technology employment to extract the wave energy. The global distribution of the wave energy resource - illustrating regional hotspots of consistent, energetic, and extractable wave power - is mapped in figure 1-4 below (from [1]).

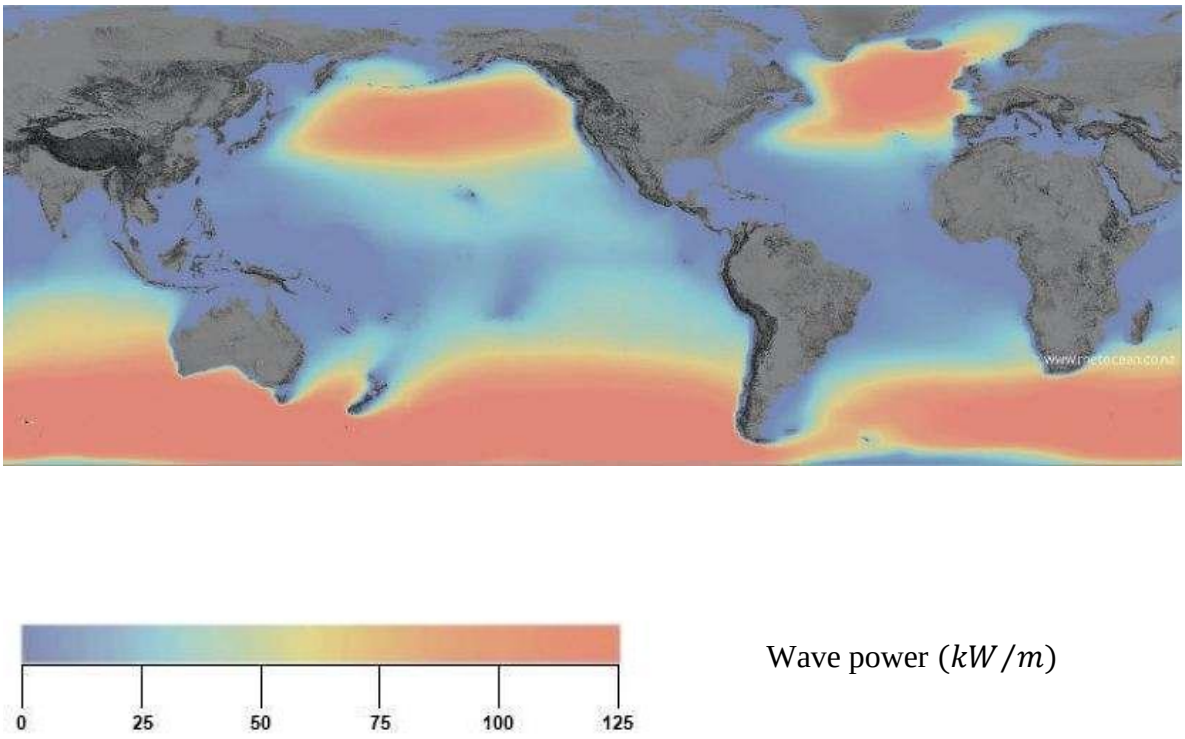


**Figure 1-4- World distribution map of wave power [1]**

The technological setbacks of wave energy converters (WECs) are many. For one, the ocean is an unforgiving environment for any machine. Costs are exponentiated for both materials and lifetime maintenance for mechanical ocean systems with the present technologies. The components and whole system have to be comparatively larger than terrestrial competitors to make them financially competitive or even worthwhile. The renewable energy issue of grid supply and demand seems to be a deterrent as well, first requiring that new energy lines be installed, sometimes at great length, with added complications of underwater, underground installations; subsequent operation provides power at nature's will, with far from 100% controllability, in an industry that requires matching electricity needs at an on-demand basis. These challenges have hindered wave energy technology development and investment until a specific WEC system proves itself commercially viable.

Large scale multi-WEC arrays, or *wave farms*, seem to be the most competitive projected strategy to enter the energy market at large, and with a definitive WEC technology yet unchosen to compose these wave farms, wave energy commercialization remains in a stalemate.

With current WEC technology still having suboptimal performance, prototypes have come to fruition mainly in the scientific research phase via universities and international laboratories, with few practical project proposals - generally for specialized and remote applications, i.e. water desalination plants and isolated island or rural coastal communities - and these remain heavily subsidized by governments, private finances, or are not developed at all.

## 1.3 Wave energy conversion technology

The concept of wave energy extraction has been around for centuries. The first documented usage was a patent issued in the eighteenth century to a father and son in France [8]. However, the technology really took up stride in the 1970s when the oil crisis reminded an energy-dependent world to look for viable, sustainable alternatives, and governments began to invest accordingly.

This trend was short-lived, only until the oil economy normalized within a few years, and to date, wave energy remains in a precommercial phase [5].

There is an accelerating rate of wave energy patents being filed in different countries. The contemporary technologies can be classified by functional kinematics, installation kinematics, and proximity to the shoreline [5]. The process of generating electricity from ocean waves may be split into three phases, composed of three staged subsystems: primary, secondary and tertiary conversion stages [14]. This delineation helps in characterizing the many WEC strategies [5]. The primary subsystem represents wave-body interaction, extracting and delivering mechanical power to the second stage system. Some WECs deliver the mechanical energy directly to the tertiary stage via electromechanical components in direct-drive technologies. When an intermediary, secondary stage subsystem is employed, it is composed of short term energy storage and power processing components [12][15]. The tertiary stage uses electromechanical as well as electrical processes; the ultimate system to receive the mechanical power and deliver electricity is called the power take-off (PTO) system [5]. At least 100 wave power pilot projects have been launched over the last few years [16][20]. More than 1000 patents have subsequently been registered [16],[17],[18],[12].

### 1.3.1 Strategies

[12] classified WECs based on their principle of operation, illustrated in Figure 1-5, below. The vertical column shows the genus, the next column is a classification based on placement, and the last column shows the mode of operation [5].

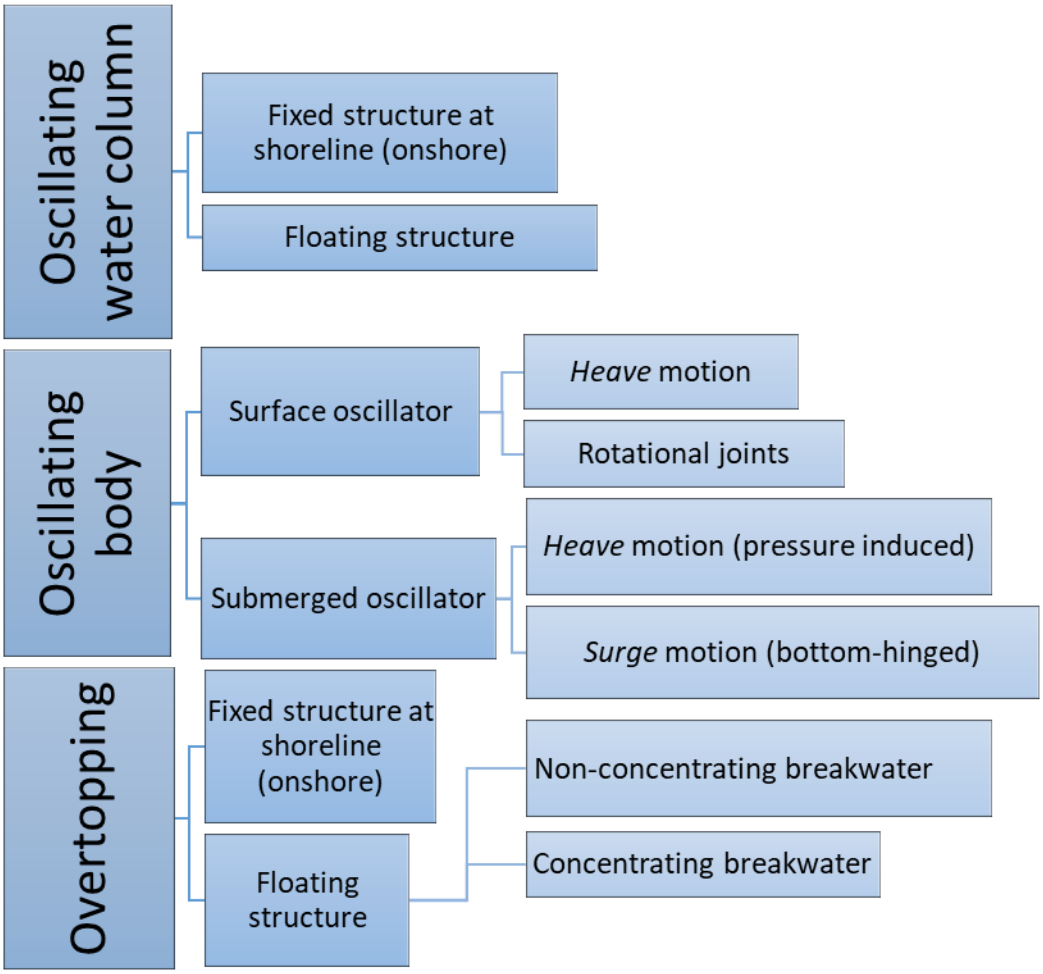


**Figure 1-5 – Wave energy technologies: classification based on principles of operation [5][12].**

The oscillating water column (OWC) concept is a twofold strategy to extract energy from water waves. OWCs are set up to allow incoming, often breaking, waves to enter a hollow chamber where they exert pressure on the vertical column of air trapped in the chamber. The air is pressured through a special turbine that maintains a constant direction of rotation regardless of airflow direction. Thus, when the water column recedes, at the instance of a wave trough, the chamber is negatively pressurized and air is sucked back into the chamber through the turbine. The Wells turbine was the first of these specialized systems to be developed, circa 1970, and is quite unique. Consequently, the OWC wave energy conversion strategy is a relatively mature technique, in fundamental function. The first wave energy device to be connected to an electrical grid was in fact an OWC deployed on the Pico island of the Portuguese Azores.

Perhaps the most commercially viable WECs at scale are oscillating body types. The oscillating body WEC strategy generates power through relative oscillatory motion between two distinct bodies. One of these bodies may essentially be a 'fixed' reference point, such as the earth (or seabed) [5].

Overtopping WECs are structured so that incoming waves surpass their vertical rise and then pool in a holding region situated above the mean free surface water line, where the collected overtopped water is may pass through a low head hydraulic turbine [5].

Actual prototype and precommercial WEC installations, again categorized based on operational genus are delineated in figure 1-6 below, adapted from [5].

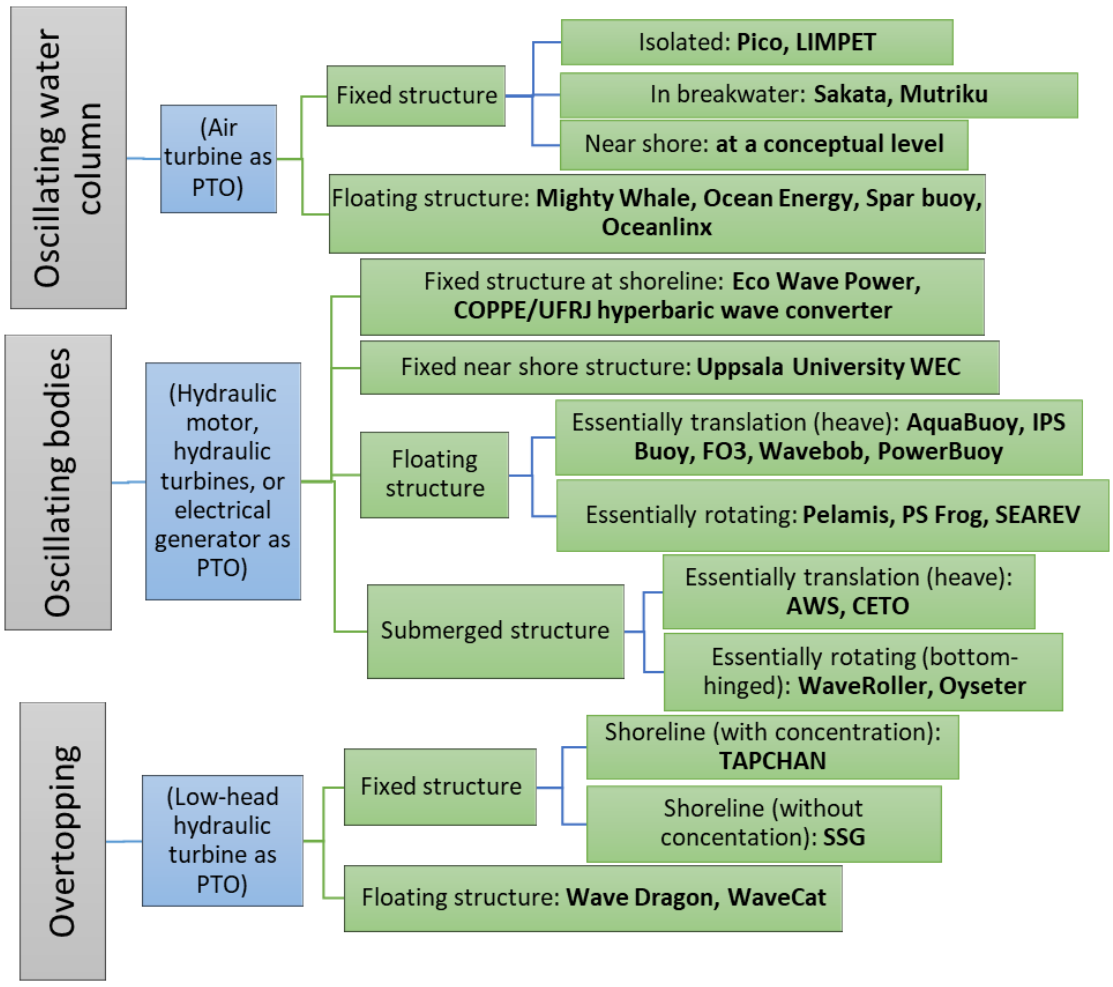


**Figure 1-6 - Wave energy technologies, actual installations, modified from [5], (based on [12][16][19]). The content is organized as follows: operational genus (green), power take-off system type (blue), and installation class and installed systems (grey)**

Additional, unorthodox concepts have appeared in the literature to date. The “Berkeley Wedge” for example operates as a wave impact energy extractor [9]. Another interesting characteristic of the Berkley Wedge is that, besides power capture from impacting waves, the device is designed to operate as a functional breakwater. The Berkley Wedge has an optimized shape to minimize viscosity effects in oscillatory motion and is expected to reduce separation drag [9]. This makes the design a suitable candidate to pair with heaving point absorber systems in a symbiotic mechanical assembly.

## 1.4 Motion constraint in WECs

A look into the literature of heaving point absorber wave energy convertors provides a solid foundation and a path for the more elaborate research into specific properties, functions, and mechanism design that this dissertation pursues.

**Table 1-1 - Approximate number of WEC end-stop/motion constraint problem instances in the current scientific literature.**

| # | ~20 | ~3-5 | 0 |
|---|---|---|---|
| | Mentions of the problem being a significant design challenge in WECs<br><br>$(\sim 90\%\ in\ last\ 2-3\ years)$ | Direct treatment of end-stop actuation limit, analytically or other | Investigations of practical design solutions addressing the WEC motion constraint problem<br><br>(+1) |

There are significant design challenges inherent to WECs. Oscillating systems as the heaving point absorber, composed of two or more large bodies reacting with each other through a power take-off, pose major engineering challenges to ensure that they can function for many million cycles, maintain alignment and withstand extreme conditions. The need to react against something - be it a second collaborating body, the Earth´s sea floor, or an equivalently *static* body - presents the significant challenge to developing practical oscillating WECs [24].

A further design requirement of heaving point absorbers is resonance. A point absorber operating in the heave mode, has a natural period of oscillation that corresponds to this plane of motion. This intrinsic system property should be matched to the largest range of statistically probable sea states near a proposed WEC installation site, for maximum energy absorption potential. By nature, heaving point absorbers tend to have a well-defined natural period in heave, so there is a small window of incident wave periods which produce the best response for ideal energy absorption through resonance.

Some control solutions have been devised to bypass the limitations imposed by the natural frequency resonance design requirement. One such solution is latching. Latching holds, or "latches" the oscillation thereby simulating a longer natural period. This solution increases the capture width of potential, optimal incident wave frequencies, but compromises with the peak absorption potential [5].

[21] describe end-stops as mechanisms that restrict the stroke length of the WEC moving bodies to restrain its displacement within certain excursion limits for operational purposes. They explain that this state saturation problem can be met by control methods that consist of an added spring and/or damper. They further point out that end-stop solutions serve particular importance in concepts that operate at high velocities, namely heaving point absorbers.

Further research is presented by [22]. Their paper analyzes the proposed problem numerically, via combined potential flow boundary element method and modified Morison´s equation viscous drag for two WEC geometries of varied radius and draft. Their aim was to discover how end-stop stiffness and constrained WEC travel distance affect the PTO forces and average annual energy generation.

[22] essentially conduct a performance analysis of WECs numerically, using end-stop control based on their mathematical model.

In the numerical modeling structure proposed by [22], two end-stops are treated as spring elements that activate only when a certain positional limit is reached. Furthermore, the case is simplified by presuming the end-stops, one as an upper boundary constraint and the other as a lower constraint, are the same stiffness and are positioned equidistance from the WEC´s still water resting position, with respect to their point of engagement.

It is important to note that the free stroke length of the WEC and end-stop positions are intrinsically linked, and that this model treats the effective end-stop length as fixed. The numerical procedure takes calculations of varied free stroke length, whereas end-stops are positioned at the ends of this stroke length [22].

[22] propose their formulation as a means to delineate the end-stop force with respect to specific design parameters it relies on. $K_{ES}$ is the end-stop stiffness, $z$ is the vertical position of the WEC, and $F_{ES}$ designates the Heaviside step-function force of constraint response of the end-stop. $z_S$ is the free stroke length of the heaving point absorber:

$$z_S = 2 \times z_{ES} \tag{1.1}$$

$$F_{ES} = \begin{cases} -K_{ES}(z - z_{ES})\ if\ \ z > z_{ES} \\ -K_{ES}(z + z_{ES})\ \ if\ \ z < -z_{ES} \\ 0 \qquad\qquad else \end{cases} \tag{1.2}$$

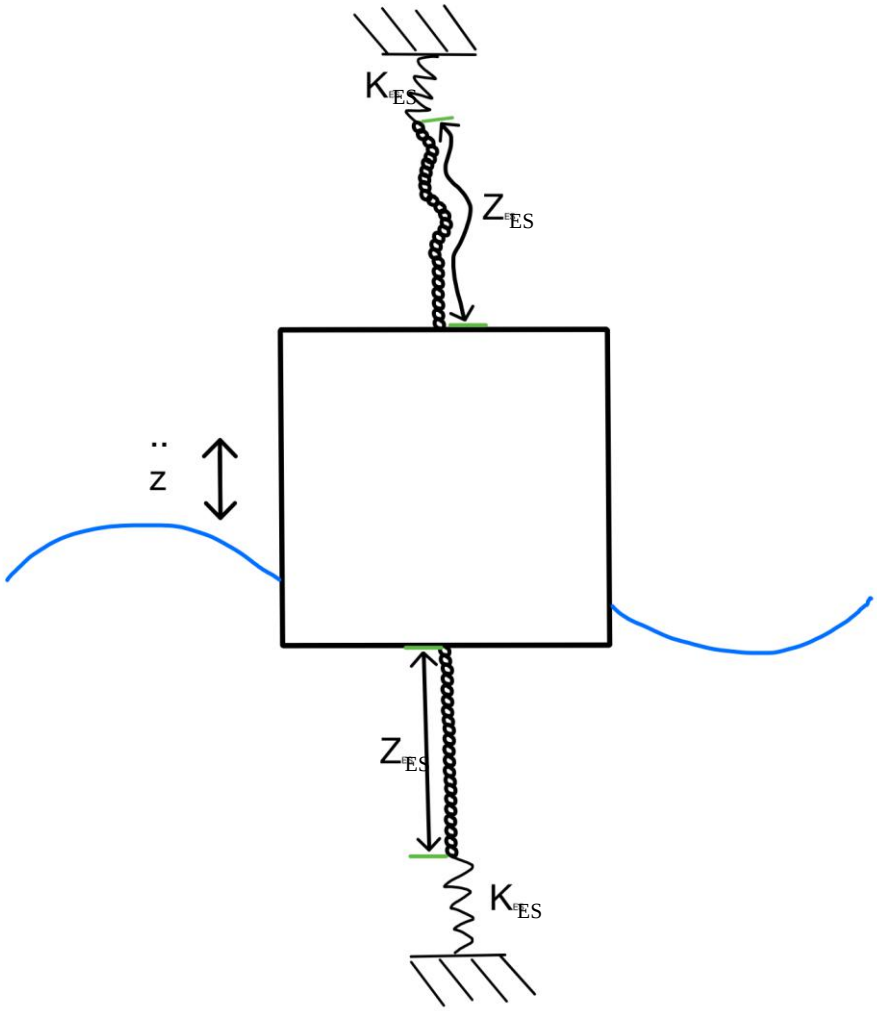


**Figure 1-7 – A schematic representation of the [22] end-stop model applied to a heaving buoy - Depicted: 2 ideal spring elements of stiffness $K_{ES}$; 2 massless, ideal chains of constraint, with extension length $z_{ES}$; and buoy heaving response $\ddot{z}$, due to incident wave excitation forces and other imposed forces upon the heaving buoy.**

In figure 1-7 a representative schematic is developed to illustrate the [22] model, upon a heaving buoy of arbitrary acceleration. The stiffness parameter, allocating the force of constraint when the buoy passes its designated heave limits, is represented by linear spring elements of stiffness $K_{ES}$. The Heaviside step-function behavior is modeled with ideal, massless, frictionless, inelastic chain elements of fixed length $z_{ES}$, these based on heuristic models of flexible marine organisms developed by [28]. The opposing nature of the end-stop forces of constraint, indicated by the negative sign in the function, is portrayed by tensile action of the spring-chain elements which are fixed to rigid walls located at the upper and lower limits of the reference frame. Thus, when z

becomes $z_{ES}$ (in an upper oscillation) the lower chain becomes fully extended and the lower spring element activates. When z reaches $-z_{ES}$, the upper chain fully extends and the upper spring is activated. $\ddot{z}$ represents buoy motion responses in heave, which defines the relative heave position of any point of the rigid buoy in time. It's bulk, although fixed volumetrically (spatially) relative to the heaving $z$ direction, is represented by a central rectangular element; which, for more complex modeling can be considered of variant mass due to the effect of hydrodynamic added mass present in mechanical ocean waves. The illustration provides a means of displaying the end-stop problem parametrically, adaptable to additional parameters or degrees of freedom.

[23] devises an expression for maximum mean power under motion constraint, implementing an analytical approach, based in hydrodynamic linear theory, and applies it for an entire theoretical wave farm, composed of multiple heaving point absorbers.

[25] make an appropriate distinction, indicating that WECs conceivably exist in two states with respect to motion constraint, the normal operating conditions of proper wave energy extraction and a survivability mode, where excess motion, from incident wave excitation, exceeds operational boundaries. Specifically, [25] point out that the wave excitation forces are too great for motion and force constraints to be satisfied simultaneously.

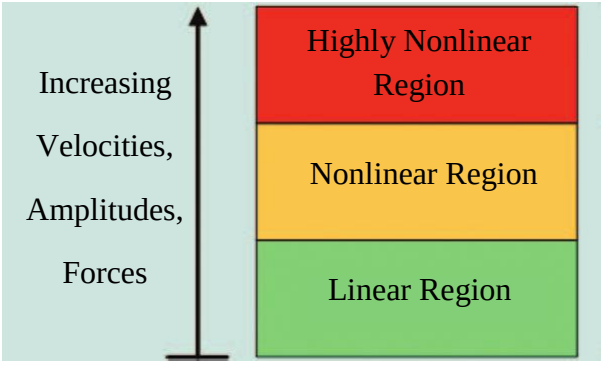


**Figure 1-8 - Effects of nonlinear behavior, adapted from [24] WEC operational modes' diagram.**

Nonlinear behavior can be extracted from the model ([22)] schematic representation in figure 1-6, exemplary of the combined spring-chain element, and its inherent discontinuity in stiffness ([28]). This phenomenon is characteristic of impact dynamics or jerk forces in tension systems.

[26] point out that reacting body heave damping is the most influential hydrodynamic parameter for verifying their numerical dynamics model; their method uses a predictive control scheme. The design implications of a reactive PTO control scheme and relative motion constraints show alarming insensitivity to motion constraint due to wave viscous *damping* on the WEC body. Their numerical results showed increased sensitivity to end-stop constraint for a WEC with a more *streamlined* reacting body. In comparison, the relative motion amplitudes of non-streamlined WEC were prohibitively large from a design perspective [26].

The practical unbalance of developing control schemes is apparently unsatisfactory on the side of motion constraint, in the current literature.

To quote [27]:

> It is well known that the output of a system is determined by the input (such as sea states, load) and the characteristics of the system itself (such as the inertial mass and the spring coefficient). So, for a WEC without constrained control, the optimal operation of the converter sometimes may exceed the physical limitations imposed by the system (such as the amplitude of velocity, motion, or force) under certain sea states. Such situations are dangerous for the practical WEC. Especially for waves with high amplitudes and short periods, the motion of the WEC can exceed the designed stroke length, which may cause a strong strike to the hull. The improved survivability is a very interesting secondary benefit with motion control. In our device today, we have motion control (limited stroke length), but the striking force can still be very high if the motion is not controlled in the correct way. (Wang et al. 2015) [27]

From the tone of the current literature, it is not too bold a statement to proclaim that if end-stops or other constraint strategies do not see abrupt performance improvement through design, WEC devices will remain uninsurable and the already sluggish pace of the industry will reach an end-stop of its own.

### 1.4.1 End-stops

From a technical standpoint, the necessity of an actuation limit and mechanical displacement or motion constraint in the WEC system stem primarily from PTO system limitations and an increased risk of *slamming* dynamics, as WEC technology develops (control, size, and velocity all scale up with technological improvement). The PTO system is arguably the most important (and the most expensive) component of a WEC, in conjunction with the primary mechanical power extractor in direct contact with incident waves, and the subsequent power transmission subcomponents, as these together serve the energy extraction functionality of the WEC.

The end-stop gets a bad rap because it essentially reduces the power output potential of a WEC, yet it plays an important role. The role of the end-stop is bar none WEC protection during operating conditions, or self-preservation. It may also provide a full or partial failsafe in case of PTO failure, if designed for such. The end-stop not only ensures mechanical reliability, but has profound impact on the industry at large, especially at its current pre-commercial phase, since WECs not designed with operational self-preservation functionality are essentially uninsurable.

As a result, WEC component systems can be functionally classified into one of 3 categories: energy conversion, support structure, and protection, shown in figure 1-9 below.

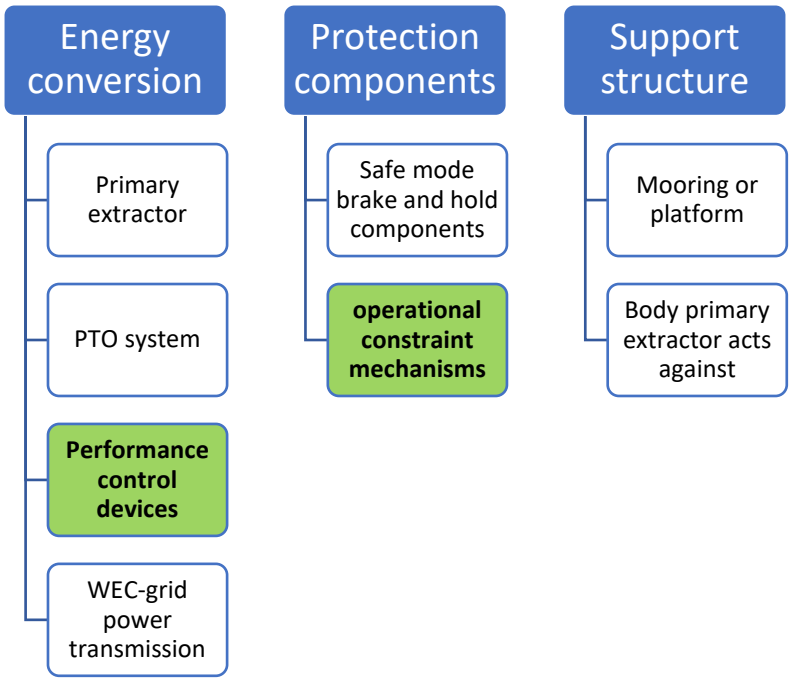


**Figure 1-9 - 3 suggested families of primary component systems for wave energy converters, classified in terms of their intrinsic device purpose. Performance control devices and operational constraint mechanisms are highlighted in green, as they are interrelated. As performance control for energy extraction improves, more attention needs to be paid to operational constraints for protection.**

At the core of the protection features in WEC systems are nonoperational *safe mode* components. However, with improving WEC performance, operational constraint mechanisms are swiftly gaining importance. Depicted by the *self-preservation circle* in figure 1-10, as technology advances, the ideal role of operational end-stop motion constraint shifts inward, accounting for more proportional importance as an independent WEC self-preservation system, first absorbing the functional responsibilities of fail-safes and eventually reducing the frequency of required "safe mode" protective measures. With WEC technological progress, and wave energy industry advancement, these operational constraints will simultaneously increase operation time potential and reduce the time in "safe mode." Non-operable conditions are not forecasted to disappear, and a safe mode feature will most likely, always be a WEC component, but with well-designed operational constraints, an ideal system, may be able to absorb some of this responsibility while keeping the WEC productive over broader conditions and intervals.

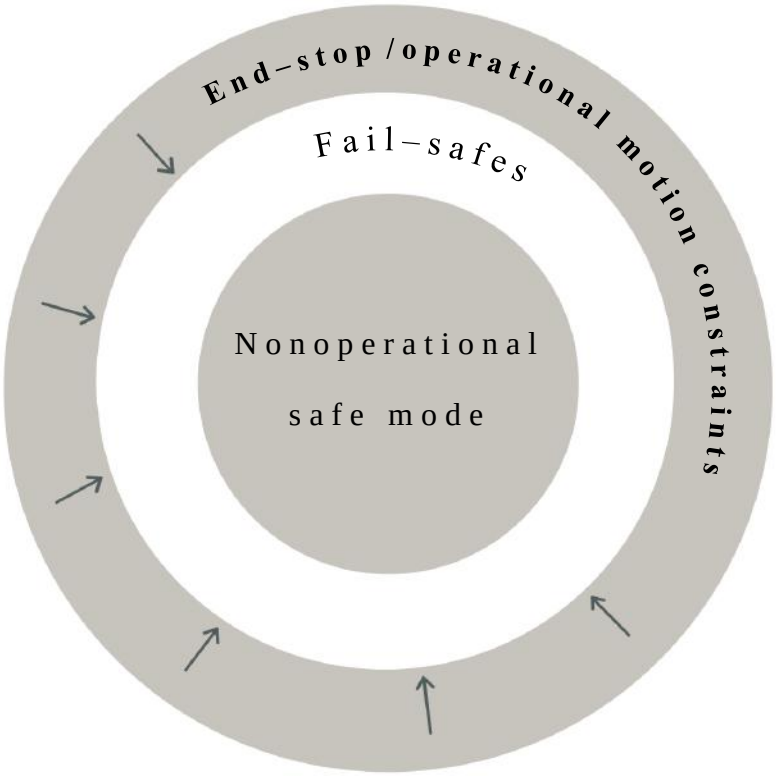


**Figure 1-10 - Representation of WEC self-preservation components' hierarchy. Nonoperational safe mode at the core, operational constraints such as end-stops begin to migrate inward as WEC systems mature, to accommodate additional protection functionality, first as fail-safes, then by increasing operational regimes, shrinking WEC safe mode downtime.**

In modern (still precommercial) wave energy converters, the nonoperational *safe mode* component system is at the core of self-preservation, or protection, features. However, with respect to technological development, it is intuitive from these figures, that end-stop/operational motion constraint investment will give the best ROI amongst self-preservation components, to reduce downtime and ideally decomplexify and decrease the necessary WEC component systems and parts in the long run. The immediate benefits of reduced safe mode downtime are twofold, the increased potential power production time and the significant residual benefit of increased operational data to inform developers and the budding industry as a whole.

For this reason, end-stop or equivalent motion control systems should be considered in the WEC preliminary design phase. [32] cautions, in conclusion of their study on control informed geometric optimization, “Our main aim is to alert designers of the need to consider control at the device design stage.” They conclude that device energy extraction can even be improved by this tactic, particularly with tight PTO force limitations.

## 1.5 Motivation & objectives

Offshore renewable energy projects face unique and trying challenges. As with any offshore structure or mechanical system. the unforgiving environment of the sea amplifies cost and vulnerability. In addition, the increased risk involved with novel, unproven renewable energy technologies, concatenates upon this reality. Naturally, methodologies and procedures have emerged to help curb cost; however, not yet to the point of definitive, technology, world-economic commercialization. Some standardization is underway.

The initial design phase of a point absorber WEC requires a number of considerations. Depending on local wave environment, choices must be made with regard to a best suited PTO system, heaving buoy size and shape, and features such as motion constraint and fail-safes. Device-specific operational constraint tactics not only add additional parts and cost to the WEC, but they affect overall system efficiency and energy conversion potential. Economic feasibility of any WEC project relies largely on these features. An elegant and economic solution to WEC operational constraint requirements, adds extreme value to the emerging wave energy industry at large.

Wave energy technology, despite its initial boon in scientific and technological development being over 40 years ago, is still in its infancy. To attain economic viability, WECs must yet overcome many challenges to make them competitive in a highly commoditized energy industry, and/or change the game. Recent years have seen advancements, as climate, meteorological and atmospheric science, and oceanography point out the pitfalls of our modern, rapt, oil-dependent economy, and worldwide investments in renewable energy mount, but even within the steady, increasing momentum of the renewable energy industry, wave power lags.

If wave energy is to make a case in the rapidly changing energy ecosystem of post-industrial humanity, it needs to be an economic contender, viz. efficient. Besides energy capture methods being suboptimal, there is another more foreboding culprit keeping the industry stagnant; that is WEC operational constraints. If it is not proven up to the task, to endure its own resonant properties and operational environment, the WEC cannot be insured and the project will not come to fruition.

As WEC control methods mature, the WECs are able to take advantage, inducing resonant response more readily, and higher excitation response. However, this necessitates the use of additional control strategies or constraints to keep the WEC operating within safe bounds. If certain device-specific actuation limits are exceeded, crucial system components can be irreversibly damaged. A judgment call must be made to balance energy conversion potential and protection of the system, at cost. This is no easy task. Yet for the current state of the industry, there is no way forward unless a conservative approach is taken to the end-stop dilemma and optimized protocol are established for the design of functional end-stop systems. This dissertation focuses on an approach to proper practical design of an end-stop system under given system limits.

Based on previous literature, whose purpose this dissertation also pursues, it is argued that an end-stop is a physically applied constraint on a dynamical system´s motion that merits inclusion in WEC preliminary design.

The objective of this dissertation's investigation into WEC end-stop motion constraint is twofold:

The first objective is to establish a WEC end-stop design framework and process. The second objective is to uncover and evaluate the primary parameters of importance for practical end-stop implementation.

## 1.6 Dissertation chapters

- **Chapter 1 — Introduction:** This first chapter reviews ocean energy in general and its place amongst other renewable sources. It then presents wave energy with respect to its place amongst other ocean energy strategies. Chapter one further divides wave energy into its primary strategies and gives a short briefing of the method and prototypes. The specific motion constraint problem is addressed and a detailed literature review sheds light on the problem as a bottleneck in WEC and WEC industry development. From here the specific motivations and objectives, as well as structure, of this dissertation research are presented.
- **Chapter 2 — Methodology:** A methodology for end-stop motion constraint design is comprehensively developed. Design tasks and design criteria are formulated to attend to motivations and objectives established in the first chapter. From there, a procedure is proposed (design strategy), and followed, to obtain design parameters. Fundamentals in wave mechanics are presented and segue into specific point absorber working principles and component parts, including end-stops. The kinematics of the problem are observed. The COPPE nearshore WEC numerical model is summarized as the method to obtain design load. End-stop strategy selection is outlined and spring and friction principles are presented in detail. Finally, a number of dynamical end-stop collision models are proposed and analyzed for impact damping with respect to the two chosen methods for analysis: mechanical spring and friction.
- **Chapter 3 — Results:** This chapter provides the various results obtained through the adopted process, sequentially. First, the end-stop design load is obtained from the COPPE nearshore WEC numerical model. A helical compression spring to attenuate this load is designed in stages. Finite element analysis is performed for static spring loading. Then a dimensional analysis is performed to assess key end-stop parameters.
- **Chapter 4 — Conclusions:** This chapter presents the prominent conclusions of the dissertation work along with inspiration for future research.

# Chapter 2

# 2. Methodology

## 2.1 Design approach

To investigate preliminary design for the end-stop system, clear criteria and objectives are set forth. The design objective is described by two explicit design tasks and one intrinsic design task, as shown in Figure 2-1. **Design task 1**: constrain motion at operational limit. **Design task 2**: mitigate dynamic impact response. The design task *intrinsic* to WEC end-stop development is to avoid or minimize any reduction of the WEC system's energy capture potential. Both explicit end-stop design tasks relate directly to WEC self-preservation, while the intrinsic task is related to system practicality.

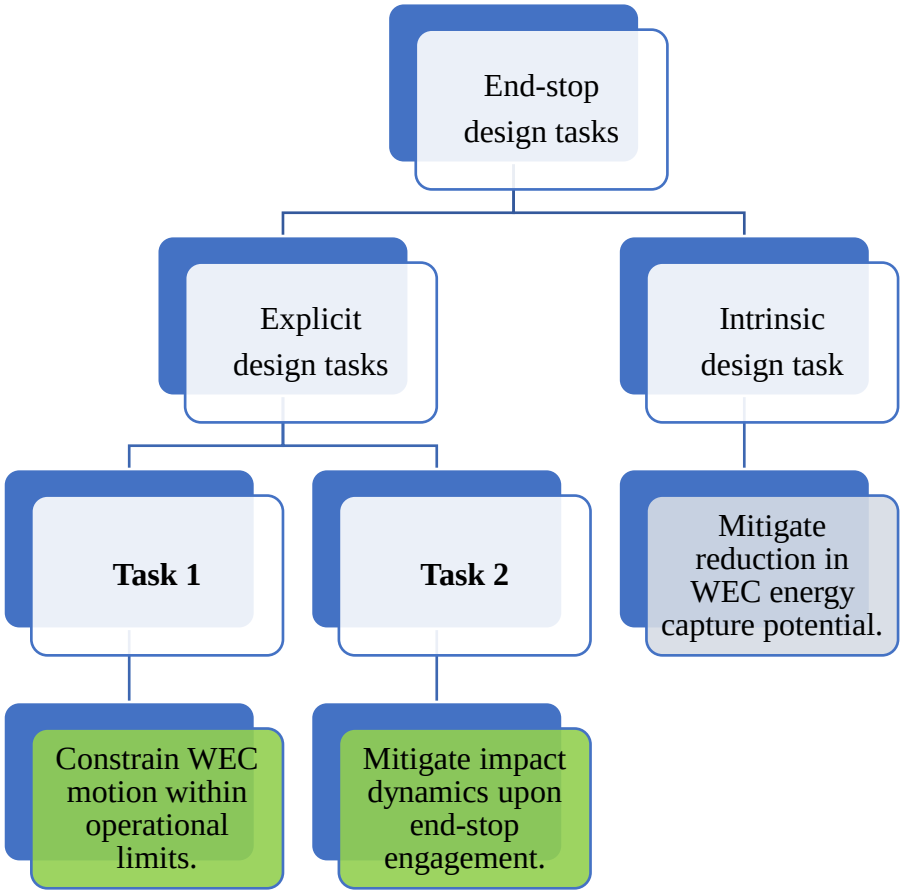


**Figure 2-1 - Hierarchical representation of the preliminary end-stop design tasks.**

The intrinsic design task implies that any minimizing effect on normative, WEC energy capture process should be kept at a minimal, or avoided if at all possible. The focus and protocol of the end-stop preliminary design rest on the 2 explicit design tasks.

For design task 1, the system actuation limit is given at $\pm 3$ meters, from mean F.S. (free surface) level. These are conservative constraints for the WEC system. Through hydrodynamic analysis and subsequent design steps, it will be possible to characterize the system response.

**Table 2-1 - Strategies related to accomplishing each explicit design task.**

| Design task 1<br><br>Constrain motion | Design task 2<br><br>Control impact |
|---|---|
| Physical strategy: Counter WEC<br><br>force at limit position with a reliable force of constraint | Physical strategy: Control kinetic energy transmission upon limit arrival |
| Possible engineering tactics:<br><br>• Direct obstruction<br>• Friction<br>• Harness tension | Possible engineering tactics:<br><br>• Energy dissipation<br>• Energy Storage<br>• Energy Conversion |

The two explicit design tasks, outlined in figure 3-1, can be tackled in different ways. The model strategies considered for preliminary analysis are (1.) provision of a force of constraint and (2.) impact energy regulation, respectively, as shown in table 3-1.

Figure 2-2 represents the respective valuation of the ends-stop's explicit design tasks as they relate to WEC self-preservation. From the figure it is apparent that a balance between the two design tasks will render more effective protection. Technical tactics are listed accordingly.

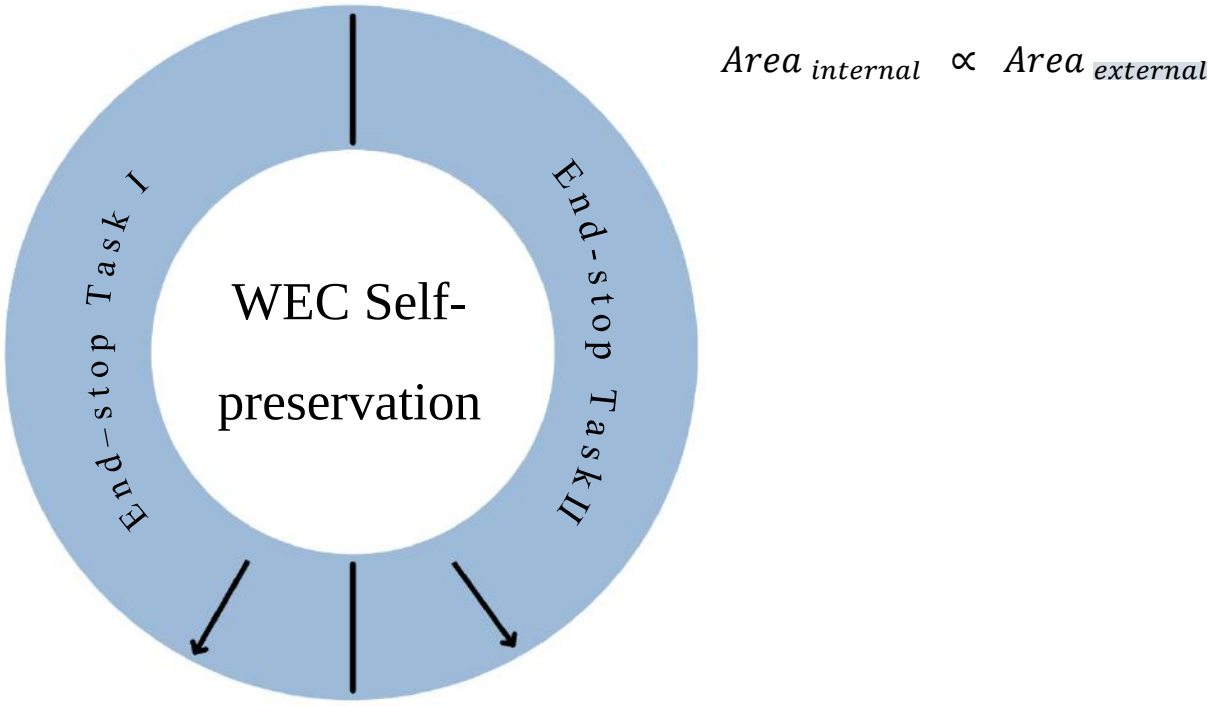


**Figure 2-2 - Graphical representation of the effect of explicit end-stop design tasks on overall WEC self-preservation ability. Concentric outer and inner hemispheres represent end-stop tasks and WEC self-preservation, respectively. The arrows designate hemisphere expansion when the respective design task is improved. Internal and external regions contain fixed proportional areas in their respective hemisphere.**

As the blue outer area and the white internal area have fixed proportional area, improvement in end-stop system task performance results in expansion of WEC self-preservation capability through the respective task hemisphere. End-stop tasks are improved independently, but each account for 50% of the self-preservation circle circumference.

### 2.1.1 Design criteria

As discussed in chapter 1.4 'Motion constraint in WECs,' there are a number of criteria to which the end-stop system must comply, the premise being that an end-stop needs to constrain the motion

of a WEC primary energy extraction oscillating body (the buoy in the specific case of a heaving point absorber), within a given limit, whilst avoiding any repercussion to the system or its operational lifespan.

To better inform the multitude of decisions during the design process, a set of qualitative, preliminary design criteria are established based on the end-stop problem characteristics. The 4 criteria chosen are defined as follows:

1. Reliability/effectiveness - ability to perform design tasks consistently
2. Robustness - ability to withstand adverse conditions
3. Integrability - ability to integrate into WEC system at large
4. Efficiency/economics - minimal material and complexity

These attributes can further be stratified by primary, contributed function to overall WEC system, as being protection or practicality, shown in table 2-2 below.

**Table 2-2 – End-stop design criteria.**

| **Criteria** | **Contribution to overall WEC system** |
|---|---|
| 1. Reliability/effectiveness | Protection / self-preservation |
| 2. Robustness | Protection / self-preservation |
| 3. Integrability | Practicality |
| 4. Efficiency/economics | Practicality |

Definitively a protection / self-preservation WEC system facet, the *reliability/effectiveness* end-stop design criteria appear in 2 parts, each correlated to an explicit design task, qualifying the design's 'functionability,' i.e. does it do its job, and how well?

Design task 1 requires that the kinematic boundary for WEC actuation be met, effectively through a force of constraint. For design task 2, the end-stop mechanism is required to 'cushion' the impact

dynamics, to prevent any damage potential. Thus, to quantify this execution of operational tasks, working force reliability and potential dynamic response range can be measured.

End-stop robustness requires optimal functionality for variable loads. Because of the high uncertainty and conservative nature of the initial design actuation limit, it is paramount to investigate a strategy with good robustness. Characteristics of a robust end-stop system include: efficacy for variable load, effective for long life, fatigue and wear resistance. Projected maintenance needs, environmental concerns, corrosion resistance, temperature tolerance, and biofouling resistance can all be incorporated in a comprehensive quantification of design robustness.

Integrability is an obvious concern for the design of any component system. However, for this preliminary phase, it is considered as a practicality issue of the design rather than a paramount self-preservation quality. The importance of system integrability is held off for subsequent design phases (intermediary, final). To determine how effectively an end-stop system integrates into the WEC some quantifiable attributes to consider are: fixtures to support structure, complexity (measured in number of steps), and connections' tolerance magnitudes.

For this preliminary design, the efficiency/economics of the system is not the top concern, but it should be considered. Amount of material/mass, complexity of design (number of moving parts), cost of materials, manufacturability, manufacturing cost, number of independent (working) components, complexity of components, total mass, and total volume may all contribute to efficiency/economics values.

In summary, table 2-3 presents the established design criteria as they correlate to the two explicit design tasks.

**Table 2-3 – End-stop design criteria with relation to design tasks.**

| *Design criteria* | **Design task 1** *Constrain motion* | **Design task 2** *Control impact* |
|---|---|---|
| **1. Effectiveness/ reliability** | Sufficient force of constraint | Manages energy dissipation upon collision |
| **2. Robustness** | Ability to endure higher loads or adverse conditions | Optimal response for design load and lesser loads |
| **3. Integrability** | Effective with high tolerance considering placement within WEC system | |
| 1. **Efficiency/ economics** | Amount of: material, space occupied, and number of mechanical parts | |

In practice, the end-stop must constrain buoy motion under normal operating conditions. In the case of the COPPE nearshore point absorber, buoy excitation is optimized with latching control, and buoy geometry and mass are tuned to the actual sea states of its proposed deployment location.

To most effectively establish relative weights, the pair-wise comparison method from Pugh method for design is used [30]. Pairwise comparison is a tried and tested method for most judiciously establishing accurate relative weights for qualitative value sets and criteria. Table 2-5 and the following calculations depict this procedure, where letters are assigned to each criterion and aligned vertically and horizontally to provide a cell in the table for each possible pair to compare (would-be redundant cells are shaded and not used). The more crucial criterion is selected for each pair comparison and tabulated accordingly. Subsequently, the frequency of each selection is accounted for and scaled. Percentages are allocated. These weighted values will be referenced to assist in further design decisions.

**Table 2-4 - Pair-wise comparison of preliminary design criteria. (based on Pugh method for design [47])**

| DESIGN CRITERIA | | A | B | C | D |
|---|---|---|---|---|---|
| Reliability/effectiveness | A | | A | A | A |
| Robustness | B | | | B | B |
| Integrability | C | | | | C |
| Efficiency/economics | D | | | | |

Reliability/effectiveness was chosen unanimously when paired up against its counter criteria. Thus, reliability/effectiveness earns 3 points, one for each victory, shown in the table. Robustness receives 2 allocations, integrability earns 1 pairwise win, and efficiency/economics receives none.

To find percentages

$$100 = 3x + 2x + 1x + 0x \qquad (2.1)$$

$$x = 16.\overline{66}$$

Rounding down to the integer value 16 results in the following weight allocation for end-stop preliminary design criteria:

1. Reliability/effectiveness 48%
2. Robustness 32%
3. Integrability 16%
4. Efficiency/economics 4% (remainder)

Quantifying these qualitative design criteria facilitates design decisions and design parameter evaluations, throughout this dissertation work, and for future works.

### 2.1.2 Design strategy

To achieve the given design tasks with the established criteria, a design strategy is necessary. The strategy (see figure 2-3 flow chart, below) is as follows. First, local sea characteristics are taken for the site of interest. Then, those sea states are used in a numerical hydrodynamic analysis, performed for a phase-controlled cylindrical buoy heaving point absorber in irregular waves. Next, based on the hydrodynamic results, an end-stop design load is determined. An end-stop strategy is chosen, and finally the solution is modeled and further design investigation made to determine device feasibility and performance characteristics according to the tasks and criteria outlined in the previous sections. Iteration is performed to split design load between component systems or in an attempt to improve the load bearing capabilities, which may even exceed the original, conservatively established magnitude. This will depend on system dynamics and further problem details uncovered through the investigation.

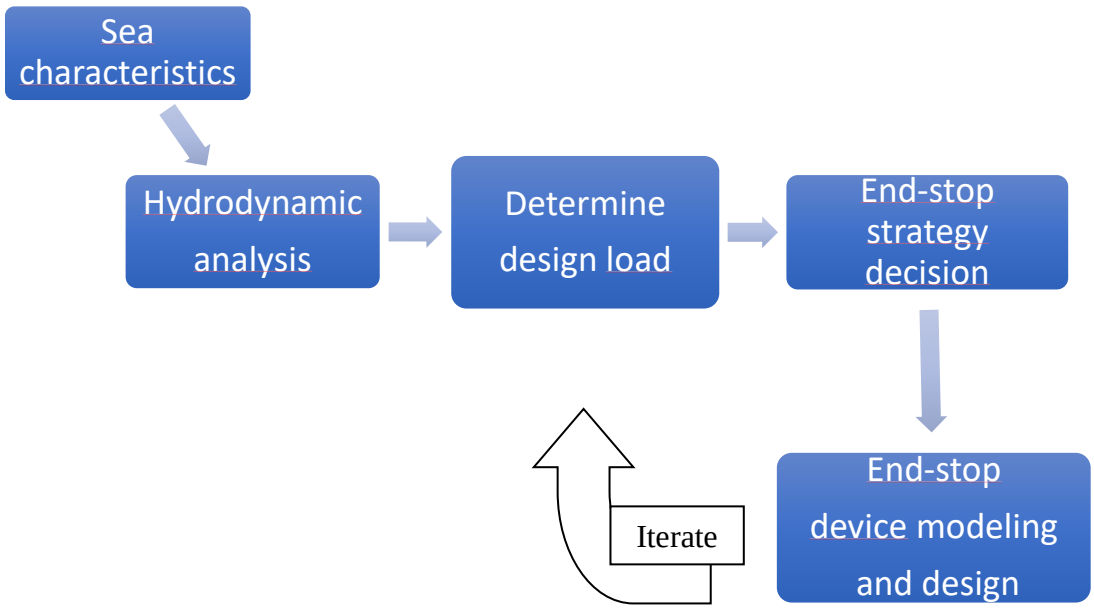


**Figure 2-3 - Preliminary design strategy procedural flow chart. Note the iteration after arriving at "end-stop device modeling and design" to enter a reassessment loop to determine design load, then make an end-stop strategy decision, and improve end-stop device modeling and design. This process is established to increase both the efficiency and efficacy for preliminary design completion.**

## 2.2 Hydrodynamics and wave mechanics

To understand how energy can be extracted from ocean waves, the specific hydromechanics, propagation dynamics, and development cycle of the waves should first be understood. Ocean wave mechanics exhibit complex behavior in general, showing extensive nonlinear effects, i.e. the cases of "breaking" waves and small-scale capillary wave effects. For efficiency and comprehensive design, a standard, approximate linear model is applied, where ideal swells are analyzed, and a numerical model adhering to this theory is used accordingly.

It should be emphasized from a phenomenological standpoint that waves are energy propagators, not mass propagators. Ocean surface waves, referred to as gravity waves, translate energy across the surface of the bulk of water.

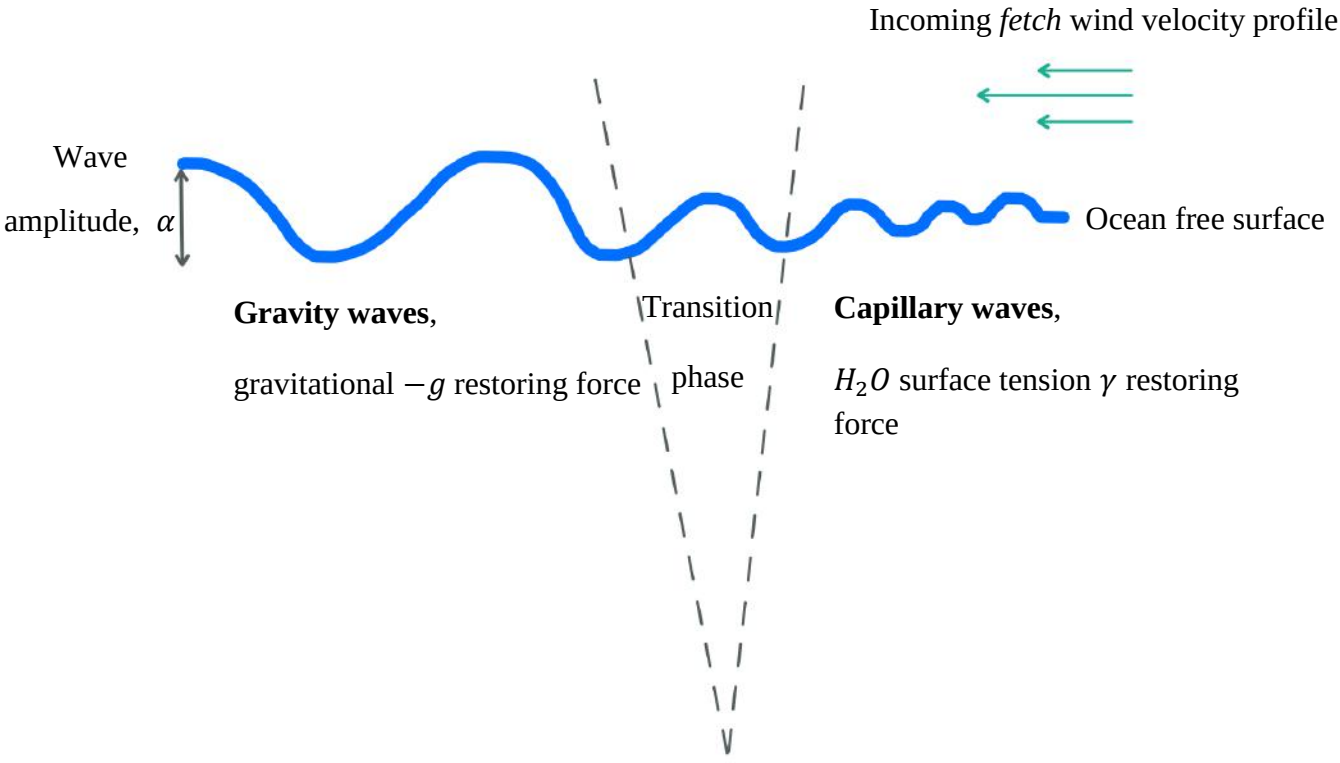


**Figure 2-4 - Development cycle of an ocean wave; beginning with a *fetch* of tangential wind above the free surface, kinetic energy is transferred from the wind to the water creating capillary waves. The capillary waves propagate by a surface tension induced restoring force. Once a wave acquires enough energy from the wind, described by its amplitude $\alpha$, transition occurs and the dominant wave restoring force shifts to gravity. This transition period is designated "transition phase." Continued growth sees that gravity propagates the waves through their deep-water lifespan.**

Figure 2-4 portrays a typical development cycle of ocean waves. The ocean free surface is subjected to consistent, tangential wind flow from above where a *fetch* aligns its wind velocity profile over some prolonged time and distance. Due to relative roughness on the free surface boundary, kinetic energy is transferred at small scales from the wind to the waves. The nature of the free surface boundary condition provokes the surface level water molecules to seek the most energy efficient equilibrium state available. In water, cohesive phenomena grant a lower energy state for submerged molecules, molecules in contact with only like molecules, and this instigates surface tension action in surface molecules. Surface tension tends the water molecules to resist shearing when subjected to tangential wind momentum. This complex interplay results in excitation of the free surface, where wave energy propagation aligns with incident wind velocity, and the water's surface tension balances oscillatory action as a primary restoring force. As a capillary wave grows; however, subject to continued wind momentum from behind, gravity becomes a more dominant actor in the hydromechanical restoration dynamics. At a certain transitional phase gravity becomes the dominant restoring force and the wave is now deemed a gravity wave. In deep water this process may continue for as long as the wind velocity is aligned with and exceeds that of the water wave.

It is now apparent in the wave power world distribution map in section 1.2.1 (figure 1-4) that the most energetic ocean wave regions can be attributed to either larger absolute fetch areas of directionally aligned wind flow or more powerful concentrated or consistent aligned fetch velocities. Combined with the influence from meteorological patterns, the relative spatial distribution of ocean shows high correlation with wave power potential. This is certainly due to the fact that, where unobstructed by continental landmasses, the fundamental hydromechanical development cycle of an ocean wave has liberty to occur and progress over a wider region. This phenomenon is observed in the large, connected region of high wave power potential present in the far southern hemisphere.

The linear approach considers a floating object and assumes a small amplitude and steepness of incident waves; the potential problem is linearized and solved around the equilibrium position of the device [29].

The inherent nonlinear characteristics of rapid buoy mass deceleration upon end-stop impact will show increased dynamical response from viscous component forces; although the aim of design

task 2 is to mitigate these dynamics by any means, a design goal is to effectuate end-stop constraint in as little space possible (from both effectiveness (1) and robustness (2) self-preservation criteria for design task 1). This becomes a question of when to shift self-preservation tactics to a nonoperational safe mode, as well as the interplay between the different device protection features. The inclusion of drag and viscous forces, or any equivalent *damping* formulation could provide insight for designability of the entire WEC protection scheme, but is not a primary focus of the end-stop preliminary design. Thus, linear theory is adopted.

### 2.2.1 Point absorber working principles

The working principles and general design parameters of a heaving point absorber are depicted in figure 2-6 below. Figure 2-6 (a.) depicts PTO with latching control components connected and the end-stop system disconnected (energy production). Figure 2-6 (b.) depicts the end-stop acting while the PTO system is temporarily disconnected (operational self-preservation). This illustration shows the operational relationships between component systems.

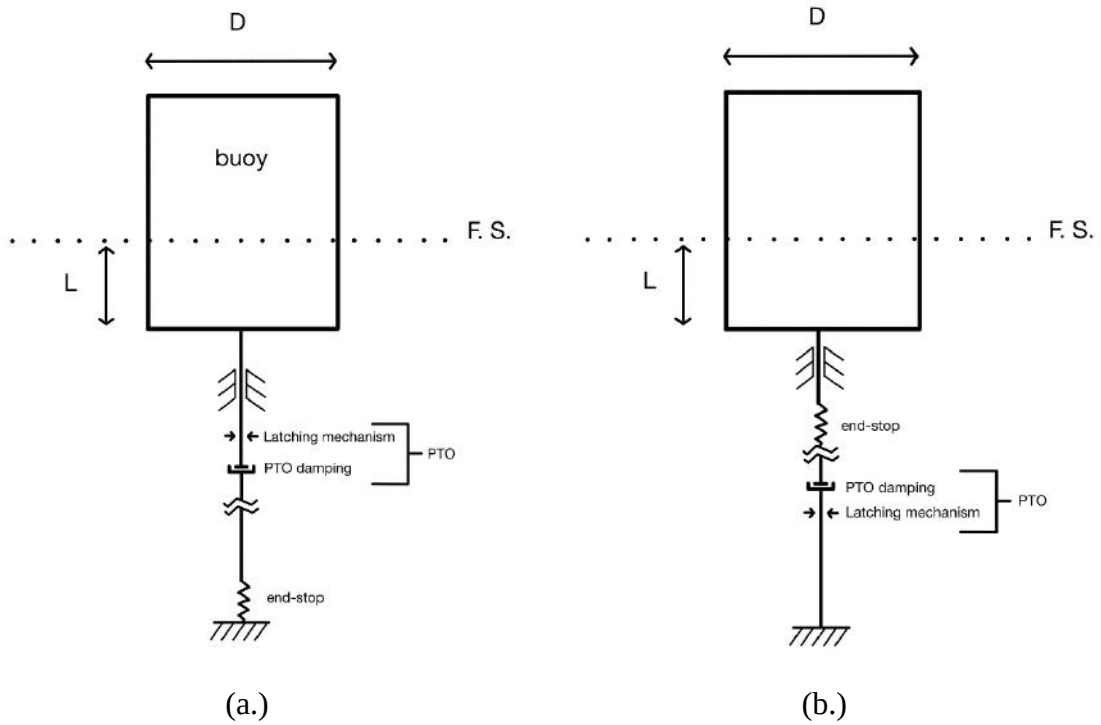


**Figure 2-5 - Heaving point absorber operational component systems. (a.) From top to bottom: buoy, heave constraint, PTO with latching control, disconnected end-stop; (b.) heave constraint, engaged end-stop, unconnected PTO and latching control systems (model adapted from [29] and [5].**

To produce power, as an oscillating body WEC, the point absorber primary extractor (buoy) must oscillate with respect to another body. The body which the extractor acts against is essentially the earth for on or near shore systems or may be a heave plate in the case of offshore installations. The specific nearshore system used in this model has a support structure connected to the seabed. This gives a fixed reference frame to interpret the interplay between the key component parts presented above.

An illustration to depict the relative arrangement and interplay of these component systems and their simplified coupling to an oscillating free surface is shown in figure 2-6 below.

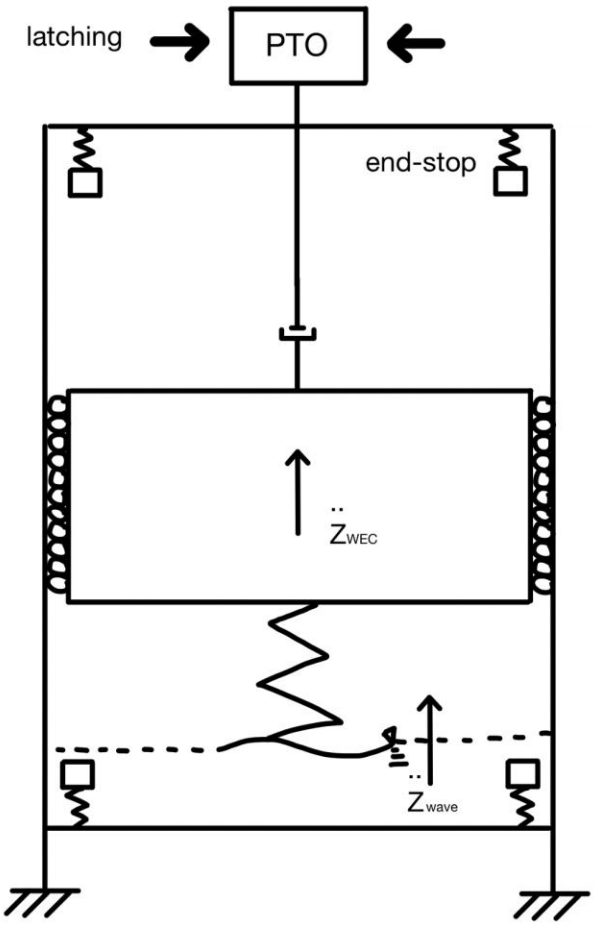


**Figure 2-6 - A schematic representation of the working parts of a heaving point absorber WEC with spring-mass end-stops rigidly fixed to some upper and lower actuation limits. The PTO damping and hydrodynamic radiation damping are represented by dashpots. Heaving buoy response is depicted by acceleration vector $\ddot{z}_{wec}$ and incident wave acceleration by $\ddot{z}_{wave}$. Buoy-wave hydrostatic coupling is modeled as a simple, linear spring element. 4 end-stops are modeled as spring-masses. The representative buoy is kinematically constrained by ideal, frictionless rollers on its lateral edges.**

### 2.2.3 End-stop kinematics

For practical design, it is important to understand both component arrangement and the environment within which a system is to be applied. From the [22] formulation in equation 1.1, the end-stop system can be broken up functionally into its upper and lower components. The kinematic conditions at each of these component end-stop locations are largely different. These dissimilar conditions present unique design challenges and dynamical problems for the upper and lower end-stop systems respectively. To allow a more in-depth preliminary design assessment, the

upper or lower end-stop should be chosen for preliminary investigation. The upper end-stop is arbitrarily chosen to be the focus in analysis. However, as with the intrinsic design task, the lower end-stop will not be completely ignored, but shows up in the qualitative design criteria of integrability and robustness, informing preliminary design selection decisions. The first order decision hierarchy is shown in figure 2-7, the chosen upper end-stop is highlighted in green.

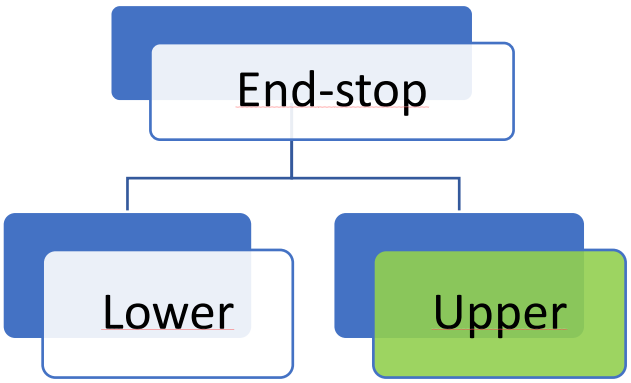


**Figure 2-7 - Sequential investigation of possible end-stop task 1 strategies (#1). Depicted are end-stop (level 0), and upper and lower (level 1) independent end-stop systems. "Upper" is highlighted in green, as the chosen reference system for preliminary design investigation. This is the premier investigative figure of a series to follow in "strategy selection" section 2.4, providing a hierarchal depiction of end-stop design strategy selection.**

In this system, inertial forces are deterministic; contact forces are forces of constraint. The hydrodynamic response of the buoy is the deterministic force, and the proposed end-stop will be a force of constraint.

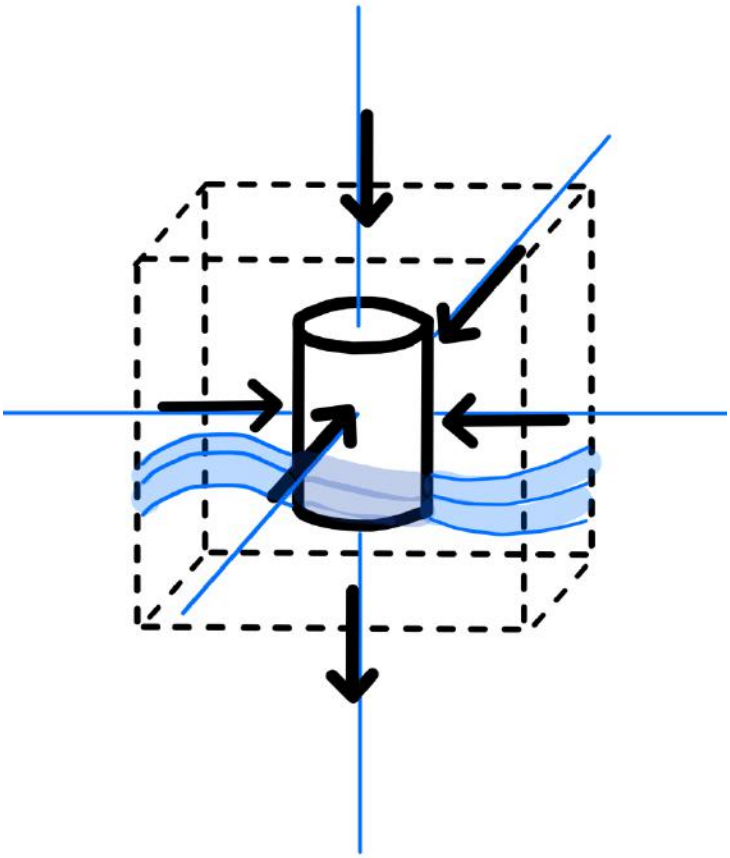

**Figure 2-8 - The three pairs of constraint force application directions for a cylindrical point absorber WEC constrained to heave motion.**

The end-stop force of constraint can be applied from three distinct axes of action: a compressive-tensile direct line collinear to the buoy cylindroid and two distinct lines where the force is applied tangential of the buoy´s circumference.

Consequentially, the tangential forces of constraint can be spread around the cylindrical surface area, and the direct forces of constraint are restricted to the buoy face area.

This analysis gives some clarity as far as geometrical possibility of the end-stop constraining force application in design task 1; however, it is barren of useful information for design task 2. This requires further kinematic analysis, beyond the buoy boundaries. An *interface* investigation is required. The two potential, end-stop strategies are assessed with respect to existing contact interfaces and their interactions.

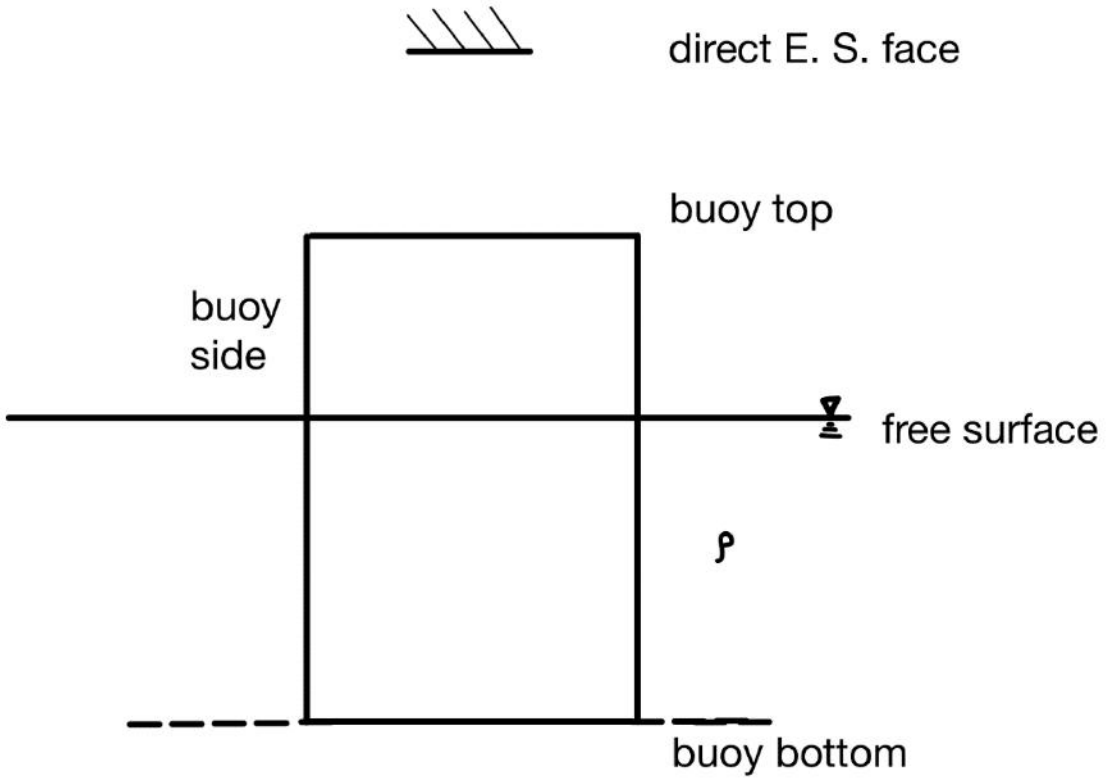


**Figure 2-9 - The kinematic arrangement, 2-D representation with constraints and boundaries in space, of a cylindrical heaving point absorber buoy with a direct upper end-stop "E.S."**

Figure 2-9 portrays the direct-facing, end-stop option. It generates some fine inquiries based on the nature of the heaving buoy environment. Where can the impact response be 'tuned?' Where will the impact vibrations dissipate, and to what degree? The idea here is to presume, but employ tactics to prevent, that the model end-stop is not a cannonball falling upon the vessel. Historically, cannonballs almost always destroy the surface of a boat, yet we know that they do not make much ripple in the water. In detailed design, even the rigidity of the buoy; therein, how the impulse vibration travels through the body, especially if the impact is a directly applied, stiff end-stop buffer. This stiffness will have to be fine-tuned for robustness, yet that is a separate hindrance. Investigating these interfaces, perhaps direct kinetic energy transfer, due to impact can be reduced, by enticing it to onset it elsewhere upon immediate collision contact. The "immediate" response

may be difficult, but there are some slower acting hysteresis responses that may prove helpful if employed, these from the natural free surface and buoy bottom interfaces, and even any viscous drag on the sides of this same model.

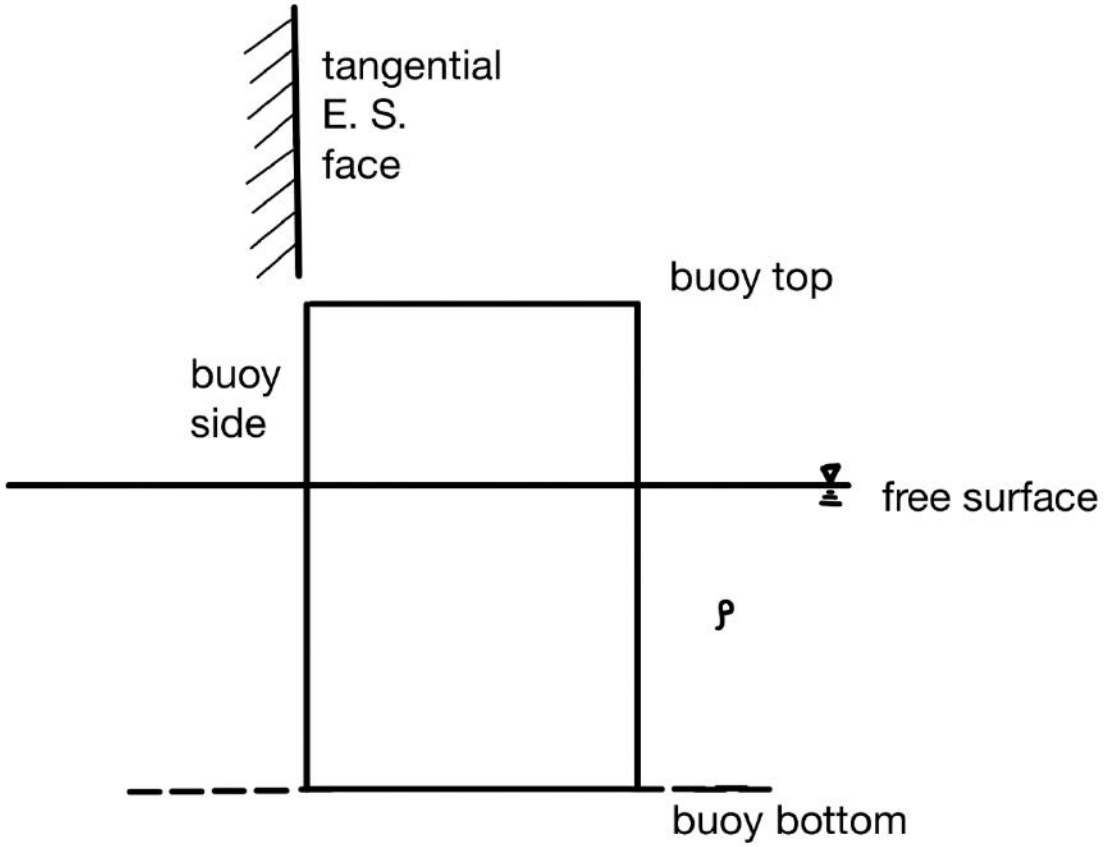


**Figure 2-10 - The kinematic arrangement with marked constraints and boundaries in 2-dimensional space, for a cylindrical heaving point absorber buoy, with a tangential upper end-stop "E.S."**

Applying the end-stop constraint exclusively to the buoy side opens another perspective, completely different from the direct model.

To be clear, the application of the end-stop force of constraint need not be direct application to the buoy cylinder; although, there inevitably must be some kind of direct fixture in contact with the buoy.

For a preliminary model it is fitting to assess the kinematics in this broad sense, because the essence of system configuration in space is absolute; no matter the size or exact positioning of the end-stop system, the buoy will need to receive the applied constraint load directly, one way or another. The intermediary measures and components, through more detailed design, will reveal optimal locale for the practical installation of the end-stop. However, those components or particular arrangements are not the focus of this work, rather, they appear intrinsically within the integrability design criteria (3).

Other potential application locales, for the practical end-stop setting, include:

1. heave stem
2. roller bearings or sliders
3. directly within the PTO

As a preliminary design constraint, the actuation limits for the point absorber buoy in heave are given as **3 meters above** and **3 meters below** the mean free surface level.

## 2.3 Hydrodynamic analysis — numerical model

The adopted model uses one-dimensional energy sea spectrum and is employed using irregular waves. [5] states the following with respect to the qualifications of a one-dimensional sea state model: "Real sea is mathematically represented by irregular waves which can be simulated as a superposition of regular waves. By considering a one directional wave propagation, a given sea state is adequately represented by a one-dimensional energy sea spectrum. Since the buoys are axisymmetric and therefore quite insensitive to wave direction, a one-dimensional spectrum will be considered in the following analyses [5]."

Numerical data were obtained for the entire potential wave spectrum shown in matrix form of representational occurrences of significant wave heights and periods for nearshore Rio de Janeiro, Brazil. Since hydrodynamic linear theory was used for the numerical model, reliability hinges on

those linear assumptions. However, it is considered a reliable representation for the sea states and nearshore region studied.

The Cummin's equation as a time domain representation of the forces in heave at play in the heaving point absorber model [5].

$$(M + A)\ddot{x}_3(t) = F_{e,3}(t) + F_{r,3}(t) + F_{h,3}(t) + F_{PTO}(t) + F_{Latching}(t) \qquad (2.2)$$

This time-domain formulation of all the forces accumulating on the buoy, should be modified to include the end-stop force, which can take the Heaviside step function form described by [22] and presented in chapter 1.

$$(M + A)\ddot{x}_3(t) = F_{e,3}(t) + F_{r,3}(t) + F_{h,3}(t) + F_{PTO}(t) + F_{Latching}(t) + F_{ES}(t) \qquad (2.3)$$

The COPPE nearshore point absorber WEC is used for numerical analysis. The numerical model is a complete wave-to-wire simulation for a heaving point absorber based on the following fundamental assumptions [5]:

- Hydrodynamic linear theory resembles real-world response.
- Point absorber motion is restricted to heave only.
- The PTO system is considered a *pure damper*.

| | | Tp(s) | | | | | | | | | | | | |
|---|---|---|---|---|---|---|---|---|---|---|---|---|---|---|
| | | 4 | 5 | 6 | 7 | 8 | 9 | 10 | 11 | 12 | 13 | 14 | 15 | 16 |
| Hs(m) | 0.25 | 0.60 | 2.00 | 8.40 | 84.00 | 79.80 | 35.00 | 19.40 | 18.00 | 5.80 | 1.20 | 3.00 | 2.00 | 1.60 |
| | 0.75 | 7.60 | 23.80 | 101.00 | 602.20 | 866.60 | 456.00 | 376.40 | 280.80 | 169.40 | 84.00 | 32.80 | 12.20 | 3.40 |
| | 1.25 | 0.80 | 12.80 | 50.80 | 199.20 | 483.60 | 480.80 | 492.20 | 404.40 | 279.00 | 137.00 | 51.80 | 15.00 | 10.20 |
| | 1.75 | 0.01 | 0.40 | 19.40 | 70.20 | 154.80 | 201.80 | 286.60 | 350.00 | 215.20 | 141.20 | 42.60 | 9.80 | 4.00 |
| | 2.25 | 0.01 | 0.01 | 0.60 | 14.00 | 63.60 | 97.40 | 147.00 | 174.00 | 162.00 | 82.80 | 22.80 | 9.80 | 11.20 |
| | 2.75 | 0.01 | 0.01 | 0.01 | 1.40 | 17.80 | 29.60 | 49.60 | 69.00 | 97.80 | 72.80 | 25.60 | 6.80 | 8.40 |
| | 3.25 | 0.01 | 0.01 | 0.01 | 0.01 | 0.40 | 10.00 | 10.80 | 20.00 | 39.60 | 31.00 | 26.00 | 7.00 | 1.80 |
| | 3.75 | 0.01 | 0.01 | 0.01 | 0.01 | 0.01 | 0.01 | 5.00 | 4.40 | 10.60 | 15.40 | 4.40 | 1.20 | 0.20 |
| | 4.25 | 0.01 | 0.01 | 0.01 | 0.01 | 0.01 | 0.01 | 0.01 | 0.20 | 4.80 | 3.80 | 0.60 | 0.01 | 0.60 |
| | 4.75 | 0.01 | 0.01 | 0.01 | 0.01 | 0.01 | 0.01 | 0.01 | 0.01 | 0.01 | 1.20 | 0.60 | 0.80 | 0.01 |

**Figure 2-11 - Matrix representation of the number of occurrences of sea waves for the nearshore region of Rio de Janeiro[5]**

Standing on the rigors of the established COPPE model, there are still a great many assumptions and limitations to this analytical code that need to be considered, some of which have been acknowledged in previous sections. This discussion evolves as the paper proceeds, with the aim to accommodate an understanding of "practical solution" needs. However, the model serves quite well to investigate the end-stop preliminary design requirements. The COPPE model is used in the following procedure.

The nearshore point absorber numerical simulation is run for all potential and predominant sea states from the joint distribution model above, with a constant PTO damping selected as 8 kN/m.

The numerical analysis models actuation forces in a kinematically constrained floating point absorber buoy, bobbing in only the heave direction. End-stops are observed as actuation limits.

Through the initial calculations of end-stop forces at the required actuation limit of the point absorber, the necessary end-stop system parameters are established.

Since the end-stop is a function of extreme displacements induced by the pairing of wave excitation forces and latching control, we are most interested in where these values are at their maximum, and specifically where the displacement reaches the established 3-meter design threshold.

## 2.4 End-stop strategies – strategy selection

There are a lot of possibilities when it comes to the motion constraint strategy of a heaving buoy. The choice was made in section 2.2.3 “end-stop kinematics,” to investigate an upper end-stop system (shown in figure 3- sequential investigation of possible end-stop task 1 strategies (**#1**)). This accounts for the level 1 design strategy decision. Level 2 composes of active and passive end-stop functionality, shown in figure 2-12 below.

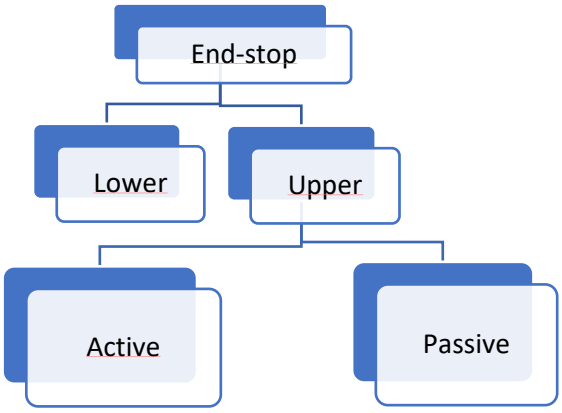


**Figure 2-12 – Sequential investigation of possible end-stop task 1 strategies (#2), depicts level 2 active and passive end-stop options.**

The difference between active and passive end-stop systems is active systems require energy input to function and passive systems do not.

Using a relatively small input energy, an active end-stop system may improve functionality for design robustness (design criteria 2). This is accomplished through active system control system design. Active controls can operate in real time, and can proportionally tune to incoming sea states as well as individual end-stop impacts. The unknowns to investigate an active end-stop solution are insufficient for a preliminary design, first, passive parameters will prove useful to later investigate improvement potential through an active approach. Besides dependency on yet undetermined parameters, an active end-stop directly affects the intrinsic design task by taking energy out of the system.

A passive solution on the other hand has a slightly more limited set of design parameters it relies upon, as it will not be implementing electronic controller components. This guarantees a stronger preliminary reliability rating (criteria 1). All parameters are still tunable, thus there is a wide range of possibility for criteria and design task fulfillment, with no inherent limitations.

An active end-stop solution may be directly implemented within the WEC PTO system. However, this depends entirely on the PTO system design, and thus has unknown integrability (design task 3) into the WEC system investigated. Additionally, the high design load of $600\ kN$ is a deterrent in PTO/end-stop hybridization. A potentially catastrophic load of this magnitude should be directed away from the valuable PTO system and its components, and explicitly protected by end-stop function. If anything, a sacrificial end-stop could prove a more economic choice than incorporating end-stop constraint work within its confines, but that all depends on the selected PTO system operating principles and type.

Rather, a passive solution is chosen based on the immature determination of better strategy intrinsic design task performance and preliminarily uncertain reliability (criteria 1), and unknown integrability and efficiency/economic (*practicality* criteria 3 & 4) of active solutions. In terms of WEC self-preservation, passive solutions are preliminarily deemed aptly conservative and prerequisite to active strategies, and thus are chosen for this initial design investigation.

A divergent 3rd level subclass of potential end-stop systems is an “energy-in” system, highlighted in figure 2-13. This system is neither active nor passive in nature, as it operates as a secondary stage, additional energy conversion subsystem for the WEC, with relatively low production potential, but functionally adequate for both tasks.

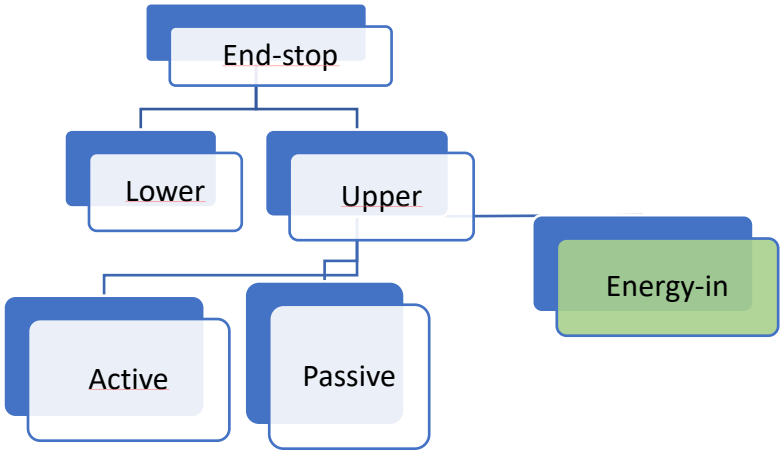


**Figure 2-13 - Sequential investigation of possible end-stop task 1 strategies (#3), depicts a proposed level 2 subclass – "Energy-in," variant to traditional active and passive constraint or control.**

Potential *energy-in* end-stop systems are developable using select piezoelectric or triboelectric materials. These materials are often employed for microscopic scale energy conversion. However, the "Berkeley Wedge" [9] is testing wave impact energy extraction at as large-scale breakwaters.

There are different types of piezoelectric materials, i.e. PVDF and PZT, with distinct material characteristics. PVDF, for example, is a relatively resilient material, Poling process to prime the material for installment may prove costly. Uncertainty of device performance and the additional design task of utilizing or transmitting the obtained energy are certain challenges. Tests will need to be performed to assess materials adequacy for the marine environment, or appropriate lattice assemblies. Future works will assess the viability of an energy-in end-stops.

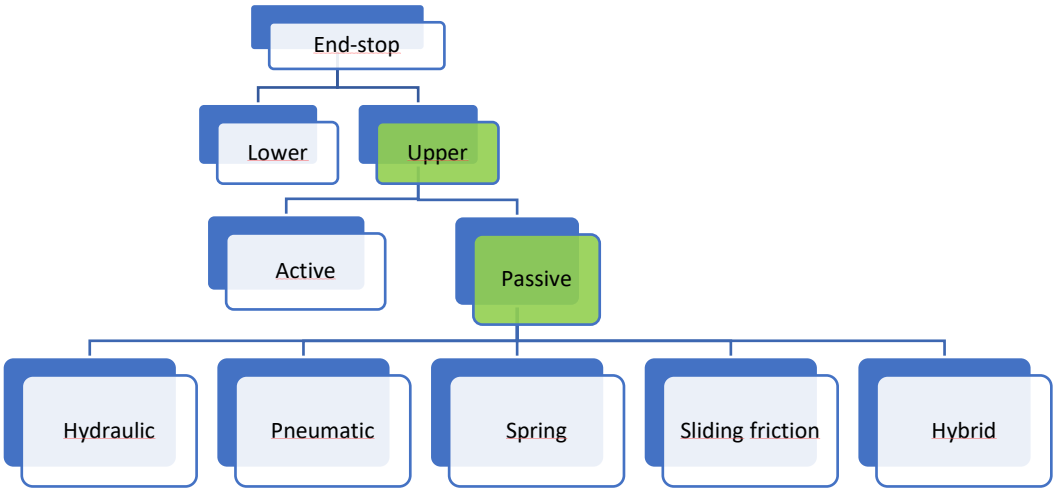


**Figure 2-14 - Sequential investigation of possible end-stop task 1 strategies (#4). The established level 1 (upper) and level 2(passive) paths are highlighted in green, and a new class of level 3 design task 1 passive end-stop strategies is presented.**

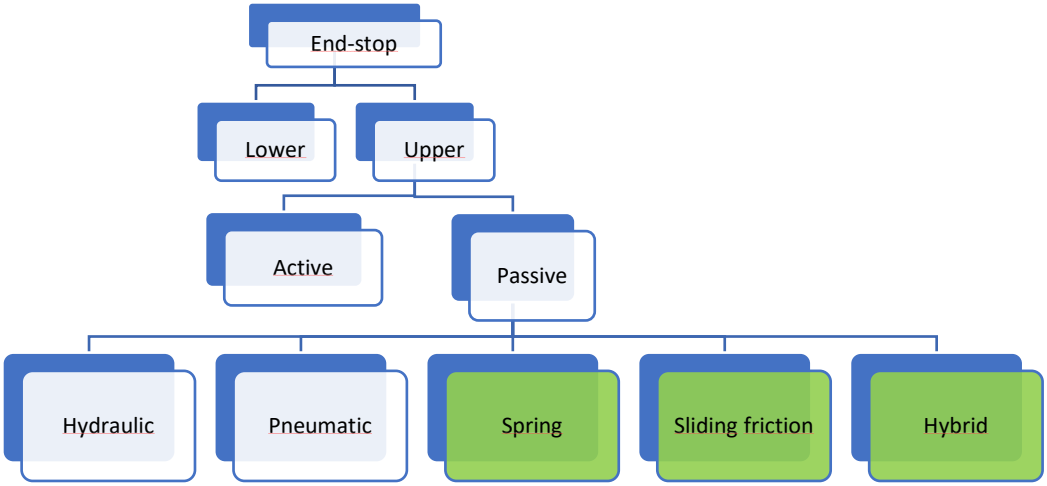


**Figure 2-15 - Sequential investigation of possible end-stop task 1 strategies (#5). Level 3 strategies are chosen- spring, sliding friction, and hybrid for preliminary investigation.**

Two distinct design strategies are preliminarily chosen: springs and sliding friction. The next 2 sections will provide background on the two strategies as they relate to design task 1, and following sections will provide detailed investigation and analysis of these potential solutions, as well as further preliminary design selections.

### 2.4.1 Springs

Essentially, springs are energy storage vessels. They capitalize on material properties and geometric configuration to produce restoring or constraining force by elastic displacement and deformation with an intrinsic stiffness $k$. The relation is described by Hooke's Law:

$$F_s = kz \tag{2.4}$$

where:

$F_s$ is the spring force, or force required to compress or extend a particular spring.

$k$ is the spring stiffness or spring rate, constant and characteristic of a specific spring.

$z$ is the linear displacement undergone by a spring, in compression or extension, relative to its static, equilibrium state.

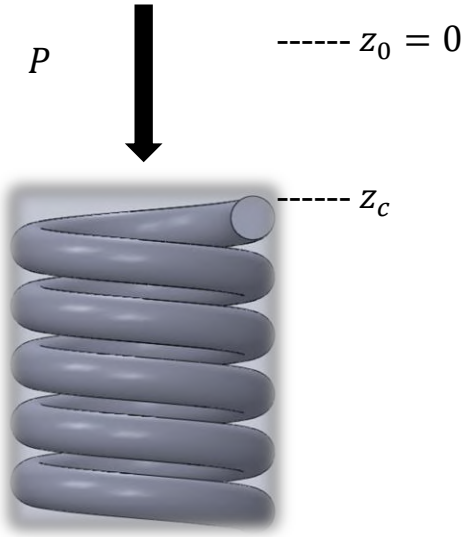


**Figure 2-16 - Diagram of Hooke's Law depicting a spring subject to deformation due to an applied external load $P$. $F_s$ is the spring force resisting load $P$. The component parameters of the $F_s$ magnitude are spring stiffness $k$ and deflection $z_c$ - $z_0$. $z_c$ is displacement after compressed; $z_0$ is $z = 0$, an equilibrium state of the spring.**

This is the same formulation that appears in the end-stop model presented in Equation 1.1 [22]. However, in spring design the formulation must be understood in depth, along with additional limiting factors inherent to practical implementation.

A spring can be taken as an ideal elastic material. It deforms to a given strain in response to a given stress, remaining until the stress is removed. Once the stress is removed, the material returns to its original shape. The elastic modulus, or ratio of stress to strain, is constant for a spring. All work done by the original stress is stored in the material then elastically recovered when the stress is removed [33]. Spring material selection criteria are as follows.

Limited materials and alloys serve for springs. Principle criteria for spring steel are high ultimate strength, high yield point, and low modulus of elasticity. These criteria are unanimous for mechanical springs to provide maximum energy storage, e.g. the area under the elastic portion of stress-strain curve.

Additionally, fatigue strength properties are a limiting factor, and are encouraged for the design of springs subject to dynamic loading. Fatigue is usually measured as cycles to yield, but the wide possibilities in load magnitude and impulses during operation, create a variant problem on the end-stop. Fatigue failure occurs well below the material yield strength and should be considered in later design phases.

There are many different types of springs. Table 2-5 shows this variety, color coded by broad functional class.

**Table 2-5 - Types of compressive springs and their properties [36]. Broad spring classes are designated in the table by cell highlight color: coil springs – blue, leaf springs – green, and disc springs – grey. Wave springs are left uncolored, being a novel design that demonstrates some properties of all three.**

| Compression Spring Type | Characteristics |
|---|---|
| Helical compression spring (coil spring) | Ubiquitous, subject to torsional shear stress, transverse shear stress, and additional stress due to curvature. [36] |
| Tension spring (coil spring) | The load bearing end is kinematically constrained to load application in a fundamentally different kinematic setup to that of compression springs. |
| Torsion spring (coil spring) | Axis of deflection and axis of applied load do not coincide. |
| Wave spring (novel) | Flat wire compression springs with sinusoidal or bell curve wire waveform, can reduce the weight and size of assembly up to 50% [37] |
| Volute spring (coil spring) | Conical shaped spring with a different contact area at each end |
| Disc or Belleville spring | Good for large loads at small deflection, as in side clamping machine tools. [36] |
| Laminated/leaf spring | Cantilever or simply supported type, called "laminated" when contains more than one leaf, can be semi-elliptical, used in automobiles [36] |

From the basic functional characteristics in table 2-5 and innate deflection kinematics, 2 design criteria are readily comparable, while the rest remain undeterminable. Based on reliability for design task 2 and robustness for design task 1, the longer extension properties inherent to coil spring configuration are desirable.

Since a compressive constraint force direction was chosen in premature determination (see Appendix C for selection protocol), tensile and torsional springs can be excluded from this design analysis. Narrowing the possibilities to compression springs for direct application, the funneled options are compared in figure 2-17. They consist of tension, torsional, and compression.

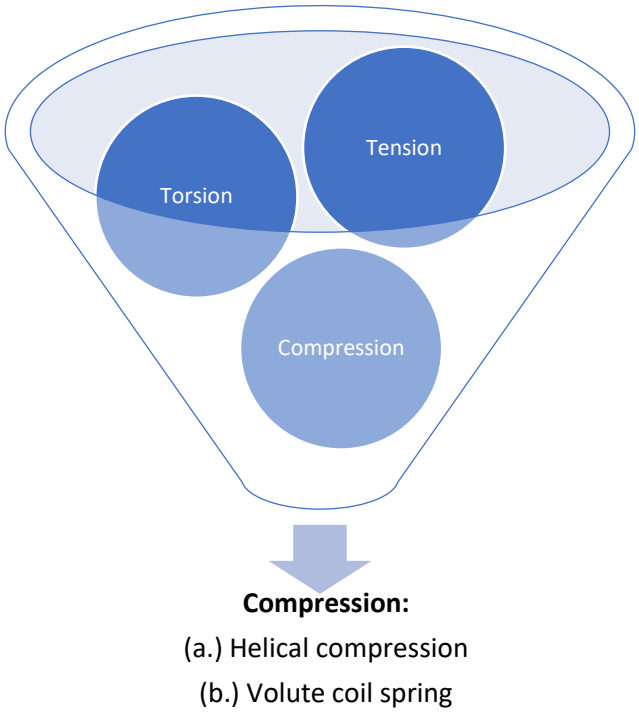


**Figure 2-17 - Functional coil spring classes and the chosen helical and volute compressive springs.**

To facilitate obtaining preliminary design results, linear helical springs, option (a.), are chosen for design investigation.

### 2.4.2 Friction

Friction may very well be the most underappreciated force in modern engineering design. Besides recent rise in tribological science publications (mainly in pursuit of super-lubricity), the most common acknowledgement of friction in contemporary engineering practice may be with the clumped derogation, “friction loss,” written off merely to ignore complex or unknown effects of friction on a given system, a means to save time. This reveals a general lack of understanding with respect to friction, and yet it remains ubiquitous. Oftentimes friction is something to mitigate, but for a tangential action end-stop, it will be investigated as a strategic asset and primary constraint force to attenuate buoy heave motion.

The phenomenological nature of friction analyses presents less definitive modelling characteristics for a friction end-stop. With the uptake of new research into tribological sciences on the micro and atomic scales, new models are under development to cope with the breakdown of traditional, macroscopic friction formulations.

Kinematically, the friction end-stop strategy composes an interface application tangential to the cylindrical WEC buoy motion.

In physical friction phenomena, both viscous and linear components are observed. In solid-solid sliding friction the empirical “AC,” Amonton-Coulomb friction (or alternatively, “Coulomb”), friction laws — also referred to as dry or sliding friction (terms are used interchangeably) - are often used, omitting viscous phenomena.

The Coulomb sliding friction formulation describes two fundamental modes of frictional behavior, static and dynamic (also referred to as “kinetic”) friction [32], as functions of a normal contact force, a static or kinetic friction coefficient, respectively, and the velocity sign of intended or acting relative motion between two surfaces, in some frame of reference. The equations are as follows:

$$F_f = \mu_k F_\perp sgn(\dot{z}) \tag{2.5}$$

$$sgn(\dot{z}) = \begin{cases} 1 \ for \ \dot{z} < 1 \\ -1 \ for \ \dot{z} > 1 \end{cases}$$

With: $F_\perp = kx$ (2.6)

Where:

$k$ is the contact stiffness

$x$ is compression distance or distance over which elastic work has been done

Where:

$F_f$ is the friction force

$\mu_s$ is the empirical coefficient of static friction

$\mu_k$ is the empirical coefficient of kinetic (dynamic) friction

$\dot{z}$ is the relative velocity between two surfaces in contact

$F_\perp$ is the normal contact force perpendicular to the line of sliding action

From this basic friction model, the force of constraint behavior is velocity dependent; in that, with some velocity the frictional force opposes motion in accordance to some dimensionless coefficient $\mu_k$ (classically obtained from empirical measurements) and the normal surface contact force $F_\perp$ (a property between two *touching* * surfaces), but when no relative velocity exists between the surfaces in contact a static coefficient of friction $\mu_s$ is used instead (which is higher in magnitude than the kinetic in all known cases).

*It must be established that two surfaces can never literally *touch.* Instead, there is some interfacial space existing between them at any given moment in time. This space between two solid sliding surfaces, and direct contact alike, is often considered and proven to be occupied by air molecules, and the closer the two surfaces get to actual contact, the stronger the opposing effect of their charged surface electrons providing an irrefutable boundary layer between two distinct objects.

It is clear that friction is a property between two surfaces, each contributing certain value to the resultant force of constraint. This presents a marked difference from forces of a spring, which contain their own unique properties consequent of material makeup and geometric configuration.

In the AC friction model, force vectors are simplified to orthogonal components and the magnitudes of acting forces simply expressed. The strength of the model is in that it relays and quantifies the distinct difference between static and dynamic sliding frictional forces.

In either case, it is apparent that the dimensionless, static and kinetic friction coefficients convey the amount of normal contact stiffness force that is projected unto this tangential friction component.

Viscous forces are often modeled as quadratic functions, implying their strong damping effect on system response. This is a desirable characteristic for design task 2 – mitigating impact dynamics.

The Froude number is a dimensionless parameter that helps to indicate whether viscous or inertial forces dominate for a given, physical system.

Material factors of importance in the tangential contact application of friction differ from those of the direct contact application from springs. Stress-strain phenomena should be examined accordingly. The *viscous* quality of friction can be contrasted to spring functionality by understanding the strain behaviors under applied stress of the respective systems. Parametrically, the elastic modulus is the quantity that allows prediction of how much a material will deform elastically when subjected to a stress, and viscosity is the analogous quantity that describes how fast a material will flow. The key difference between elasticity and viscosity is whether the strain reaches a limit or increases continuously in response to constant stress. Ideal viscous materials change strain in proportion to the time the stress is applied, thus the ratio of stress to the rate of strain defines the viscosity [33]. Behaviorally, a viscoelastic material under stress will comply under smaller stresses and resist larger stresses. This shear material property is significant for a

tangential friction end-stop strategy. Optimizing viscous material properties equate directly to the intrinsic design task fulfillment and the robustness (design criteria 2) of the end-stop subjected to variable loads.

Although the mathematics of viscous friction phenomena will be omitted in the dynamical models, it should be noted that they remain an important design consideration, and experiments or numerical simulations are needed to determine whether they play a dominant role in the system dynamics.

Another factor to consider in friction collision is *stick-slip*. Stick-slip friction dynamical behavior is the result of the abrupt difference between the static coefficient of friction and kinetic coefficient of friction where a consequent acceleration lurch in motion occurs periodically during a sliding interaction between two surfaces. Since no surface is considered perfectly flat or one-dimensional, for all intensive purposes, at any given moment certain surface asperities will catch and resist movement within the sliding interface. This can and will occur at any scale, but at the microscopic level it is difficult to observe without proper instrumentation, and even more difficult to predict, with no generally acceptable model with high reliability. [53] observe stick-slip friction during experimentation of "static" friction traction between individual paper sheets in their investigation of interleaved phone books and a friction amplification phenomenon. To extract the delicate dynamics of stick-slip phenomenon, further research will have to be done.

Another way to study friction motion constraint, is to look at friction motion propulsion. In nature, evolution has provided legless reptiles, along with many aquatic creatures, an optimized locomotion based on anisotropic friction. Furthermore, the ideal frictional trait for a directional end-stop is directionally independent friction force comportment. This would be the most effective (design criteria 1) and efficient (design criteria 4) approach to friction application for a passive system, and thus will be investigated in detail.

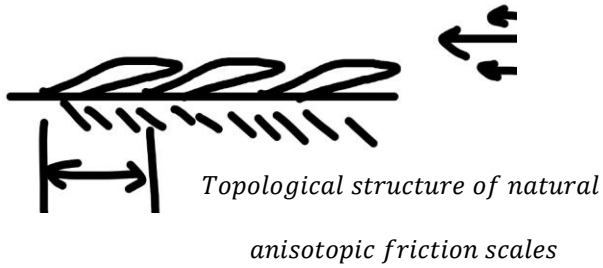


**Figure 2-18 - Schematic representation of scales subject to incoming motion. Sliding friction as well as viscous forces can be used to model the nature of the force of constraint they impose to resist motion.**

The limiting factors in a friction end-stop are definitively normal contact force together with wear. For a WEC end-stop in a humid environment the change in frictional performance on a wetted surface also needs to be accounted for and measured. The acting force can either be contained or exposed, based on hydrophobic properties of the natural topologies, examined below.

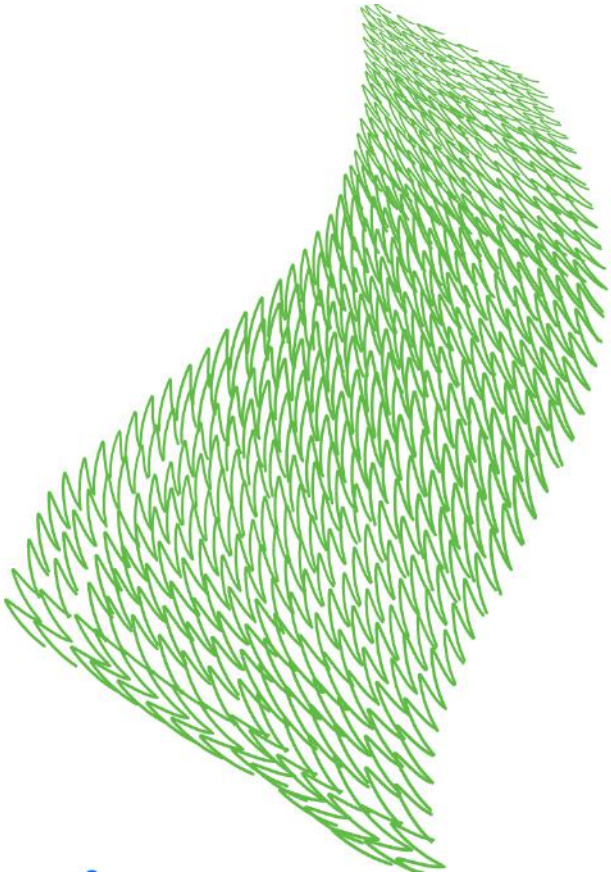

**Figure 2-19 - A 3-D theoretical representation of a biomimetic, patterned, anisotropic friction surface. This pattern can be manipulated, and geometrically and materialistically tuned, for best, desired frictional performance properties.**

These scales give the snakes a preferred direction of motion, which makes snake movement a lot like that of wheels, cross-country skis, or ice skates. In all these examples, sliding forward takes less work than does sliding sideways [44]. Additionally, the Froude number for these snakes shows that the dominant forces in their propulsion are decidedly viscous, and not inertial. Thus, their propulsive force goes directly to motion, directly to their forward velocity (instead of inertial acceleration), entirely due to this anisotropy and their body and scale control during undulation [44].

[44] measured the directional, friction forces of a variety of snake species.

**Table 2-6 - Directional friction forces shown by static friction coefficient of a snake on rough cloth surface (top) and smooth glass (bottom); $\mu_f$ when slid forward, $\mu_b$ when slid towards the tail, $\mu_s$ when sliding towards its flanks, from [44]**

| $\mu_f$ | $\mu_b$ | $\mu_s$ |
|---|---|---|
| $0.11 \pm 0.011$ | $0.14 \pm 0.015$ | $0.20 \pm 0.015$ |
| 0.14 | 0.14 | 0.16 |

The coefficients in table 2-2 show the important fact that the friction force does not depend on the snake scales alone, but also on the roughness of the substrate along which it is slithering [44]. Additionally, it is the laterally directed friction that has the highest magnitude.

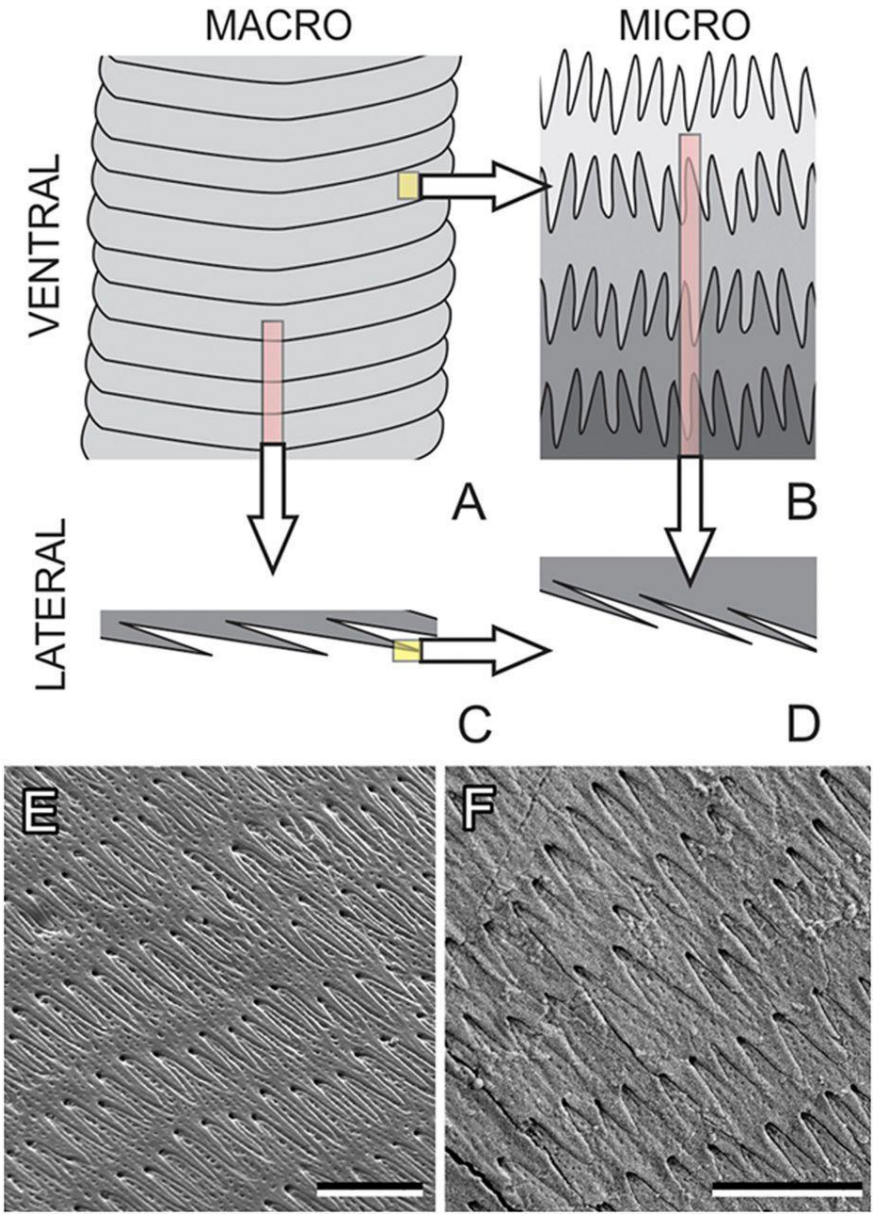


**Figure 2-20 - Snake ventral scales microscopic view [44]**

The complex multi scale patterning of the propulsion surface of these reptiles can be mimicked to provide a controlled, directionally dominant friction for use as a directionally constraining end-stop component.

Typically, vibrations are seen to overcome friction, and this is the case with the static friction of a still snake, but this effect changes nature when in motion, and instead of the multiplanar undulation

diminishing the force, it indeed contributes and couples to the anisotropic pattern to produce an efficient drive.

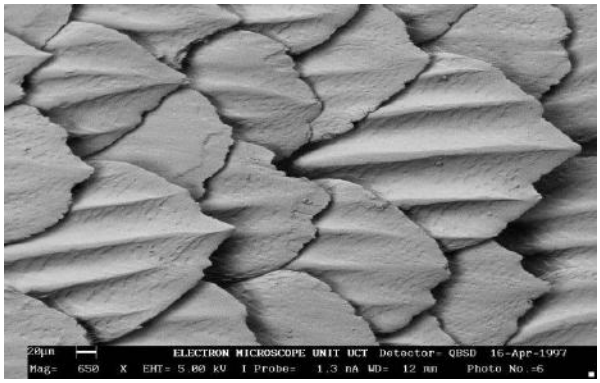


**Figure 2-21 - Shark skin denticles microscopic view [48]**

Another benefit of the anisotropic friction is the antibiofouling and hydrophobic properties. This would assist the preservation of AC dry friction applicability in a humid, marine environment, while simultaneously preventing flora and fauna from attaching to the system when in nonoperational mode. Apparent in figure 2-21, shark skin is composed of tiny rectangular scales topped with smaller spines or bristles. The surface pattern makes it difficult for algal spores to attach or get a grip. Brennan constructed artificial composite to emulate this form, composed of plastic and rubber coating. The artificial denticles measure 15 microns, with additional smaller ribbed asperities like those visible in the photo of figure 2-21 [48].

Friction may also display stick-slip phenomena. Stick-slip is a spontaneous jerking that occurs in sliding friction due to the difference in magnitude between kinetic and static coefficients of friction- sticking provides static friction resistance, but upon subsequent release the sudden drop to the kinetic coefficient produces a lurch or acceleration in the system. This can be observed when trying to move furniture along a rug.

## 2.5 Impact damping

The kinematic conditions, presented in section 2.2.3, allow up to 3 pairs of contact interfaces for end-stop force of constraint engagement. Inhibited to 2 degree of freedom, all of the potential lines of impact, or collision paths, run parallel, along these planes of heave. The

These inherent conditions are applied to develop efficient practical practices to better achieve design tasks and criteria.

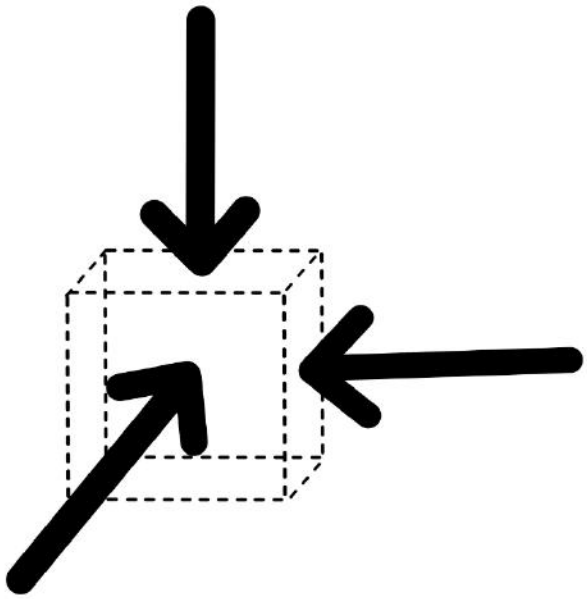

**Figure 2-22 - Potential planes of end-stop collision in three-dimensional space, where the possible lines of impact all run vertically in the same heaving *z* direction as the WEC buoy itself.**

To navigate the dynamical problem of motion constraint in WECs, it must first be understood the hazards of unconstrained WEC motion. There are two main dynamical problems when a WEC with its primary conversion stage oscillator is optimally or suboptimally tuned for energized resonance. First, the PTO system can receive dynamical forces that it is not equipped to handle. This could result in catastrophic failure or unnecessary fatigue to the crucial, and costly PTO

system. Many different types of PTO systems exist, but any implemented system will have certain limitations, and maximum jerks or loads for its particular design specifications. Second, in certain operational wave conditions, a heaving buoy can be subjected to *slamming*. Slamming not only harms the buoy (primary extractor) but, depending on the specific WEC design and PTO coupling strategy, can harm the PTO system and other crucial component systems with jerk and impact loads. When higher kinetic energy is involved in a given collision, solids tend to exhibit more liquid-like behavior. This can be observed in slow motion capture of high energy impacts between solids, where bending and vibration modes truly resemble *flow* like a liquid.

From the kinematics and interface formalizations of the problem, it is clear that there are two constraint forces of interest for this preliminary end-stop design: normal force and friction force, which have been described in previous sections. For the friction force, just the kinetic formulation is of interest for impact dynamics analysis, equation 2.5.

With a strategic basis established, coherent tactics for modeling of all collision types under investigation: mass-mass-support structure, friction tangential sliding surface collisions, allisions coupled to equivalent hydrostatic spring force are described in the next sections.

It is apparent from the kinematics analysis in section 2.2.3, that the heaving point absorber in 3 dimensions, may be subjected to detrimental impact dynamics to its force of constraint, load-bearing components, in multiple planes, depending on end-stop configuration and ultimate strategy selection.

Principles of an impact:

1. Interface waveform between colliding bodies
2. Coefficient of restitution – this parameter implies: impact energy regulation
3. Line of impact

Thus, in order for a collision to occur, there must be a contact interface, at the meeting of two distinct surfaces.

Another property of collisions is the coefficient of restitution $e$. This dimensionless parameter gives rich insight into the nature of any impact. Formulated in equation 2.7, the coefficient of

restitution is the ratio of kinetic energy in a collision/contact system after the contact, to the kinetic energy present in the system, before first contact was established.

$$e = \sqrt{KE_{after}/KE_{before}}$$

$$e = \sqrt{\frac{1}{2}mv_2{}^2/\frac{1}{2}mv_1{}^2} \qquad (2.7)$$

$$e = \sqrt{v_2{}^2/v_1{}^2}$$

$$e = v_2/v_1 \qquad (2.8)$$

Equation 2.8 shows how, assuming constant mass, the pre and post-collision kinetic energy formulation of the coefficient of restitution can be equated to a ratio of the relative velocity before ($v_1$) and after ($v_2$) the collision occurrence, established in equation 2.8.

The values for $e$ often fall between 0 and 1, where 0 is a perfectly inelastic collision and 1 is a perfectly elastic collision. However, $e$ may also have a value less than 0, if the momentum vector of both colliding objects coincides in the same direction after the collision, implying one colliding body did not return from the impact, and effectively become part of the momentum of the other,

or passed directly through. This possibility is represented schematically in Figure 2-23 below, where one colliding mass can be imagined as a dense fog of particles engulfing, but simultaneously attenuating the kinetic energy of the other, incoming, colliding mass. This formulation of $e < 0$ will prove useful for modeling dynamical phenomena of tangential, friction surface collisions.

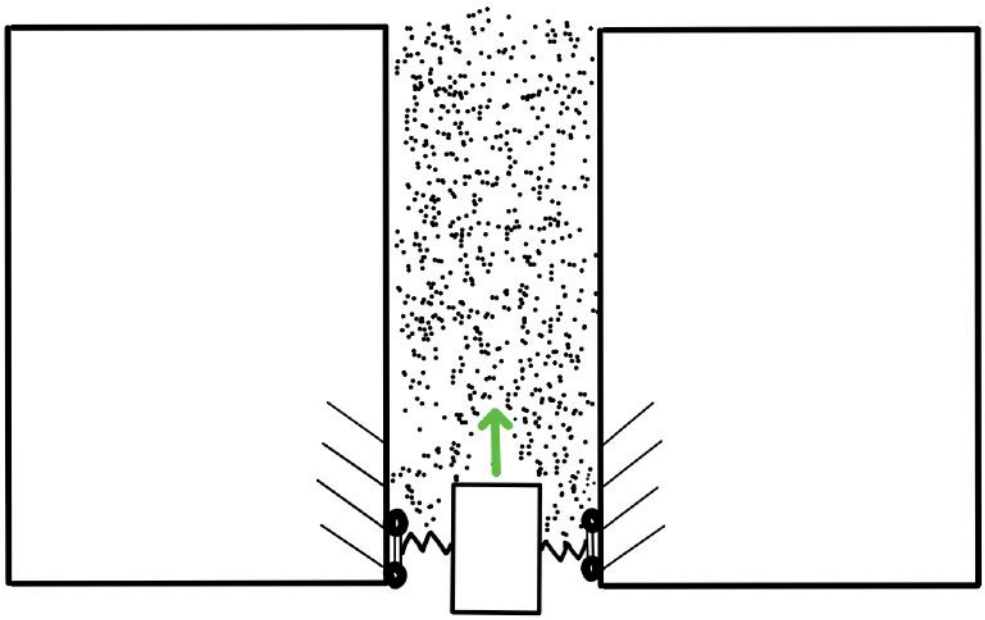

**Figure 2-23 - A representation of an $e < 0$ (negative coefficient of restitution) collision in one-dimension. A heaving, rigid-body mass is constrained by a pair of frictionless, ideal rollers between two ideal, rigid walls. A mass of particles with some density exists between these fixed wall constraints. The relative velocity vector is represented by a green arrow; where, upon collision, the heaving mass is not immediately halted by the collective mass of particles, and its motion continues, whilst sharing momentum with collided particles. Momentum and kinetic energy are conserved.**

Another conceptualization of a negative coefficient of restitution is a plaited net, where an arbitrary portion of the mass is permitted to pass through the gaps, and another portion is hindered by the force of constraint of the stiffness of the net's component weaves.

The third variable to define for a collision is the line of impact. The line of impact is significant, as it lays the groundwork for determining appropriate dynamical models for friction. The line of impact in a friction, or tangential, collision lies through the midpoint of the contact interface

between the tangentially colliding surfaces. This line of motion is comparable to the line of least action designed in mating gear wheels, where the line of least action is aimed to coincide with each point of gear tooth-gear tooth contact through the full rotational motion of the mechanical gear system.

The two possible lines of impact are shown schematically as red, dashed, vectors, in figure 2-24 below. They establish the focal line of where impact dynamics occur, as a line of action, through an interface. They do not correspond to forces or velocities acting on moving or stationary masses. The lines of impact are a dimensionless rendering of the positions along which a coefficient of restitution *e* can be defined, which will describe the velocity, and specifically the momentum behavior of the collision system response after the collision contact and its initial transfer of kinetic energy. The vector direction designates the primary occurrence of action in the collision interface under analysis.

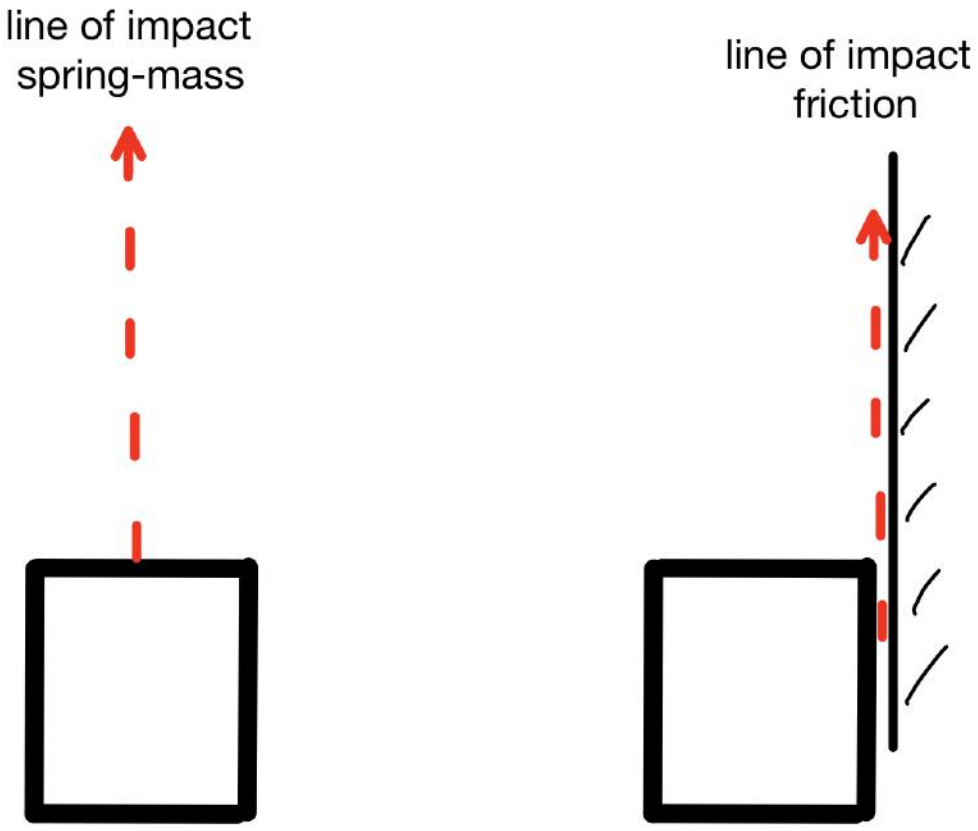


**Figure 2-24 - Depiction of the 2 possible lines of impact, depending on end-stop strategy.**

Figure 2-25 is a structural model for the interfacial region in which the surfactant molecules are represented as flexible chains of rigid spheres. The distance between the spheres is arbitrary but sufficiently large that the disturbance neighborhoods of the individual spheres do not overlap [57].

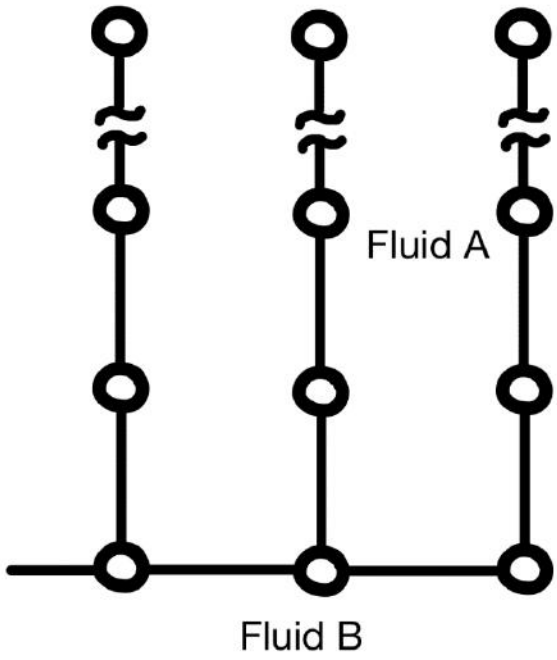


**Figure 2-25 – Interface model.**

The distinct end-stop strategies have unique interfacial interplay, reliant on their particular arrangements. This perspective of the system assembly presents strong dynamical implications. The two particular operational collision interface arrangements are shown in figure 2-26, according to the chosen preliminary design strategies under investigation: spring and friction.

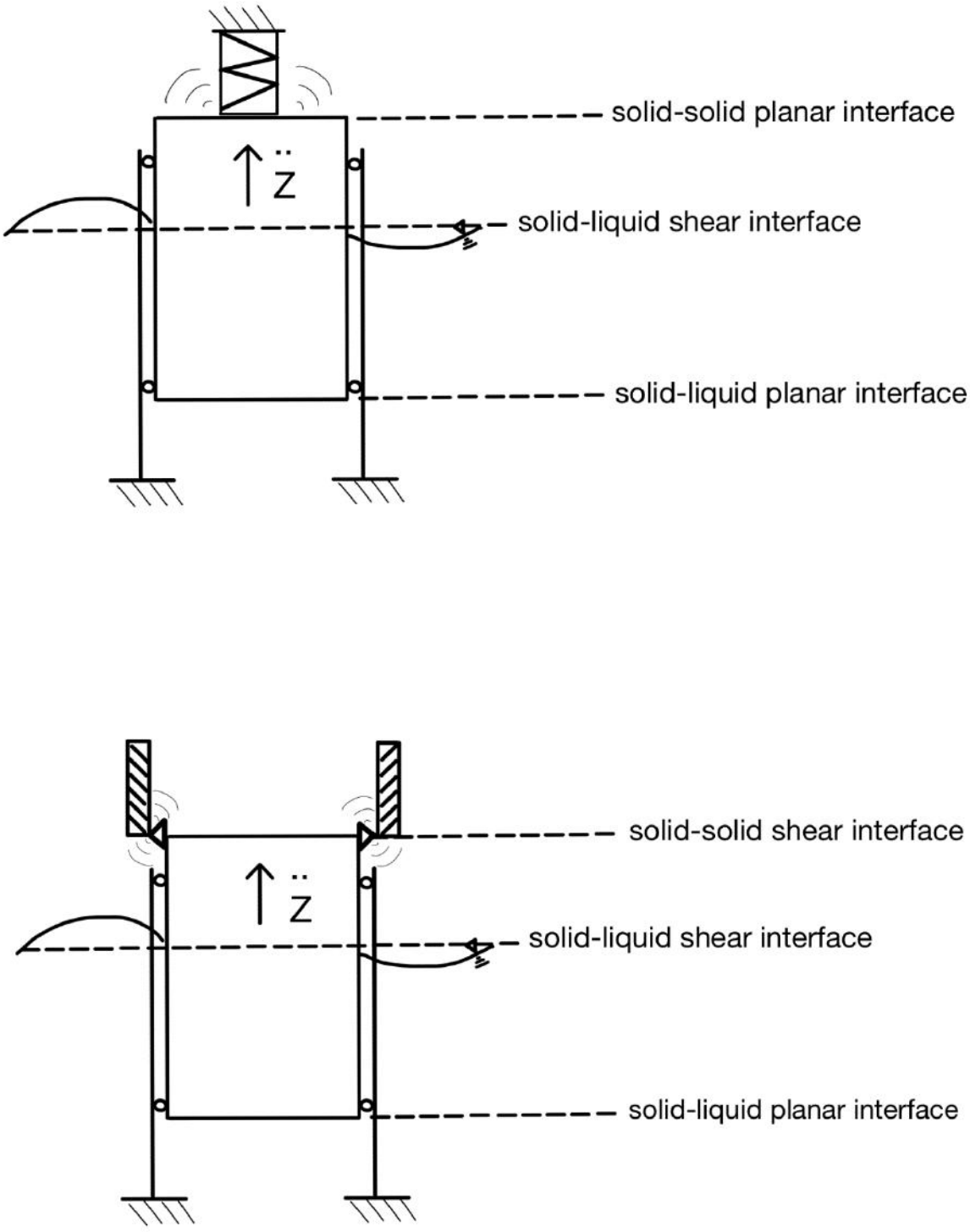


**Figure 2-26 - Representation of the primary, unique interfacial zones occurring in a spring-mass end-stop (top) and a frictional end-stop (bottom), which react upon collision impact (neglecting air).**

In a collision, energy dissipation and exchange of momentum are inevitable [86]. In the preliminary, dynamical models of the following sections, these characteristic phenomena are neglected, and in essence, a worst-case scenario for the end-stop collisions is imagined, in which no energy is lost, or dissipated, from the colliding bodies. This conservative approach allows preliminary tuning of key parameters for subsequent iterative design, and gives a focused and comparative analysis to primary mode detrimental effects. The dynamics analyses that follow are a first sweep approach to establish end-stop design principles and possibilities and are intended to lay a groundwork for future WEC research.

With respect to the design criteria, optimal end-stop parameters for reliability/effectiveness equate to controlled heaving mass displacement under design load for design task 1, and robustness equate to damping for design task 2.

Optimal parameters can be obtained by theoretical analyses of the response of each model described in the following sections. Comparative analysis can reveal and be evaluated through the established design tasks and design criteria from chapter 3.

The schematics of the models presented in this section have certain analogous nomenclature that are shared between them, to give immediate relatability and a cohesive, overall view of how the dampers would function in the end-stop system.

All collisions are modeled as momentarily elastic, hence a spring contact force. This portrayal of the collision physics allows for diverse, but comparable models, even with uncanny differences in magnitude. They are modeled as equations of state rather than complete, to isolate parametric qualities in the collision, namely various frequency behaviors. However, this simplicity in impact dynamics modeling, being fundamentally tied to end-stop design task 1, should not obscure the precedence of the second design task in the damping investigation. For this, the all-too-familiar coefficient of restitution is adopted to parametrically treat the pertinent kinetic energy problem, in the preliminary modeling framework.

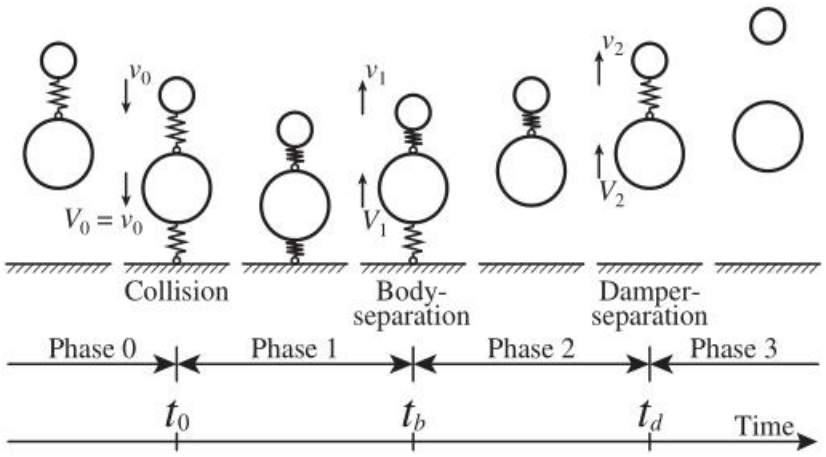


**(a.)**

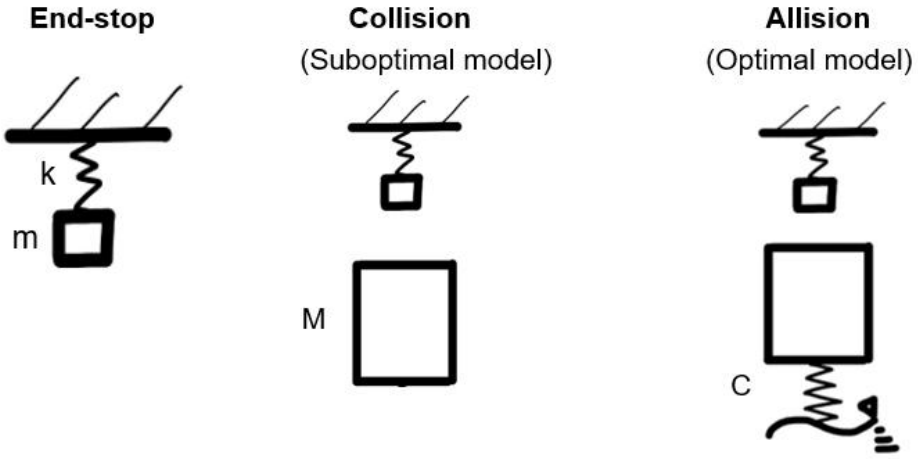


**(b.)**

**Figure 2-27 – (a.) Representative framework strategy used in dynamical modeling, from [50] Notice the contact stiffness induced upon collision impact, and the simplistic, effective spring, mass approach to MEID damper modeling, also note the significance of the velocity vector as a model guideline. (b.) Fundamental parts composing the various dynamical end-stop models to follow, modeled after [50] – from left to right: end-stop composed of a spring-mass unit; end-stop and mass for the suboptimal dynamical model, to interact in "collisions;" end-stop and mass elastically coupled to oscillating free surface for the optimal dynamical model case in "allisions." k = end-stop stiffness, m = end-stop mass, M = heaving mass, C = hydrostatic linear stiffness.**

The [50] framework provides a means to construct certain parametric similarity between microscopic and macroscopic models and spring-mass and frictional models alike, to draw

physical meaning. Thus, it is the predominant system used for dynamical modeling in this paper. [50]

A closer look at the problem: Before conducting a preliminary dynamical analysis of the end-stop collisions, in and of themselves, an analytical model is proposed to describe the unfortunate, expected scenario of a WEC with no end-stop, *slamming*. Figure 2-28 is a schematic representation of a theoretical slamming instance on a cylindrical, oscillating buoy with body-free surface interface contact described with simple spring elements.

To provide a baseline comparison for performance of the analytical, impact damper models, and to aid in design choices, a simplistic model of WEC slamming is theorized.

As mentioned in chapters 1 and 2, a main concern, and motivation, necessitating motion constraint in WECs, is slamming. Slamming occurs when the free surface interface between a vessel and the sea collide with impact. This impact is notable for causing damage in boats, especially high speed, exposed to wave action. Slamming is known to induce extremely high loads on ship structures, being a major design concern. WECs are no different. To assess general end-stop effectiveness against a baseline *worst-case scenario* parameter and to assess potential dynamics induced by an over-excited WEC experiencing slamming, compared with different known modes of slamming amongst marine vessels, a model for this dynamic phenomenon can be established. Presented below is a schematic of a point absorber WEC in one-dimensional heave motion experiencing a slamming impact. $C$ represents the collision contact stiffness between the buoy lower face and the ocean free surface at the exact moment first contact is established, $M$ represents the mass of the buoy, and $g$ represents acceleration due to gravity.

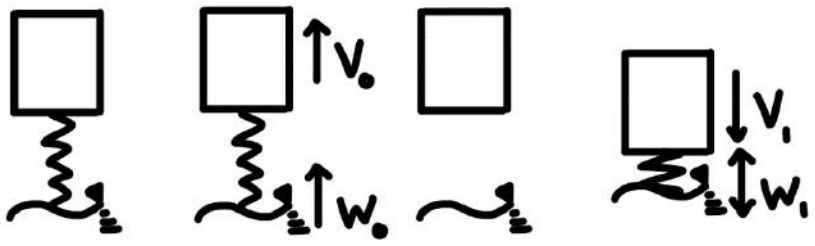


**Figure 2-28 - Schematic representation of the mechanical transitions of one-dimensional motion WEC slamming upon the oscillating free-surface.**

The equation of state derived for this slamming model is

$$\ddot{z}(t) = \begin{bmatrix} -g \\ C/M - g \end{bmatrix} = \begin{bmatrix} -g \\ \Omega^2 - g \end{bmatrix} \tag{2.9}$$

where $\Omega^2 = C/M$

Although the collision instance can be modelled parametrically, the dynamics of a slamming occurrence are highly complex. The stiffness parameter $C$ between the free surface and buoy for any distinct slamming instance is highly variable, and depends strongly on the relative velocities between the bulk body of the water (waves) and the falling buoy. It will also depend on surface area and shape of the buoy bottom face, along with momentary free surface roughness and wave action. If an incident wave is approaching a peak, for instance, the opposing velocity vectors will increase the impact force and kinetic energy involved in the surface collision. This is expressed by a higher $C$ magnitude. It is obvious that every slamming collision is unique; however, with wave hydrodynamics data and WEC geometric parameters and response, it is possible to estimate analytically.

### 2.5.1 Spring-mass collision

Spring-mass dampers are all but commonplace in high fidelity vibration mitigation. Impact scenarios are no different. The spring-mass model is a classical, representative tool to study real world collisions and make choice design.

The equations of motion for the theoretical dampers are derived as linear, second order, ordinary differential equations, based on mass and spring elements.

The models are intended to shed light on the contacting phase in which the WEC is subject to an impact force.

The following describes the one-dimensional motion spring-mass end-stop model. The model contains two masses, $m$ and $M$, that correspond to the end-stop mass and heaving mass, respectively. The heaving mass represents the mass of the buoy plus its intrinsic added mass from the accompanying wave, or the portion of that mass a single end-stop aims to attenuate, depending on the number of end-stops in the system by the following relation:

$$M = (buoy\ mass + added\ mass\ at\ the\ instant\ of\ collision)/\#\ of\ parallel\ endstops \quad (2.10)$$

The masses´ displacements in time are described by $z(t)$ and $Z(t)$, for $m$ and $M$, respectively. $K$ denotes the contact stiffness at the collision interface and $k$ denotes the spring stiffness of the end-stop. The representative collision model is schematically depicted in Figure 2-29. Here, "collision," $t = t_0 = 0$, is defined as the first moment at which the surfaces make contact, when the absolute displacement of the heaving mass and end-stop mass become zero [$z(t_0) = Z(t_0) = 0$]. The velocities of the heaving mass and the end-stop mass at this moment are $V_0$ and $v_0$, respectively [$v(t_0) = V(t_0) = 0$]. In an instant, the heaving body mass disconnects from the end-stop and the displacement becomes zero again [$z(t_1) = Z(t_1) = 0$]. This moment is defined as "body-separation," [$t = t_1$]. After body separation, the collision interface spring is eliminated and the two bodies respond independent of one another. The intervals $t$such that $t \leq t_0$, $t_0 \leq t \leq t_1$, and $t_1 \leq t$ are called "Phase 0,"Phase 1," and "Phase 2," respectively. This and subsequent models are developed based on the MEID model presented in [50].

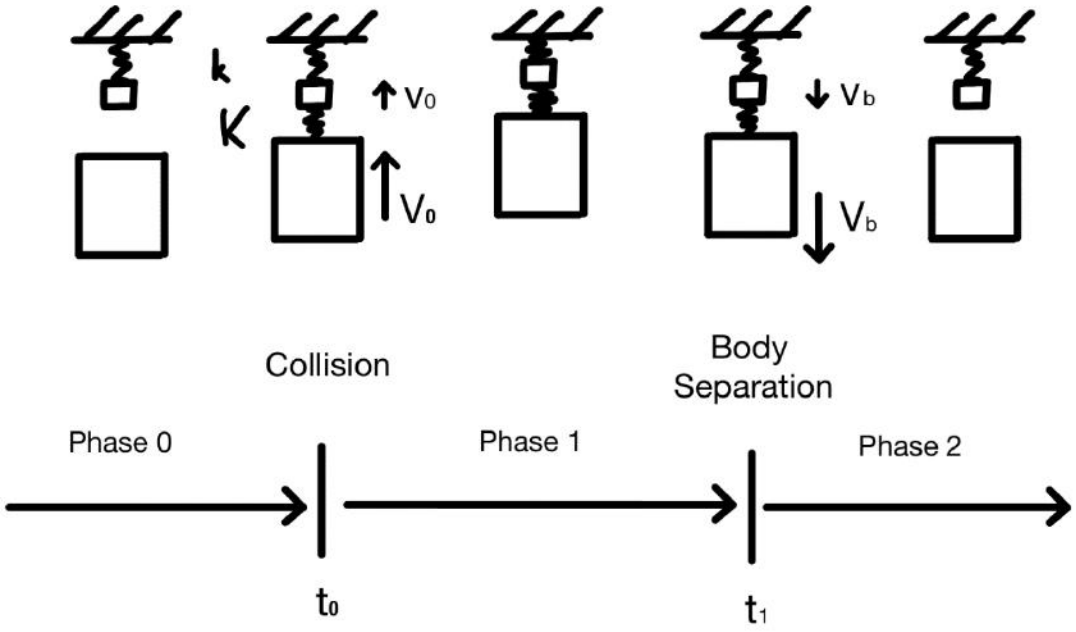


**Figure 2-29 - Schematic representation of the mechanical transitions of one-dimensional motion spring-mass end-stop collisions.**

Derived equations of motion:

$$\ddot{z} = \begin{bmatrix} 0 & -k/(M+m) \\ -(k+K)/m & K/m \end{bmatrix} z(t)$$

$$= \begin{bmatrix} 0 & -k/(M+m) \\ -(\omega^2 + \Omega^2/\rho) & \Omega^2/\rho \end{bmatrix} z(t), \quad z(t) = \begin{bmatrix} z(t) \\ Z(t) \end{bmatrix} \tag{2.11}$$

where $\rho = m/M$, $\omega^2 = k/m$, and $\Omega^2 = K/M$

For a more comprehensive dynamical model of a spring-mass damper WEC end-stop, an allision model is proposed.

In a practical sense, the WEC collision with its end-stop can be more appropriately described as an *allision,* the mariner´s term for a collision between a moving vessel and stationary body at sea. This distinction is important because the dynamics are unique for a floating vessel, even more so when coupled to a wave. With allision, a special case arises; in essence, at first contact due to both linear and nonlinear hydrodynamic effects, a percentage of the entire ocean´s bulk body (inertial, viscous, and everything in between) as well as the individual, incident wave is resisting the stop.

To formulate the end-stop allision model, the hydrostatic and hydrodynamic forces acting on the buoy are represented as a spring-mass. This requires a number of assumptions, many of which are already embedded in the original, hydrodynamics model used to establish the preliminary design load. Again, linear hydrodynamic theory is assumed. Furthermore, the acting forces on the rigid bodies in the dynamical system are reduced to linear, spring-mass interactions as well. Within the scale of time of the acting allision impact, the dynamics are represented schematically by figure 2-30.

Essentially, allision implies this hydrostatic coupling of a vessel to the sea bulk mass by the implicit fact that the vessel mass rests at equilibrium between the opposing forces of hydrostatic buoyancy (upthrust) and deterministic gravitational potential, displacing a mass of water.

Figure 2-30 shows the one-dimensional motion spring-mass end-stop allision model. The model contains the same two masses, $m$ and $M$, that correspond to the end-stop mass and the appropriate (from equation 5.5). Their displacements in time are described by $z(t)$ and $Z(t)$, respectively. $K$ denotes the contact stiffness at the collision interface and $k$ denotes the spring stiffness of the end-stop, and C denotes the linear hydrostatic spring coefficient. The representative allision phenomenon of the model is schematically depicted in Figure 5-4. Here, "allision," $t = t_0 = 0$, is defined as the first moment at which the solid body faces allide, when the absolute displacement of the heaving mass and end-stop mass become zero $[z(t_0) = Z(t_0) = 0]$. The velocities of the heaving mass and the end-stop mass at this moment are $V_0$ and $v_0$, respectively $[v(t_0) = V(t_0) = 0]$. Thereafter. the heaving body mass immediately separates from the end-stop and the displacement becomes zero again $[z(t_1) = Z(t_1) = 0]$. This moment is defined as "body-separation," $[t = t_b]$. After body separation, the allision interface spring is eliminated and the two

bodies respond independent of one another. The intervals $t$ such that $t \leq t_0$, $t_0 \leq t \leq t_1$, and $t_1 \leq t$ are called "Phase 0," Phase 1," and "Phase 2," respectively.

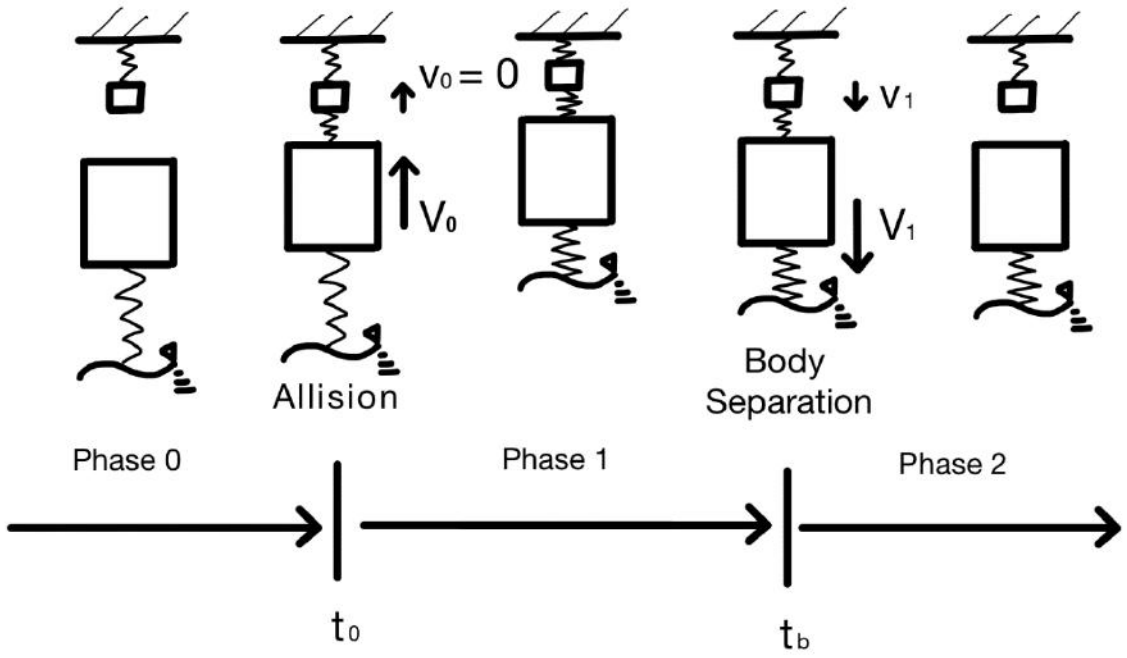


**Figure 2-30 - Schematic representation of the mechanical transitions of one-dimensional motion heaving WEC and spring-mass end-stop allisions.**

$$\ddot{z} = \begin{bmatrix} -(k+K)/M & (C/M) - K/(M+m) \\ -(k+K)/(M+m) & K/(M+m) \end{bmatrix} z(t)$$

$$= \begin{bmatrix} -\Gamma_{\text{all}}{}^2 & \Omega_{\text{all}}{}^2 - \omega_{\text{all}}{}^2 \\ k - \omega_{\text{all}}{}^2 & \omega_{\text{all}}{}^2 \end{bmatrix} z(t), \quad z(t) = \begin{bmatrix} z(t) \\ Z(t) \end{bmatrix} \tag{2.12}$$

where $\rho = m/M$, $\omega_{\text{all}}{}^2 = K/(M+m)$, $\Omega_{\text{all}}{}^2 = C/M$, $\Gamma_{\text{all}}{}^2 = (\text{k} + \text{K})/\text{M}$

$\rho$ is the mass ratio.

$\omega_{all}^2$ is the allision frequency response of the adjoined heaving mass and end-stop mass, with respect to the end-stop intrinsic spring stiffness.

$\Omega_{all}$ is the allision frequency response of the heaving mass to the water.

$\Gamma_{all}$ is the frequency response imparted on the heaving mass from the combined end-stop stiffness and the solid allision interface contact stiffness.

### 2.5.2 Friction collision

The following section presents novel, analytical models to describe the functionality of proposed impact dampers

The coefficient of friction, like the coefficient of restitution, is a dimensionless property attributed to an interaction between a pair of surfaces. The coefficient of restitution relates the interaction with respect to relative movement orthogonal to the surface pair interface. The coefficient of friction relates the interaction with respect to relative movement (or tendency towards movement) tangential to the surface pair interface but is derivative of normal force magnitude in the orthogonal direction.

Since both parameters are properties of a pair of objects, to model a ‘friction surface impact’ consider the following:

Impact along a friction surface, in a strictly theoretical sense, can be defined from the system kinematics, as occurring along the tangential, interface plane. Defining *the line of impact* in this way means it is parallel to the relative vector of motion between the two faces, and since we are looking at nonviscous friction only, the resisting friction force can be modeled as a simple linear spring component, albeit containing the AC kinetic friction coefficient to normal force ratio within.

The basis of the virtual work model for friction is based on the principle of least action. The following friction collision model was derived.
In the virtual work model, the line of impact is considered the line of least action, synonymous with the line of pitch for an ideal gear assembly. The line of impact is an important consideration, defining a friction "collision." Coefficient of restitution, $e < 0$ and is modeled as a disintegrating mass into the larger heaving mass.

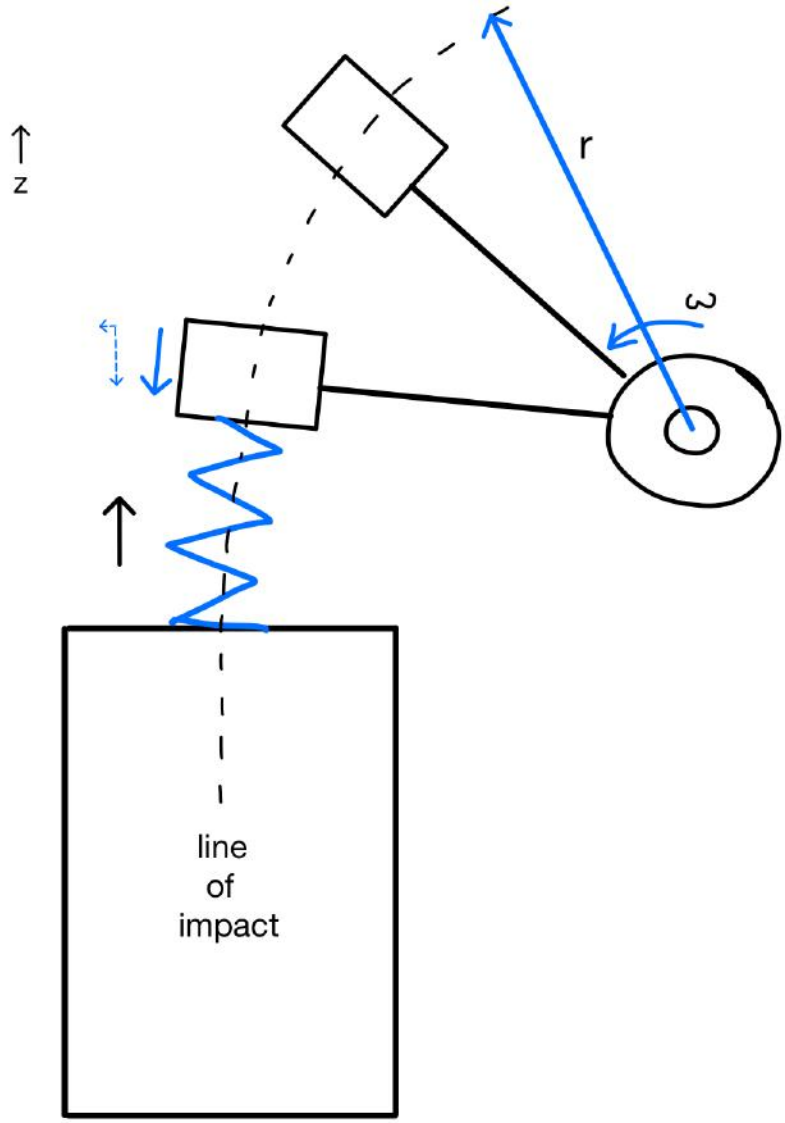


**Figure 2-31 - Conceptual schematic of the "virtual work," friction, collision interaction between a heaving mass and the *virtual*, tangential end-stop representation; shown: virtual collision line of impact (in reality it would be the midline between the tangentially colliding surfaces); z axis of heave motion; $\omega$ virtual, rotational velocity of the consecutive micro-asperities of the tangential, end-stop surface; $r$ virtual radius of micro-asperity from an imaginary gear of wheel upon which it rotates**

This model, in effect, represents friction as a deterministic force in the equation as opposed to a force of constraint, hence the term "virtual." According to the principle of least action, the work done by the real surface upon impact, can be equated to this rotating system.

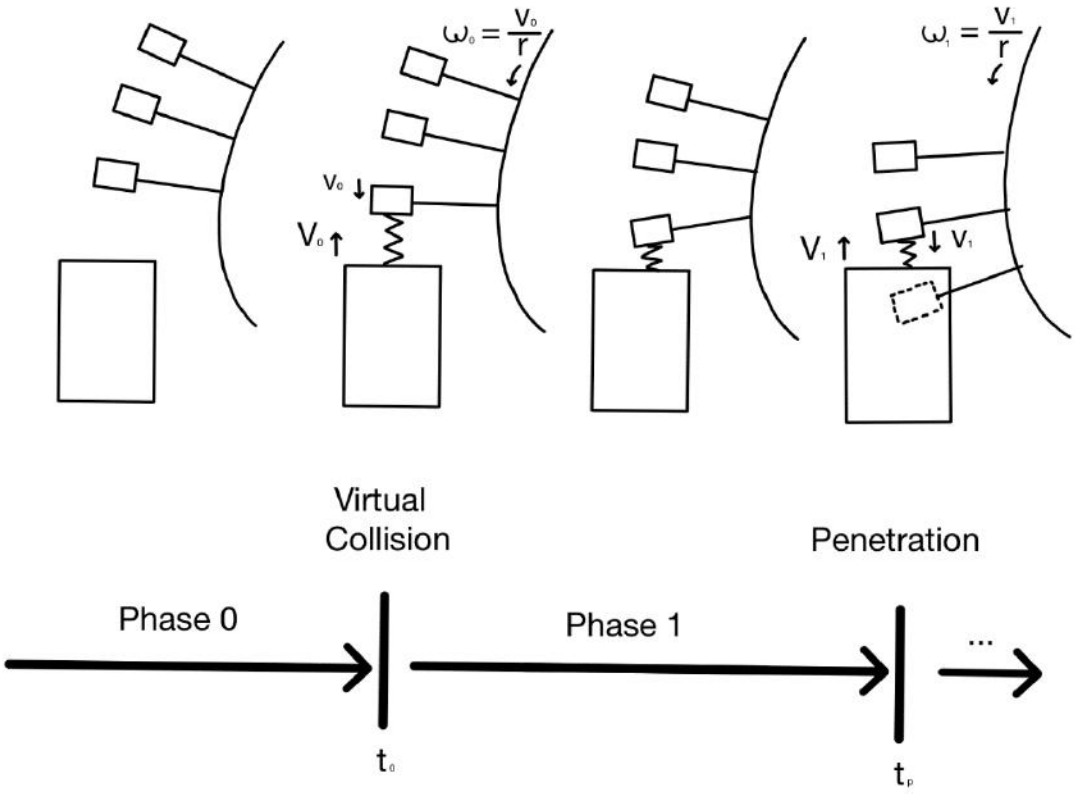


**Figure 2-32 - Schematic representation of the mechanical transitions of "virtual work" heaving mass and friction end-stop micro-collisions. Because the collision coefficient of restitution is negative$e < 0$, the colliding asperity mass is imagined to be absorbed by the incoming buoy mass at $t_p$, some moment of instantaneous micro-asperity penetration.**

Derived equations of motion:

$$\ddot{z} = \begin{bmatrix} -km/M(M-m) & -k/m \\ -2k/(M+m) & -\dfrac{k}{m} \end{bmatrix} z(t)$$

$$= \begin{bmatrix} -k\rho/(M-m) & -\omega^2 \\ -2k/(M+m) & -\omega^2 \end{bmatrix} z(t), \quad z(t) = \begin{bmatrix} z(t) \\ Z(t) \end{bmatrix} \tag{2.13}$$

where $\rho = m/M$, $\omega^2 = k/m$, and $\Omega^2 = K/M$

This virtual work model for anisotropic friction collisions may also elegantly capture stick-slip friction dynamics at certain scales depending on the collision frequencies of the virtually driven rotating virtual end-stop apparatus.

Recent studies have investigated the locomotion of snakes and legless reptiles, as an anisotropic friction phenomenon [43].

The following models are formulated on this basis:

1. The anisotropic friction damping strategy is based on the frictional, propulsive force in snake locomotion.
2. Models two-dimensional micro-collision of the heaving mass with the anisotropic friction surface
3. Considered internal and external forces pressing the heaving mass to the friction surface and resisting any tendency to move through it with a large stiffness

$\theta$ is the pitch angle the scale asperity is angled upwards

k is the normal stiffness of the scale asperity

$\Delta$ is the collision stiffness between the heaving mass and the scale

The case of the very last scale inducing a change of sign on the velocity of the heaving mass is called *body separation*; the negative coefficient of restitution case is called *penetration* in the models.

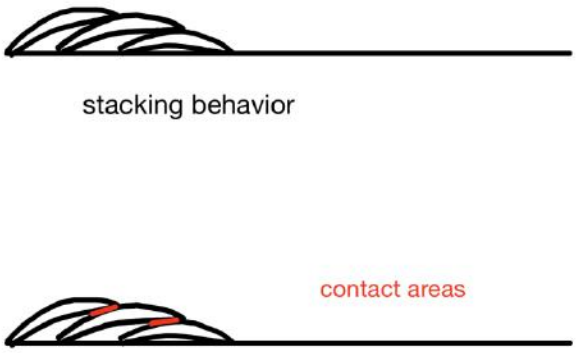


**Figure 2-33 - Schematic representation of the mechanical snake scale stacking behavior**

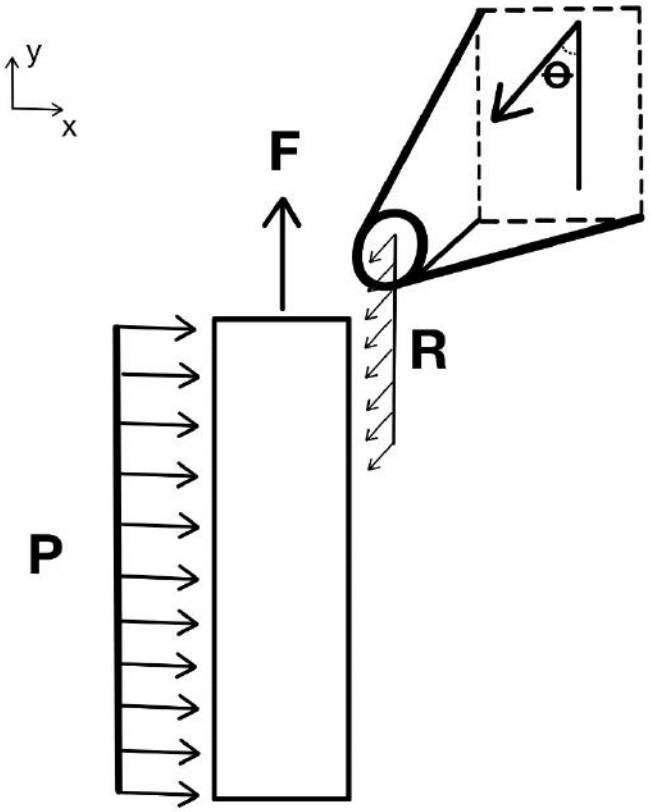


**Figure 2-34 - Force diagram of anisotropic friction surface response showing pitch angle $\theta$; normal force of the collection of individual 'scale' asperities *R*;the dominant forces between-a counteracting pressure from the particular, dominating forces of some internal buoy pressure; the stiffness of its outer shell, any horizontal component of the incident wave, and the normal force on the opposite constraint plane cumulatively designated *P*; the total, heaving force of the buoy-wave couple *F*.**

The behavior of the forces of constraint in this model are clearly presented in Figure 2-35.

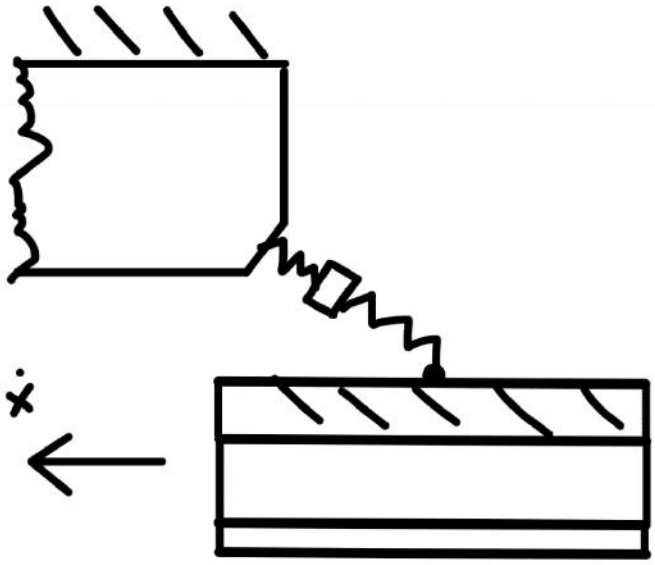


**Figure 2-35 - Abstract, representative schematic of an angled micro-asperity at the collision interface boundary between two distinct bodies of opposing, relative velocity $\dot{x}$.**

Scales, denticles, bristles, spines, or any other tangential, *friction*, obstruction, to be implemented as an end-stop component, are modeled as simple, spring-mass systems with some designated pitch angle, $\theta$. This simplistic representation of an incremental portion of a tangential, microscopic, collision interface gives some lucidity to the complex, multi-dimensional, surface-surface response of the system.

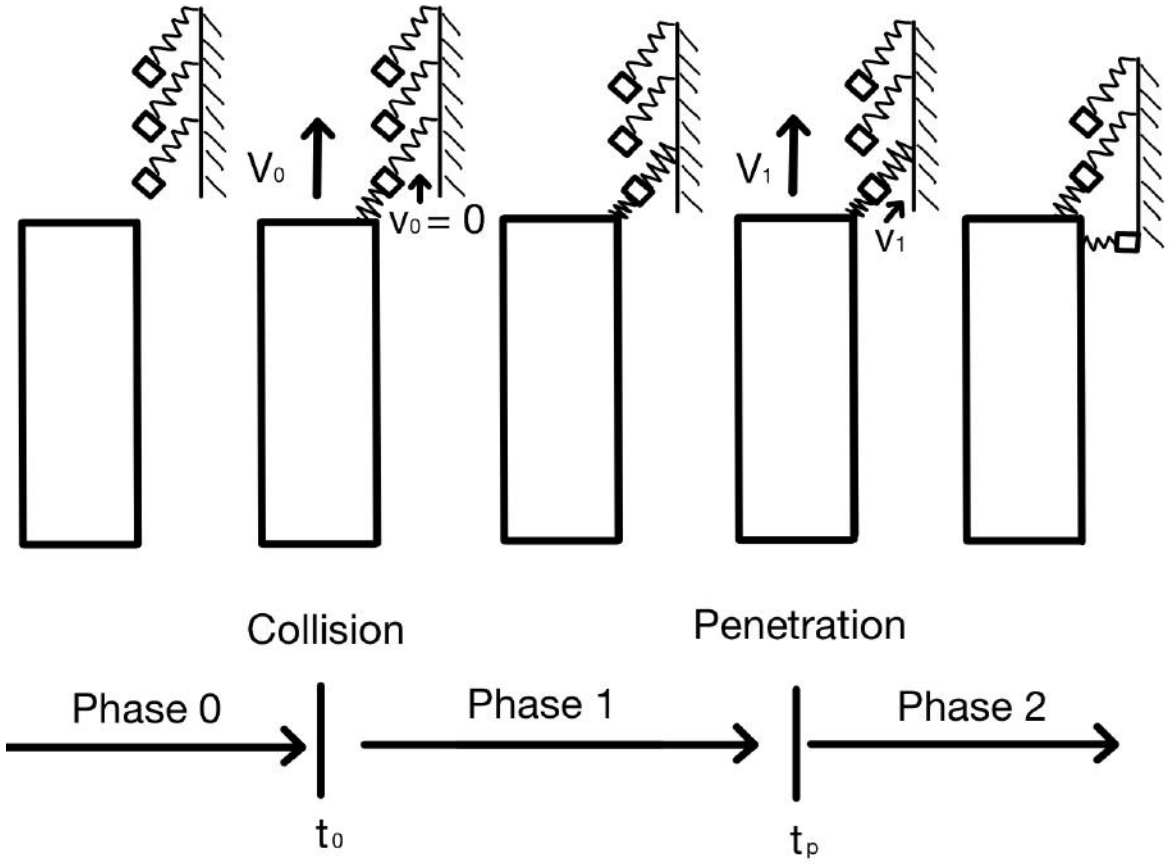


**Figure 2-36 - True orientation, macroscopic, depiction of the anisotropic friction model representing the mechanical transitions of one-dimensional motion, heaving WEC -anisotropic friction end-stop collisions.**

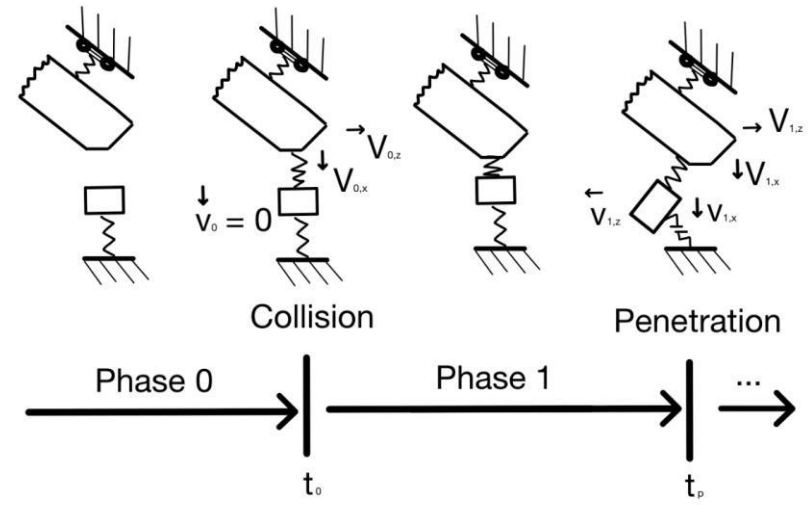


(a.)

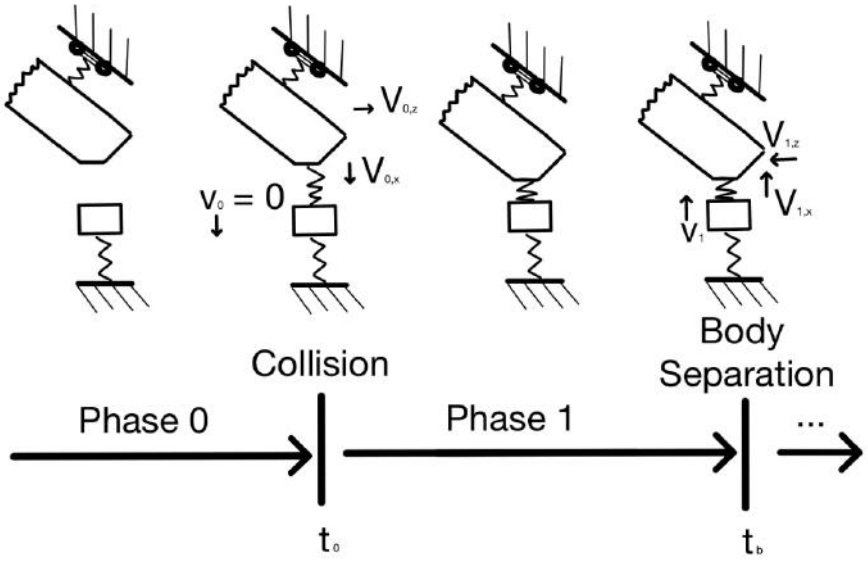


(b.)

**Figure 2-37 – (a.) & (b.) Adjusted reference frame, microscopic, depiction of the anisotropic friction models representing the mechanical transitions of one-dimensional motion, heaving WEC-anisotropic friction end-stop collisions. (a.) represents a negative coefficient of restitution $e < 0$, where at $t_p$, both collision bodies assume the same momentum vector. (b.) represents the moment along some friction surface collision when the heaving body is stopped or deflected by the final surface micro-asperity with which it will make contact during a full interval of micro-collisions.**

Derived equations of motion:

$$\ddot{x} = \begin{bmatrix} 0 & -k/(M+m) \\ -(k+\Delta)/m & \Delta - \mathrm{K}\sin\theta/m \end{bmatrix} x(t)$$

$$= \begin{bmatrix} 0 & -k/(M+m) \\ -\omega^2 + (\Omega^2/\rho) & \Omega^2 - (\xi^2/\rho)\sin\theta \end{bmatrix} z(t),\ x(t) = \begin{bmatrix} x(t) \\ X(t) \end{bmatrix} \qquad (2.14)$$

$$\ddot{z} = \begin{bmatrix} 0 & -k\,tan\theta/(M+m) \\ 0 & \frac{\Delta}{m} tan\theta + K\,cos\theta/M \end{bmatrix} z(t)$$

$$= \begin{bmatrix} -k\rho/(M-m) & -\omega^2 \\ -2k/(M+m) & -\omega^2 \end{bmatrix} z(t),\ \ z(t) = \begin{bmatrix} z(t) \\ Z(t) \end{bmatrix} \qquad (2.15)$$

where $\rho = m/M$, $\omega^2 = k/m$,$\Omega^2 = \Delta/\mathrm{M}$, and $\xi^2 = K/M$

To face the challenge of an impractically large normal force in the basic friction end-stop model, a passive amplification strategy is presented, based on layered and angled tangential, contact surfaces.

A comprehensive model of the interleaved phone book enigma is studied. Although this model presents robust, friction enhancement properties via paper sheet layering-induced normal force amplification, alterations must be made to attain the necessary functionality for a practical end-stop. In general, three main challenges arise:

1. Adapt: static → kinetic coefficient of friction
2. Convert: tensile → compressive force of constraint
3. Repeatability

i.e. the need for static constraint kinetic allowance to attenuate the heaving mass with longer action (for task 2 effectiveness); the preferable switch from tensile to direct compression loading of the component sheets (elected in the premature determination - Table C-2); and the crucial ability to effectively perform repeated constraint over the lifetime of the WEC.

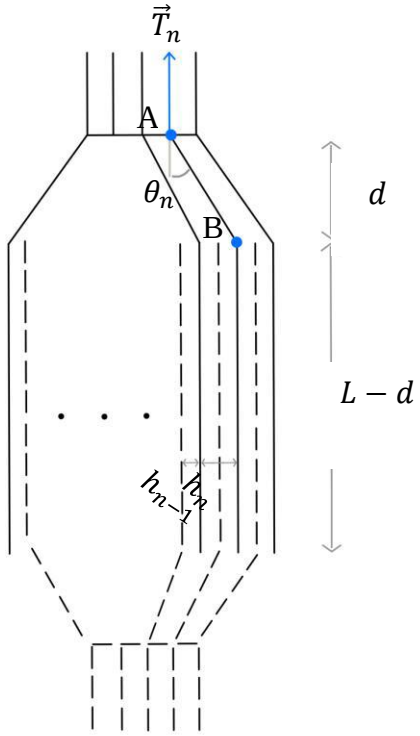


**Figure 2-38 - A schematic representation of the "interleaved phonebook" assembly detailed by [53] through experimentation.**

[53] formulates a dimensional, differential model of the enigma's physics, where they discover a single, dimensionless, amplification parameter describing the tractive resistance force to applied tension at the book ends.

The challenges of  layering the supplementary local normal force exerted by each consecutively external sheet upon internal sheets located relatively nearer to the assembly center.

$$H_n T_n = T_n \tan \theta_n \tag{2.16}$$

Following the AC laws, the change in traction at the onset of sliding is observed as:

$$T_n - T_{n+1} = 4\mu_k H_n T_n \tag{2.17}$$

Where:

$T_n$ is the traction load at the nth sheet, shown in blue in figure 5-8

$T_{n+1}$ is the traction force at the subsequent page

$H_n T_n = T_n \tan \theta_n$ is the supplementary local normal force exerted by each consecutively external sheet upon internal sheets located relatively nearer to the assembly center

$\mu_k$ is the kinetic coefficient of friction

4 comes from the 2 separate books and 2 separate sides to each page

The [53] model is formulated as follows:

$$T'(z) + 2\alpha z\, T(z) = 0 \qquad (2.18)$$

Where:

$$z = n/M$$

Their dimensionless amplification parameter can be described as follows:

$$\alpha = 2\mu_k \epsilon M^2/d \qquad (2.19)$$

Where:

$M$ is the number of total sheets in the assembly

$\epsilon$ is the elasticity of a sheet

$d$ is the modeled distance between the start of the layered portion of the sheets and the kinematic end confinement (book spine)

And $M \gg 1$

By introducing the boundary condition $T(1) = T^*$, [53] obtain, through integration, the local traction force $T(z) = T^* \exp[\alpha(1 - z^2)]$ and the total traction force in the self-similar form:

$$\frac{\mathcal{T}}{2MT^*} = \sqrt{\frac{\pi}{4\alpha}}\exp(\alpha)\,\mathrm{erf}(\sqrt{\alpha}) \tag{2.20}$$

In their experimental model, [53] note that $T^*$, although comparable to the weight of a butterfly, is a critical boundary condition, being amplified by orders of magnitude over successive sheets in the interleaved assembly. This condition is consequent of the elasticity of a single paper sheet. They explain, "The outer sheets have a tendency to be flat and resist slightly the bowing induced in the contact region, thus creating a small normal force resulting in a small friction force." [53]

These simple geometric and mechanical formulations of friction amplification through sheet stacking by [53] provide a parametric basis to begin strategic treatment of the problem of passive controllability for a friction end-stop normal force. Eventually, this could be tuned to real seas.

In principle, the same technique can be used to amplify the normal force of layered, friction end-stop surfaces, although the fiction coefficient will be the decidedly smaller in magnitude, kinetic variant. There are however, major differences in practical, system application that present unique challenges for this potential, friction end-stop design feature. These are outlined in table 2-7.

**Table 2-7 - Signature application differences between the [53] interleaved phonebook assemblies and a potential stacked, friction sheet, tangential end-stop.**

| | Interleaved phonebooks | End-stop |
|---|---|---|
| 1 | Static friction *lock* | Kinetic sliding friction |
| 2 | Tensile force of constraint | Preferably compressive force of constraint |
| 3 | One-time use | Repeatability |
| 4 | *Common* materials and composition | Optimized materials and configuration |

Combining this model with the anisotropies of the biomimetic design presented in the previous section, certain challenges may be alleviated. Figures 2-39 and 2-40 showcase the sheet layering applied to end-stop wth micro and nanoscopic, frictional anisotopy incorporated (asperity size exagerrated in depictions). The arrow designates the momentous, heaving mass velocity being transferred to the frictional forces of constraint, between sheets.

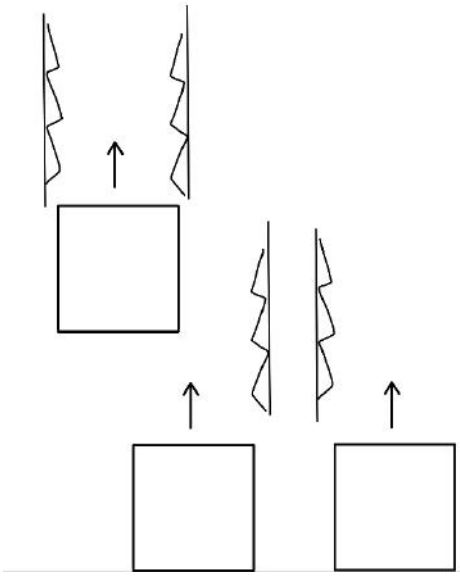

**Figure 2-39 - Representation of proposed, friction sheets equipped with anisotropic friction micro asperities, a combination of this model and that of the anisotropic (snakeskin) friction model.**

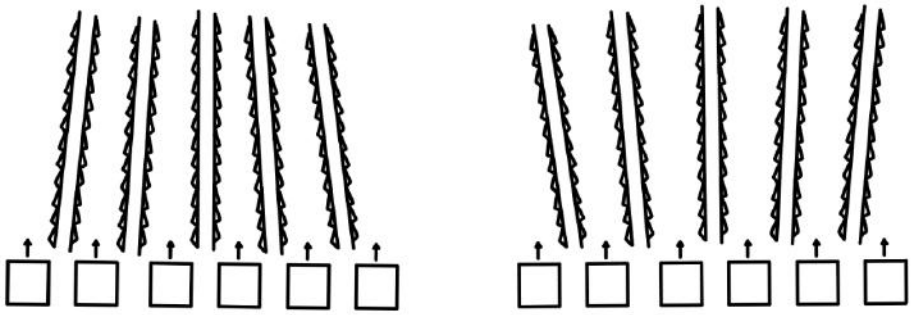

**Figure 2-40 - – Schematic representation of the 2-dimensional modes of layering configuration and constraint action possibilities between friction sheets equipped with anisotropic, micro-asperities, with incoming potential motion occurrences between each layer.**

The old adage beckons to use the right tool for the task. In reality, the end-stop will be damping water in motion. We do not dampen moving water with springs, we dampen it with paddles. Although, the dynamics in human-paddle manipulation is complex (and both viscous and inertial forces are involved) the analogy allures practical intuition to the true design task at hand. The following allision formulations of the various friction solution models describe it mathematically.

A negative coefficient of restitution, $e < 0$, collision is represented in Figure 2-41. Now, coupling the heaving mass to the hydrostatic stiffness term, $C$, an allision formulation can be imagined. This addition to the collision model is depicted in the figure below, and subsequent models can be attained to present the collision → allision alterations for the corresponding models presented in the previous sections. Schematics of these models can be found in the appendix.

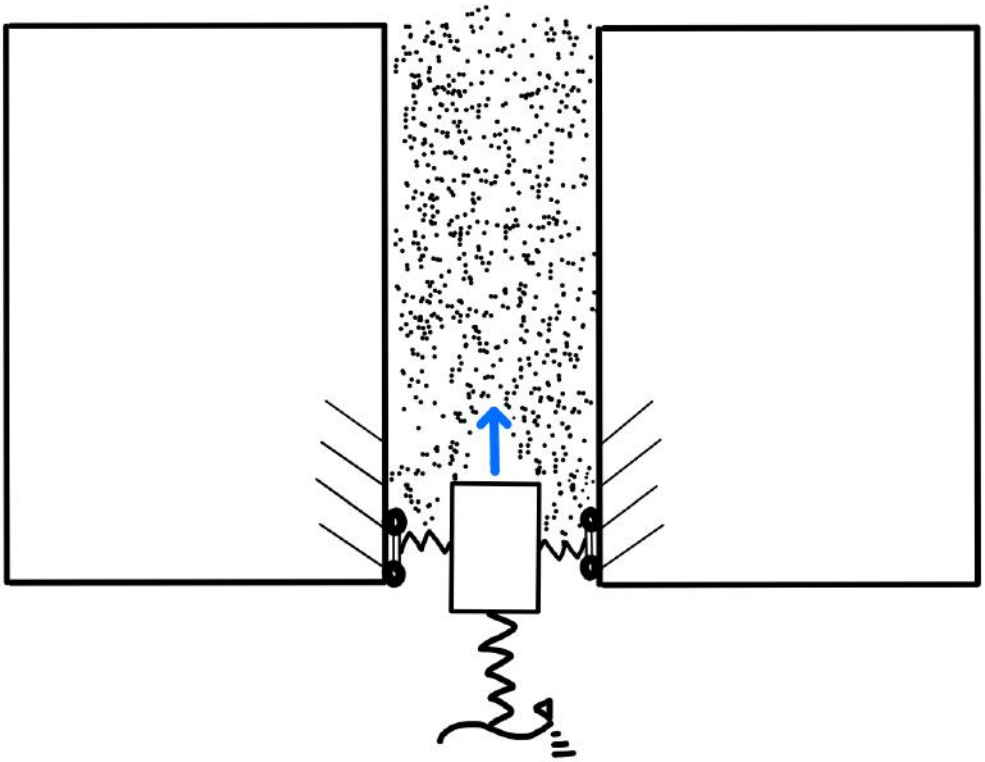

**Figure 2-41 - Heaving mass coupled to hydrostatic spring force, as it engages in collision with a mass of particles immediately to its front, relative velocity vector represented by a blue arrow. This interaction has an $e < 0$ (negative coefficient of restitution), and shows distinct dynamics to the previous representative system, as it now contains the representative spring coupling, of a simplistic, linearized, hydrostatic force model maintaining it neutrally buoyant, during dynamic incident wave action.**

As the heaving mass enters and *allides* with the mist, the hydrostatic spring may be compressed and resist this impediment on its motion. The result is complex dynamics, determined by the

incident ocean wave properties of period $\tau$, and amplitude $h$. The consecutive models, express this additional term, as the undetermined variable $C$ for hydrostatic behavior upon a cylindrical point absorber based upon simplistic, linear hydrodynamic theory. Since the perimeter, or circumference, of the buoy remains constant with the simple, cylinder shape, only the water height relative to the sunken draft is variable, the spring can be considered, this linear term. This hydrostatic $C$ spring only couples to the system during an $e < 0$ allision, if the collision is sufficiently stiff in relation to the rise speed (related to the wave $\tau$ and amplitude $h$) of the corralling water wave mass around the buoy.

The consecutive models represent the formerly presented, friction systems with this additional hydrostatic $C$ term incorporated, to investigate the difference in response for this crucial factor, with respect to tangential allision, negative coefficient of restitution $e < 0$ end-stop solutions.

**The "virtual work" formulation of end-stop allision, and select models are portrayed in Appendix B-4**

# Chapter 3

# 3. Results

## 3.1 Hydrodynamics – end-stop design load

The results of the numerical simulation show strong peak forces within the end-stop application zone. The implementation of latching control provides regular displacement and velocity amplification with arbitrary peak excitements, seen in figures 3-1 and 3-2, respectively.

A conservative force measurement is desired for the following reasons:

1. Model ignores forceful viscous effects, which will appear in impact conditions.

2. Model neglects periodic tidal free surface level changes.

3. There is designer motivation to investigate more robust end-stop functionality to substitute nonoperational mode protection tactics and fail-safes.

Figure 3-1 and 3-2 show the maximum WEC forces in terms of significant wave heights and peak periods, respectively.

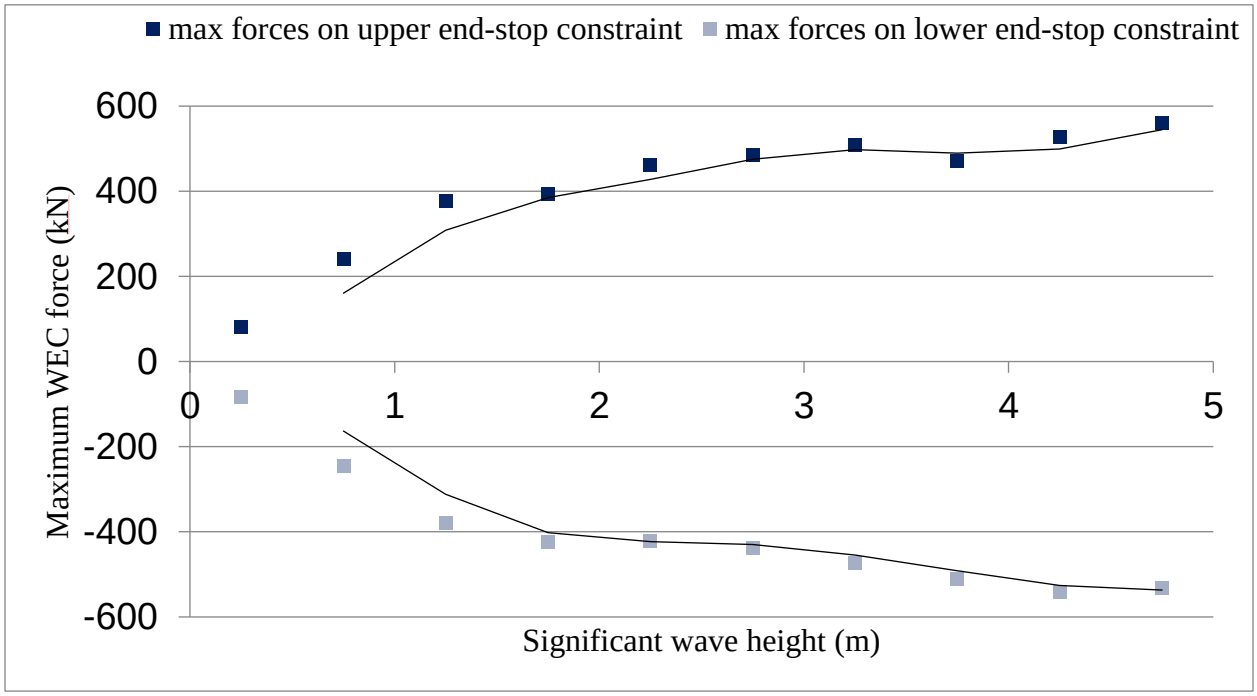


**Figure 3-1 - Maximum forces at end-stop application zone as a function of significant wave height for the COPPE nearshore point absorber WEC numerical model; *x-axis* – significant wave height in meters, *y-axis* – instantaneous force in kilonewtons.**

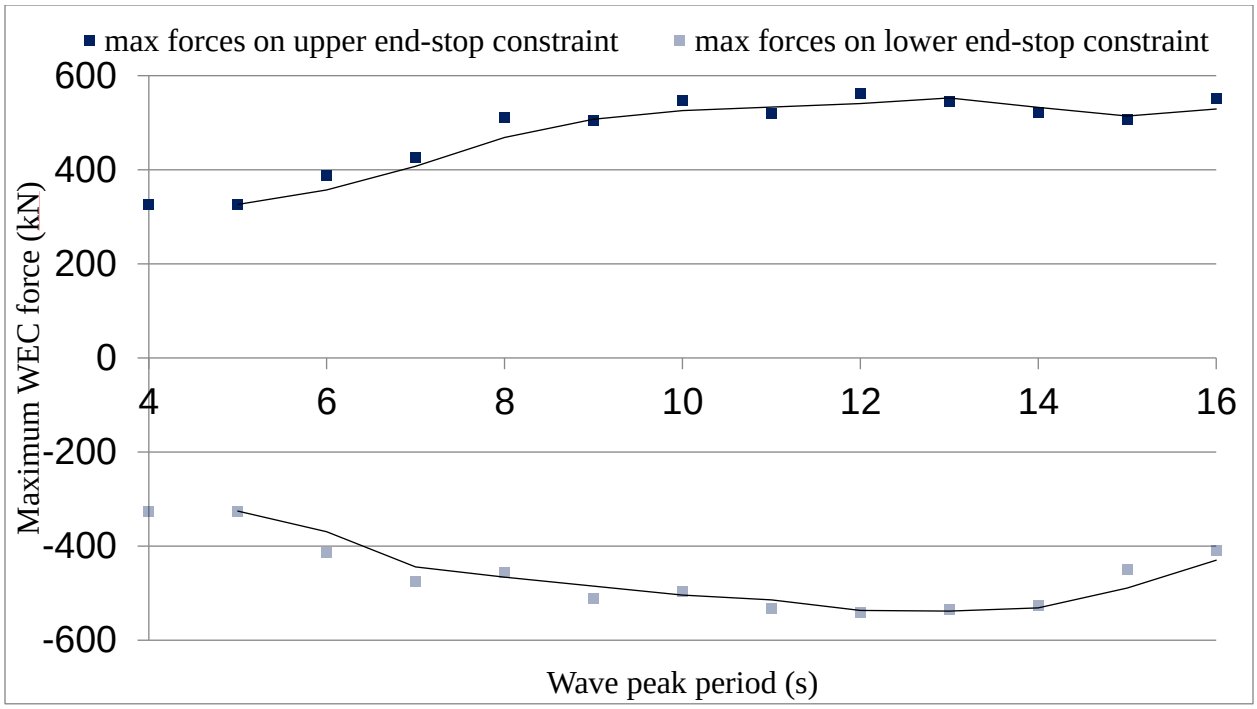


**Figure 3-2 - Maximum forces at end-stop application zone as a function of peak period for the COPPE nearshore FPA WEC numerical model; *x-axis* – wave peak period in seconds, *y-axis* – instantaneous force in kilonewtons.**

For a first pass, conservative design parameter, a magnitude of 600kN is chosen for the end-stop design load. As seen in the figures above, this threshold value can be taken for both upper and lower end-stop design loads, plotted in blue and red, respectively.

Figures 3-3 and 3-4 show the typical behavior for the statistically typical 12 second peak period, but with a large, but infrequent significant wave height of 4.25 meters. The displacement, in 3-3, is seen to pass the designated 3-meter actuation limit at around 450 seconds.

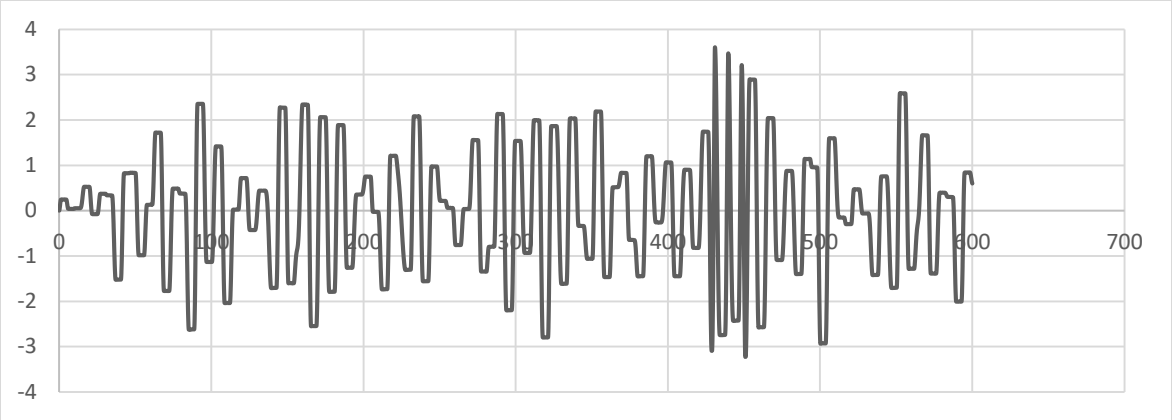


**Figure 3-3 - Time domain displacement of the COPPE numerical model with latching; *x-axis* - runtime in seconds, *y-axis* – buoy displacement in meters.**

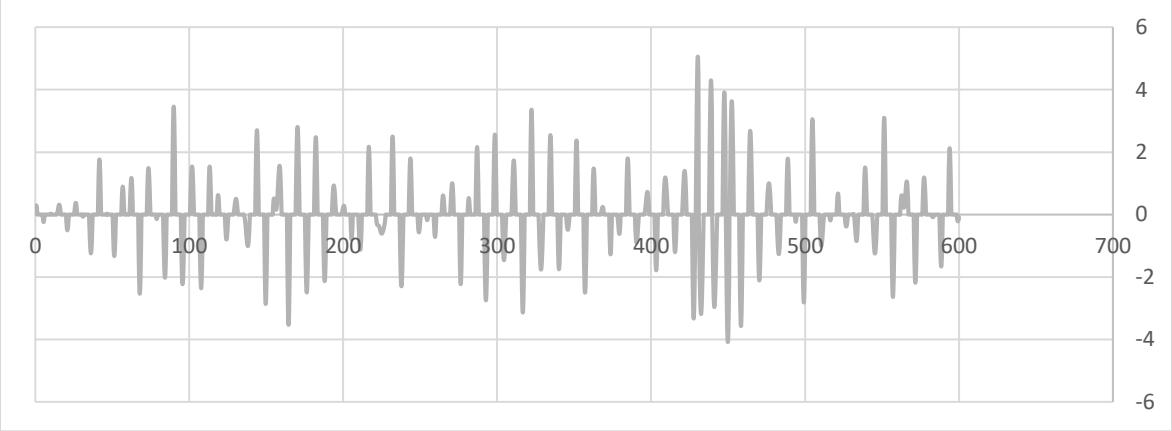


**Figure 3-4 - Velocity behavior of the COPPE numerical model with latching; x-axis - runtime in seconds, y-axis – buoy velocity in meters per second.**

## 3.2 Helical compression spring mechanics of materials and theoretical background

Helical compression springs are ubiquitous in mechanical systems. They operate according to the basic Hooke's Law formulation presented at the beginning of the last section and have a number of practical applications in mechanical engineering design. Rao 2010 and Budynas 2011 present comprehensive mechanical spring design, analytical methods [36][38], which are paralleled and slightly modified to fit end-stop spring design needs. The first design task for motion constraint

reliability, will be to discover the possible failure modes and identify the limiting factor. Helical springs are a mature technology and the primary failure mode is known to be shear stress under applied load. When an axial load is applied to a spring, the spring wire experiences torsional shear stress and transverse shear stress, as well as an additional stress due to curvature [36].

The total shear stress of a helical compression spring under axial load is described by the following equation:

$$\tau = \frac{8FCK_W}{\pi d^2} \tag{3.1}$$

where:

$\tau$ is the induced shear stress

$F$ is the applied load

$C$ is the spring index, or coil to wire diameter ratio

$K_W$ is the Wahl curvature factor

d is the wire diameter

and

$$C = \frac{D}{d} \tag{3.2}$$

where:

D is the helical spring coil diameter

$$K_W = \frac{4C - 1}{4C - 4} + \frac{0.615}{C} \tag{3.3}$$

The total shear stress$\tau$from equation 4.2 relies on a number of variables, the most significant variable being spring wire diameter $d$, of which $\tau$ has a cubic relation.

Commonly employed diameter ratio, $C$ ranges from $C = 4$ to $C = 10$ [36].

To better understand the stresses in a helical spring

From [38], figure 3-5 shows a round-wire helical compression spring loaded by the axial force F. D is the mean coil diameter and d as the wire diameter. Now imagine that the spring is cut at some point (b) in the figure, a portion of it removed, and the effect of the removed portion replaced by the net internal reactions. Then, as shown in the figure, from equilibrium the cut portion would contain a direct shear force F and a torsion T = FD/2

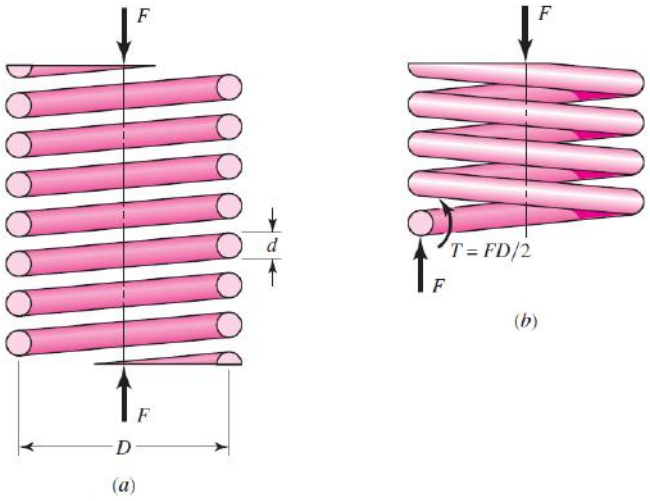


**Figure 3-5 - (a) Axially loaded helical spring; (b) free-body diagram showing that the wire is subjected to a direct shear and a torsional shear, from [38]**

The curvature of the wire will increase the stress on the inside of the spring, with a slight decrease on the outside. This curvature stress is primarily important in fatigue because the loads are lower and there is no opportunity for localized yielding. This is a concern for an end-stop under variable loading (criteria 1 and 2, lifetime reliability and robustness). However, for the first preliminary

design phase, motion constraint potential (design task 1) is the focus, and a static loading condition will provide model results that can be subsequently iterated and analyzed. An interesting caveat in the analytical method pointed out by [38] is the uncertainty and conservativeness in the need to include this additional stress parameter in static load design. The application of the end-stop is subject to a unique loading condition (as will be seen in the dynamical models), and it is determinably *not* static, but the tolerances and factor of safety embedded in the literature's design protocol will inform the valuable insight a simple numerical model can provide, to understand the nature of the analytical estimation, and hone in on true parameter magnitudes. [38] explains that for static loading, these stresses can normally be neglected because of strain-strengthening with the first application of load. Unfortunately, it is necessary to find the curvature factor indirectly because the published equations also include the effect of the direct shear stress. The Wahl curvature factor is just one of the accepted such values.

The deflection-force relations are quite easily obtained by using Castigliano's theorem [38]. From [38], the total strain energy for a helical spring is composed of a torsional component and a shear component. Thus, the strain energy is:

$$U = \frac{T^2 l}{2GJ} + \frac{F^2 l}{2AG} \tag{3.4}$$

Substituting T = FD/2, l = πDN, J = πd4/32, and A = πd2/4 gives:

$$U = \frac{4F^2 D^3 i}{d^4 G} + \frac{2F^2 Di}{d^2 G} \tag{3.5}$$

where $i = i_a$ = number of active coils. Then using Castigliano's theorem to find total deflection z yields:

$$y = \frac{\delta U}{\delta F} = \frac{8FD^3 i}{d^4 G} + \frac{4FDi}{d^2 G} \tag{3.6}$$

Since C = D/d, equation 3.6 can be rearranged to give:

$$y = \frac{8FD^3 i}{d^4 G}\left(1 + \frac{1}{2C^2}\right) = \frac{8FD^3 i}{d^4 G} \tag{3.7}$$

The *spring rate*, also called the scale of the spring, is k = F/y, thus:

$$k = \frac{d^4 G}{8FD^3 i} \tag{3.8}$$

From [38], four types of ends can be used for compression springs, and will affect the overall material doing work. A spring with plain ends has a noninterrupted helicoid; the ends are the same as if a long spring had been cut into sections. A spring with plain ends that are squared or closed is obtained by deforming the ends to a zero-degree helix angle. Squared and ground ends supply a better transfer of the applied load. According to [36], good design practice designates using squared and ground ends.

## 3.3 Preliminary analysis

As with the complete end-stop system design, component compression spring design proves an iterative, parametric process. There are 2 phases to designing the helical spring,

**Table 3-1 - Two distinct phases of helical spring design.**

| Helical spring design phases: | Design |
|---|---|
| Phase 1 - mechanics of materials | Cylindrical beam deflection (uncoiled) |
| Phase 2 – kinematic behavior | Spring coils and sizing |

In phase 1, the first parameter of interest, the limiting factor and mode of spring failure, is shear stress, $\tau$ described by equation 3.1. The dominating variable in the shear stress formulation is indisputably spring wire diameter $d$. Thus, the primary level parameters in helical spring design choice can be described as follows:

**Table 3-2 - Primary level parameters for phase 1 helical spring design (blue) and their corresponding design tactic or determining factor (green).**

| F | $\tau$ | $d$ |
|---|---|---|
| Applied load | Allowable shear stress | Wire diameter |
| Hydrodynamic analysis (from chapter 3.3) | Material selection | Comparative analysis |

Since the preliminary design load F has been established in chapter 3, allowable shear stress $\tau$ (a material property) and wire diameter $d$ (geometric/kinematic property) will be sought in relation to one another for the possible spring indexes $C$and Wahl curvature factor $K_W$.

**Table 3-3 - Level 2 parameters for phase 1 helical spring design (green) and their corresponding design tactic or determining factor (grey).**

| $C$ | $K_W$ |
|---|---|
| Spring index | Wahl curvature factor |
| Manufacturability and wire diameter $d$ | Dependent on C |

There are two good reasons not to simply choose a large wire diameter:

1. The analytical models presented in [36] and [38] are intended for relatively smaller width spring wires (reliability/effectiveness and robustness design criteria 1 and 2)
2. Excess material and manufacturing costs and additional costs for environment-proofing the excess material (efficiency/economics design criteria 4).

   A single equivalent spring is deemed infeasible for the material selection phase of spring design, and a preliminary system configuration must be established based on multiple springs in parallel. To keep end-stop system bulk to a minimal (design tasks 3 and 4), and polling regional steel bar manufacturers' catalogs, 30 mm wire diameter is established as a preliminary cut-off, maximum wire diameter. This limit exceeds the design diameters suggested by both [36] and [38] methodologies, but not excessively. After graphing the relationships in figure 4-4, [39] is perused for possible candidate steels.

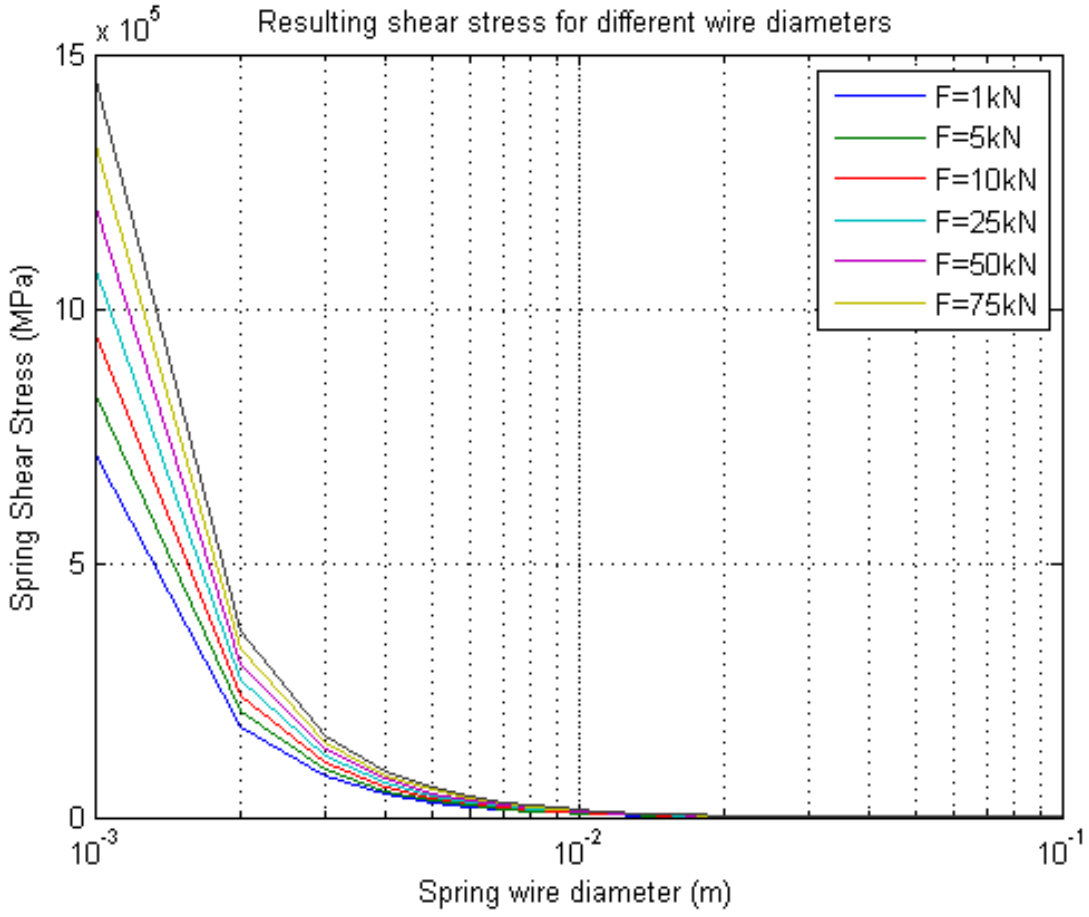


**Figure 3-6 - Logarithmic behavior of the wire diameter on the magnitude of shear stress**

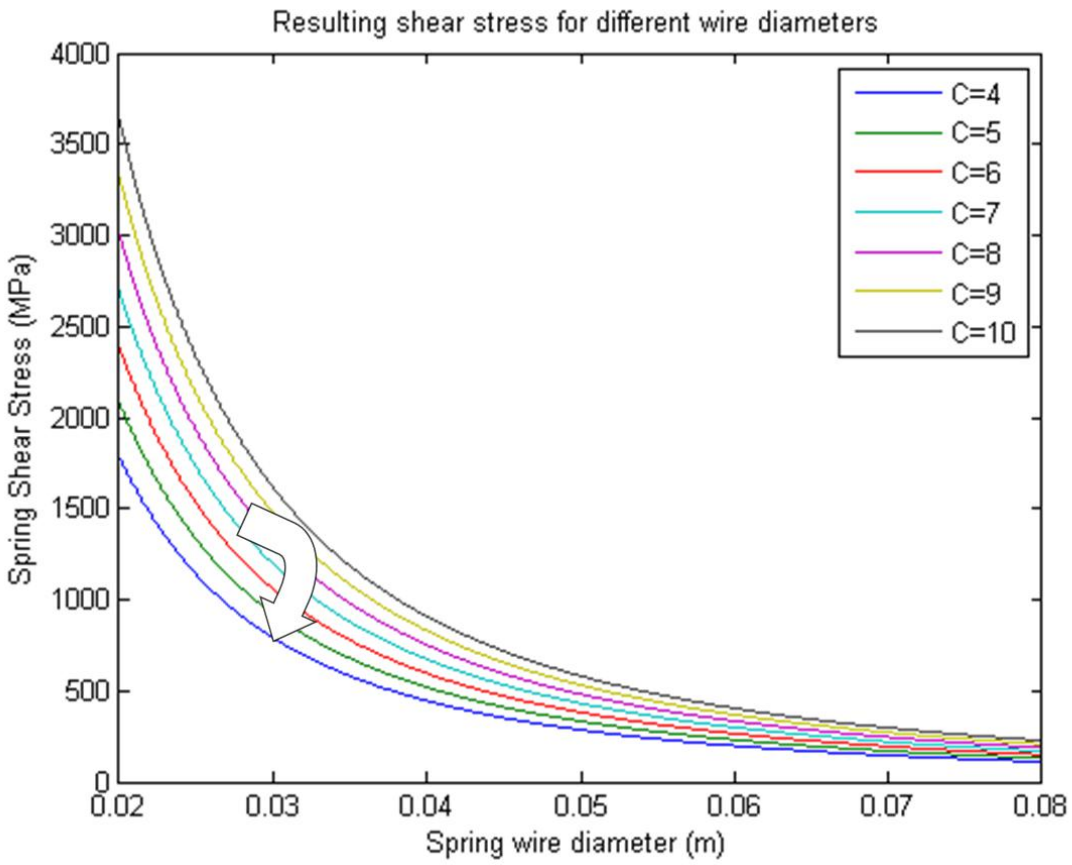
Resulting shear stress for different wire diameters
Spring Shear Stress (MPa)
Spring wire diameter (m)
C=4
C=5
C=6
C=7
C=8
C=9
C=10
4000
3500
3000
2500
2000
1500
1000
500
0
0.02
0.03
0.04
0.05
0.06
0.07
0.08

(a.)

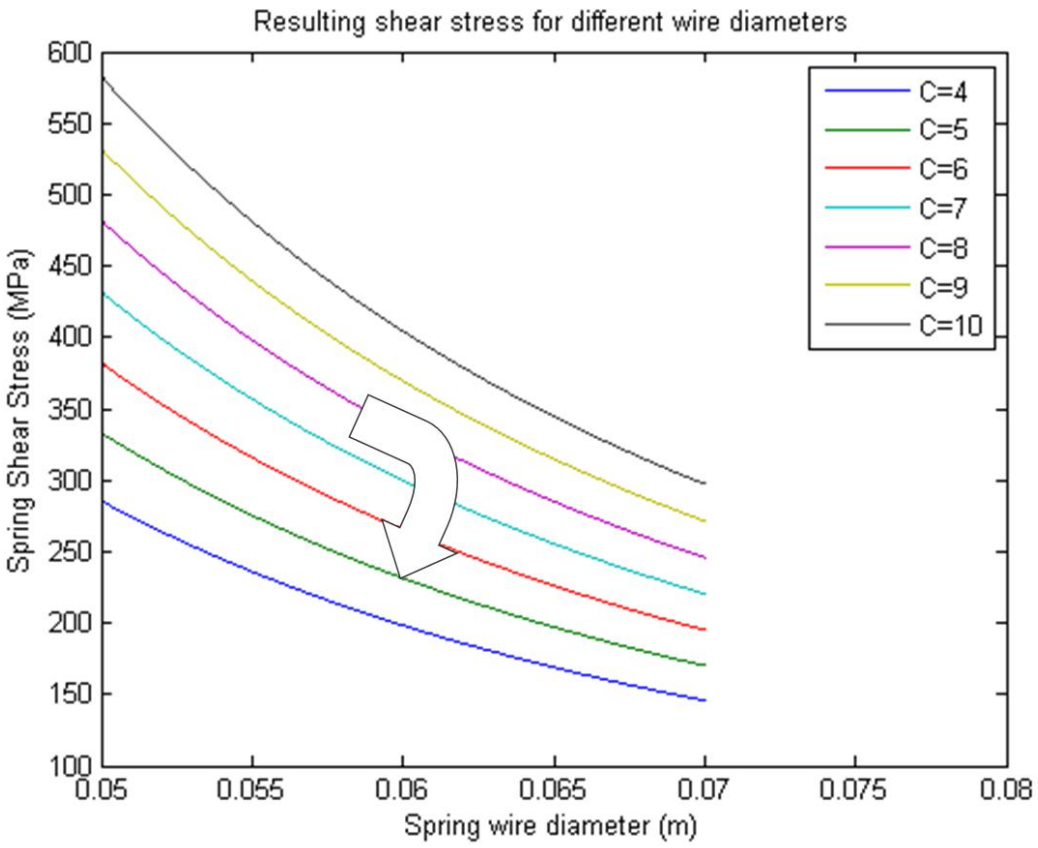


(b.)

**Figure 3-7 - (a.) & (b.) Different zoom perspectives for graph of spring wire diameter vs allowable shear stress for variable spring indexes for optimal 8 parallel compression spring system configuration, subject to $75kN$ design load. Optimal steel: d = 0.03 m, C = 4.**

The high shear stresses induced at small and medium wire diameter sizes are only attainable by some special composite materials, unnecessarily expensive for a WEC self-preservation component. The desired material is a structural, ferrite-pearlitic steel, preferably low carbon and low-alloy for efficient economics, design criteria 4. The primary parameter to protect during the life of the spring is still wire diameter. Therefore, any material property that may defend this fundamental should be sought. Table 3-4 shows the selected optimal material, from this analysis.

**Table 3-4 - Optimal material selection for end-stop helical compression springs from [39].**

| Steel | Condition | Tensile strength (MPa) | Yield Strength (MPa) | Elongation in 50 mm, % | Reduction in area, % | Hardness, HB |
|---|---|---|---|---|---|---|
| 4150 | Oil quenched from $830^{\circ}C$ | 1310 | 1215 | 13.5 | 47.2 | 375 |

With an optimal material selected, phase 2 follows, calculating optimal sizing parameters.

**Table 3-5 - Helical spring end-stop design parameters. Recall 1 and 2 are the WEC self-preservation design parameters and 3 and 4 are the practicality design parameters.**

| | Mechanics of materials (Phase 1) | | Kinematic behavior (Phase 2) | | | Extracted parameters (Both phases) | |
|---|---|---|---|---|---|---|---|
| | $UTS$ Yield strength | $G$ rigidity modulus | $d$ wire diameter | $L_o$ Spring free length | $i$ number of coils | $k$ stiffness | $m$ mass |
| 1. Reliability/ effectiveness | √ | | √ | | | √ | To be determined TBD |
| 2. Robustness | | √ | | √ | | √ | TBD |
| 3. Integrability | | | | √ | | | TBD |
| 4.Efficiency/ economics | | | √ | | √ | | TBD |

The principle weighted design criteria, effectiveness/reliability (1.) calls for adequate material yield strength, sufficient wire diameter, and an effective stiffness, being a result of these first 2 parameters. After selecting these properties, the reliability/effectiveness can be summed up by the design load extracted from Hooke's law.

To assess robustness (2.), the full range of heaving loads, from 1 to $75kN$, that the optimal end-stop springs may endure are included in the *sizing* graphs in the following section.

### 3.3.1 Optimal design parameters

Spring design parameters are obtained for the optimal oil quenched 4150 steel by combining the mechanics of materials spring design formulations with the 4 end-stop design criteria. These optimal parameters and their relationships are shown in the following graphs.

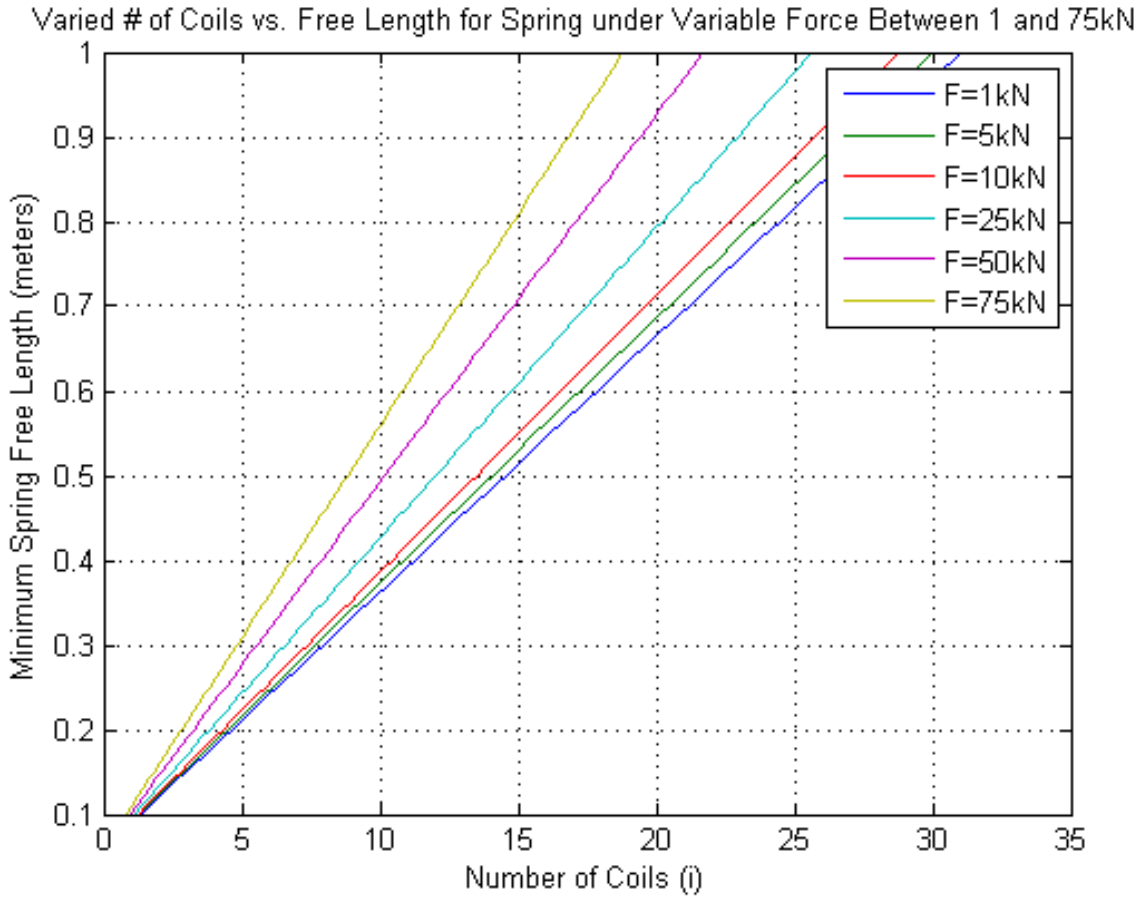


**Figure 3-8 - Number of coils *i* vs. minimum spring free length $L_0$ (in meters) for the loads on an optimal, individual end-stop spring. Optimal spring design load is 75kN (shown in yellow). A range of other possible heaving loads are graphed and labeled as well to assess design criteria 2 (each potential load is designated by a color).**

Since this is the minimum spring free length, in terms of reliability (design criteria 1), all values vertical of the lines of respective loads are considered effective. However, for the two practicality criteria (design criteria 3 and 4) and considering the intrinsic design task, there is a limit to the selectable free lengths. In robustness consideration (design task 2) it can easily be concluded that the minimum spring free length should correlate to the 75kN design load to account for all load potentials. The difference between minimum spring free length increases between loads with increased number of coils. Thus, to achieve a spring size that is effective for the variable load potentials, the smaller the spring free length, $L_0$, and the smaller the number of coils, $i$, the more consistent the sprig will behave in practical operation. This is more explicit in figure 3-9, which shows spring deflection vs number of active coils.

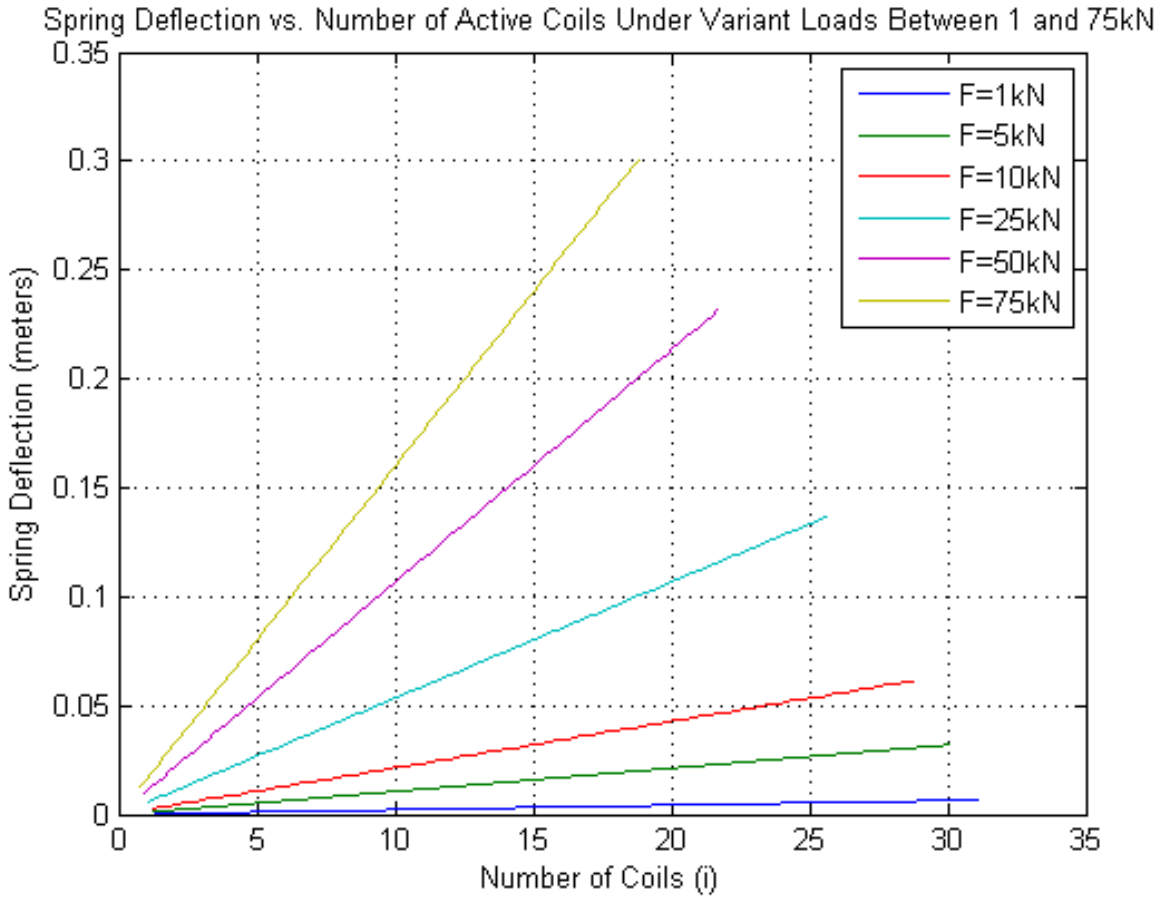


**Figure 3-9 - Number of coils *i* vs. spring deflection (in meters) for the loads on an optimal, individual end-stop spring. Optimal spring design load is 75kN (shown in yellow). A range of other possible heaving loads are graphed and labeled as well to assess design criteria 2 (each potential load is designated by a color).**

Recall that the analytical spring design protocol from [36] and [38] are for small spring deflection $z$ relative to spring free length $L_0$. Figure 3-8 shows how increasing the number of coils increases spring free length, while figure 3-9 shows how increasing the number of coils increases the spring deflection. There are a number of considerations. Deflection should be minimized for the intrinsic design task, allowing a larger, unconstrained heaving space for the buoy to produce power in operable conditions. Deflection mitigation also shows up in efficiency/economics (4.) *practicality* design criteria, due to the assumption of small deflection relative to free length from the analytical design protocols in the literature [36][38];this is backed up by the mechanics of materials theory shown.

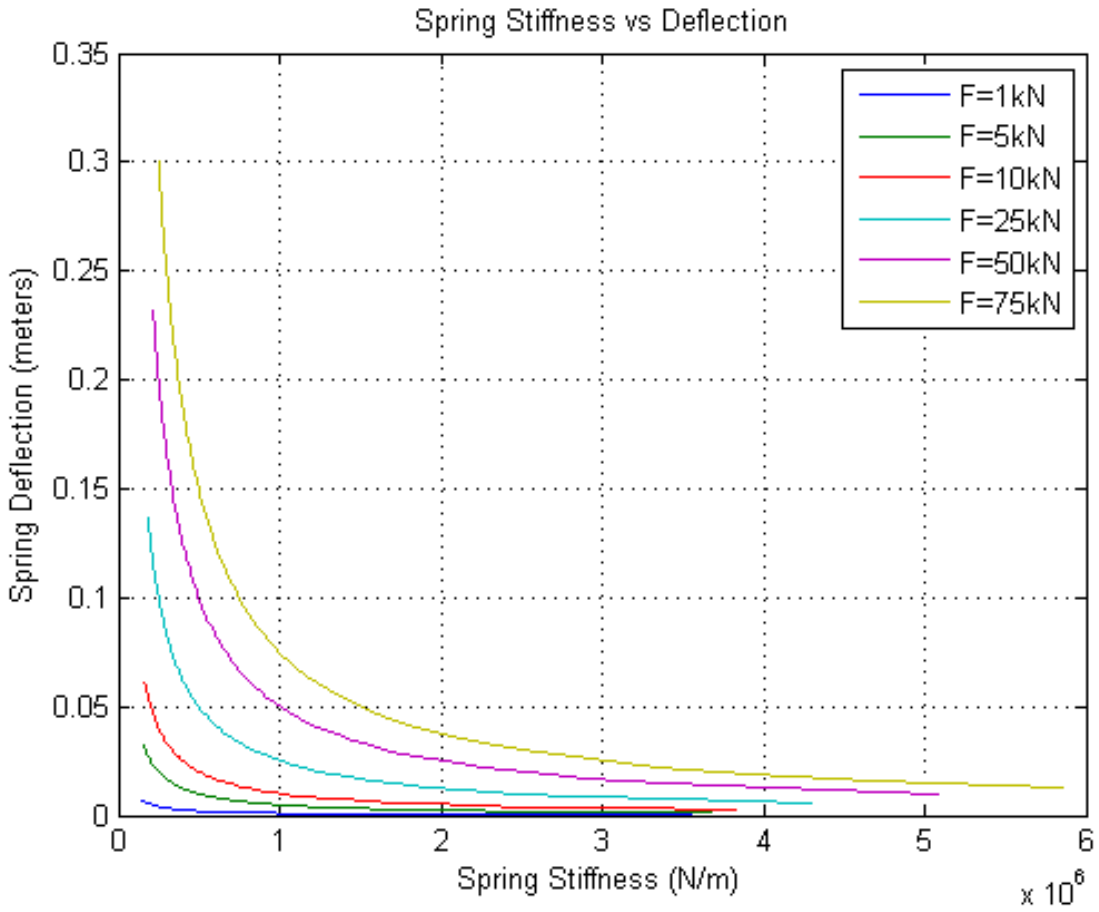


**Figure 3-10 - Spring stiffness vs. deflection for robust load design**

The characteristic material design parameter of a spring is its stiffness. The characteristic kinematic, or compliance, parameter is its deflection. Figure 3-10

The same analysis is extended for a suboptimal material selection. A parametric comparison is shown in table 3-6. The suboptimal material curve is presented in the next section, where the suboptimal material is subject to finite element analysis as a conservative preliminary design approach, and to understand the conservative factor related to analytical results.

**Table 3-6 – Optimal vs. suboptimal spring material parameters for end-stop.**

| | Optimal | Suboptimal |
|---|---|---|
| Number of parallel springs | 8 | 12 |
| Wire diameter (mm) | 30 | 60 |
| Spring index (C) | 4 | 5 |
| Spring design load (kN) | 75 | 50 |

## 3.4 Finite element analysis – numerical analysis

To obtain numerical data with respect to the load capacity of preliminary class spring end-stop systems, finite element analysis is performed on a suboptimal steel design unit. The goal is to understand system class viability with relation to design task 1, and to assess analytical error in the parametric datasets procured in this chapter.

**Table 3-7 – Spring dimensions**

| Y | k | N | d | D | L0 | Pitch |
|---|---|---|---|---|---|---|
| mm | N/mm | # | mm | mm | mm | mm |
| 104.7 | 477.2 | 10 | 60 | 300 | 860 | 80 |

The suboptimal steel was obtained from in-house measurements, modeled through elastic-plastic J2 flow theory with isotropic hardening assuming Young modulus of 206.8 GPa, Poisson coefficient of 0.3 and yield stress of 413.6 MPa. Figure 3-11 shows the true stress versus logarithmic plastic strain employed in the numerical analysis.

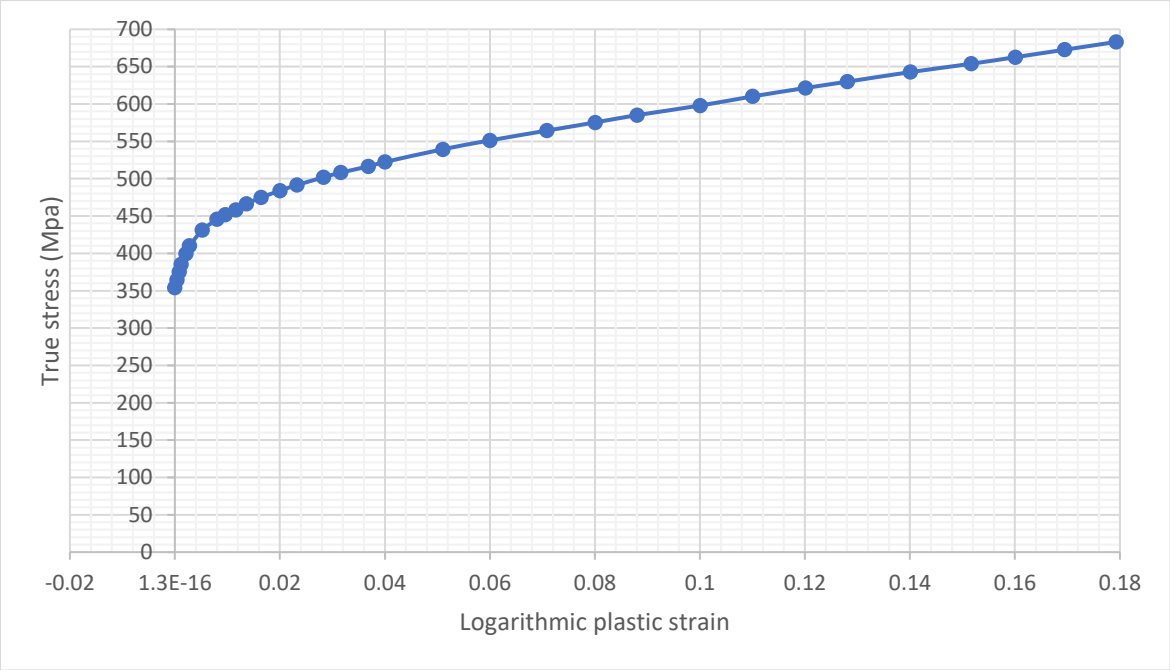


**Figure 3-11 - True stress versus logarithmic plastic strain of API X-60 steel grade.**

The numerical analyses are performed using the finite elements (FE) Abaqus commercial software [39]. The spring geometry was modeled in Solidworks. The geometry was modeled as follows: N=10, pitch 80 mm, dimeter of wire is of 60 mm and spring coil diameter set to 300mm.

The spring support surfaces are used to compress the spring FEA model, see Figure 3-12. To simulate coil contact during deformation, touching type contact elements were used to model boundary non-linearity. Coulomb's friction model was used to account for coil friction. A value of 0.1 is considered for the coefficient of friction, steel on steel. The boundary conditions were rigid surfaces, displacement controlled with quasi static analysis.

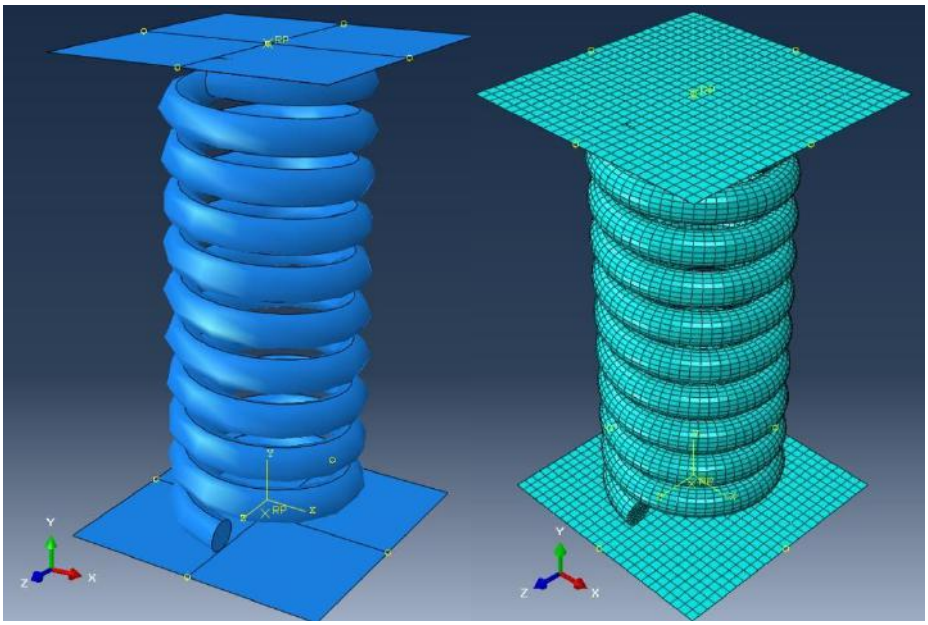

**Figure 3-12 - Spring FEA numerical model with boundary condition and mesh respectively.**

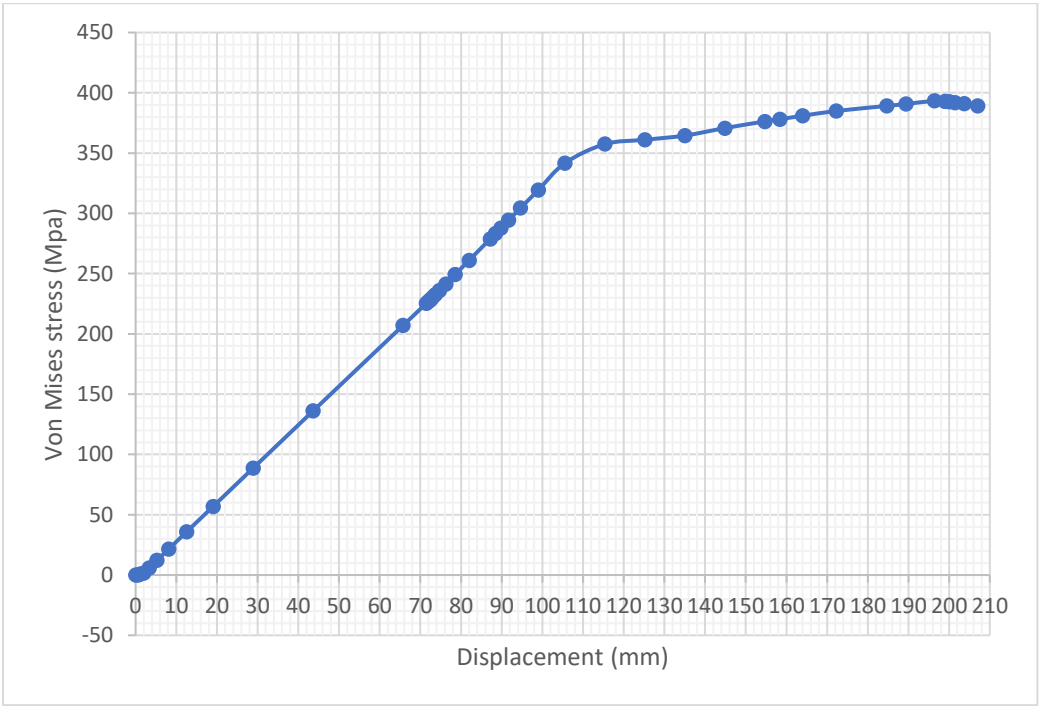


**Figure 3-13 - von Mises stress versus displacement.**

Critical stress conditions during spring compression are shown in Figure 3-13, by Von Mises stress vs. displacement. At about 110 mm the spring starts to experience nonlinear plasticization

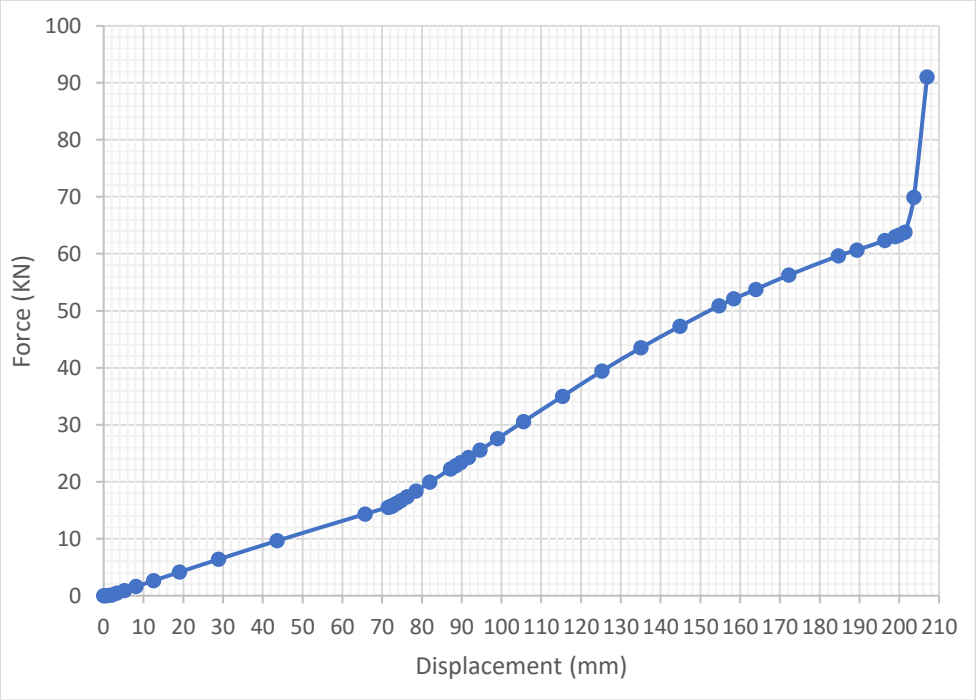


**Figure 3-14 - Predicted load versus deflection curve.**

Figure 3-14 shows force vs. spring dislocation obtained through the FE analysis. It is apparent that there are 3 distinct regions of dislocation behavior under the applied load. The first region of lowest slope linear displacement can be observed for about 15kN, to a dislocation of 70 mm. This initial behavior corresponds to the spring end conditions, which are not ground or squared, but fixed between two flat plates. During this initial compression mode, the spring experiences a disproportionate displacement along its free length ($L_0$), where both ends compress independently to about half of the wire diameter/pitch. Subsequently, a primary mode of compressive behavior occurs between ~70-200 mm dislocation, from 16-64 kN applied load. During this interval slight nonlinear behavior exhibits better than analytically predicted response. This can likely be attributed to Coulomb friction forces damping a small portion of the force, a loss in stored energy perhaps, but an improvement in damping.

After this second mode of dislocation, operational limits are reached and the spring experiences yield as it transitions to plastic deformation. This critical point is observed at around 205 mm displacement and as the numerical material yield strength is overcome.

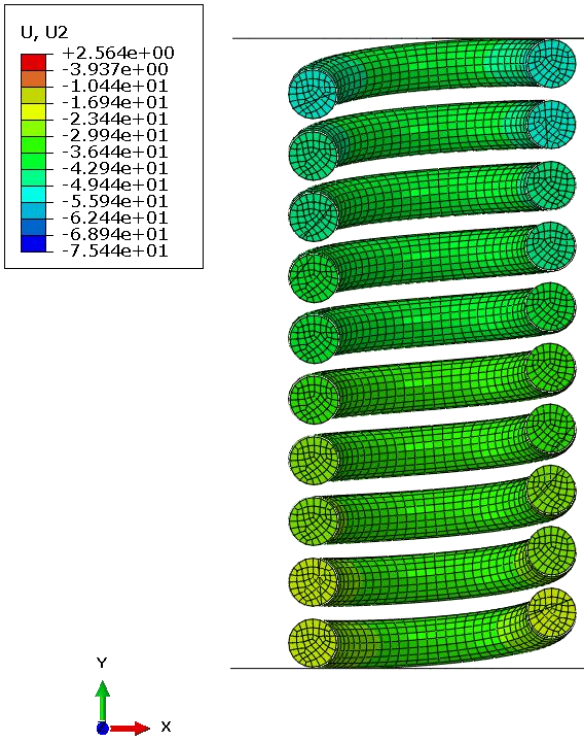


**Figure 3-15 - FEA resultant with 75.4 mm displacement.**

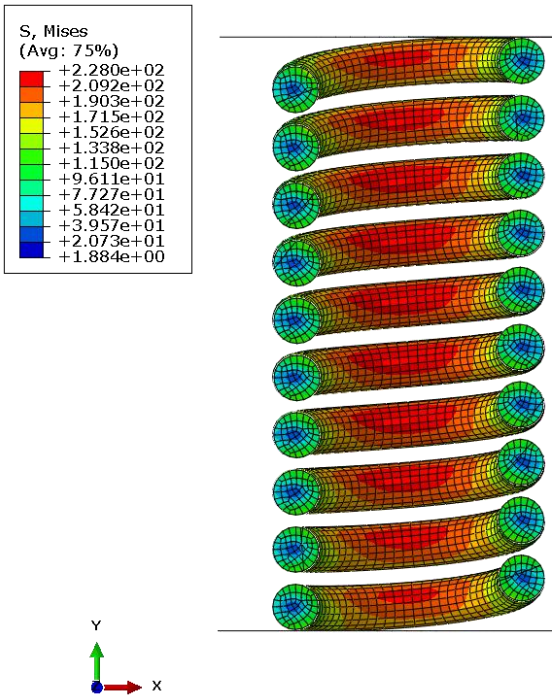


**Figure 3-16 - Field stress of von Mises to displacement 75.4 mm.**

Prior to yield limit, the Von Mises stresses are exhibited in Figure 3-16, where it is apparent that the inner axis of the spring experiences the highest stress. This behavior in helical compression springs is as expected and is verified by the literature. This unfortunate disproportionality in stress distribution for helical springs has to be the main flaw in the simple, and time-tested design. The cylindrical centers of the spring wire experience the lowest stress in comparison.

The next figures show the result with displacement 108.1 mm.

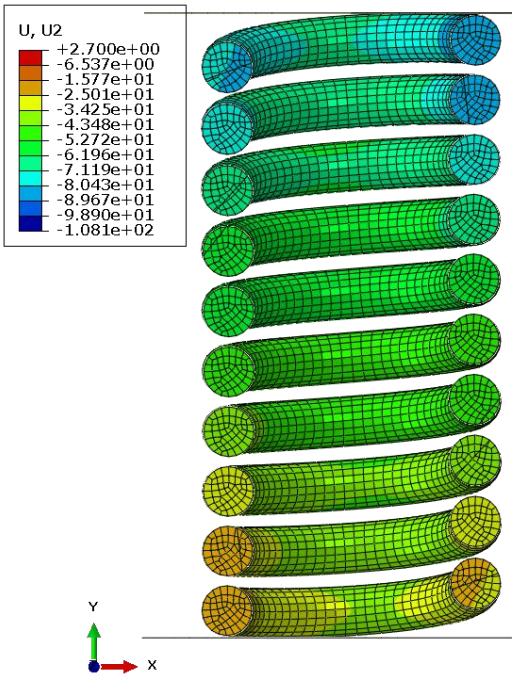


**Figure 3-17 - Displacement 108.1 mm.**

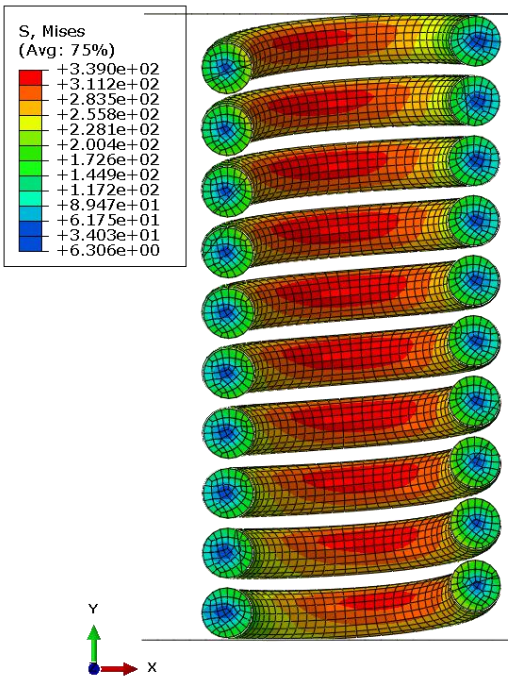


**Figure 3-18 - Field stress of von Mises to displacement 108.1 mm.**

The next two figures show the results with displacement 205 mm.

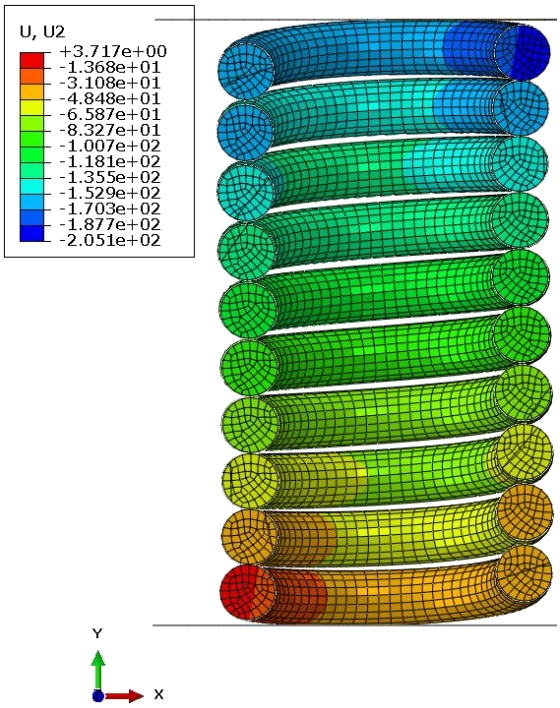


**Figure 3-19 - Displacement 205.1mm.**

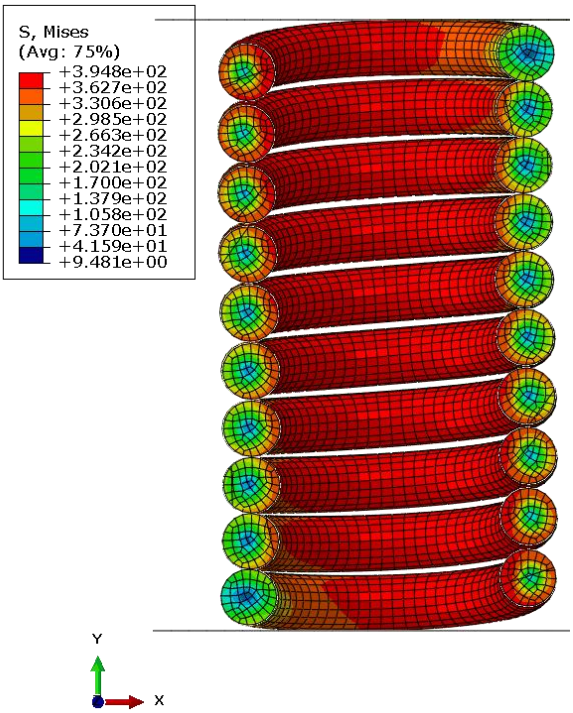


**Figure 3-20 - Field stress of von Mises for displacement of 205.1 mm.**

By this deflection, 205.1 mm, the critical Von Mises stresses have spread to engulf a large portion of the outer surface of the full length of the cylindrical wire.

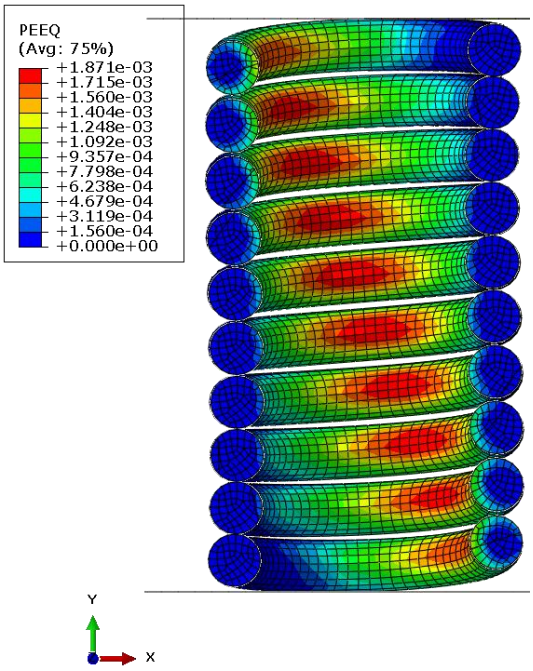


**Figure 3-21 - Field stress of equivalent plastic strain to displacement 205.1 mm.**

The first locations to experience plastic strain are predictable from the prior figures, and they occur along the inner face of the coiled cylinder. It is interesting to note that the and follows the helix in a diagonal to the other far end one half rotation from its initial point of contact with the flat plate. The initial point of contact on the ends has now become a larger region of planar contact, where the cylinder is protected from the major cause of plastic strain, from the torsional shear stress from the cylinder´s inherent twisting as compressive load is applied.

The following figures show the results with displacement 209.8 mm.

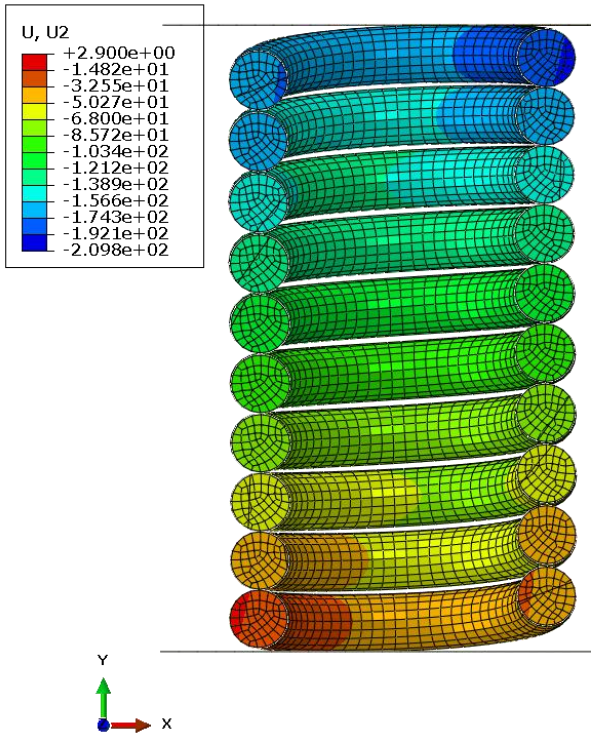


**Figure 3-22 - Displacement 209.8 mm.**

By now, the spring has chosen its weak point due to complexities in its geometry from the various numerical iterations upon its mesh. One end succumbs before the other by very nonlinear and hard to predict behavior.

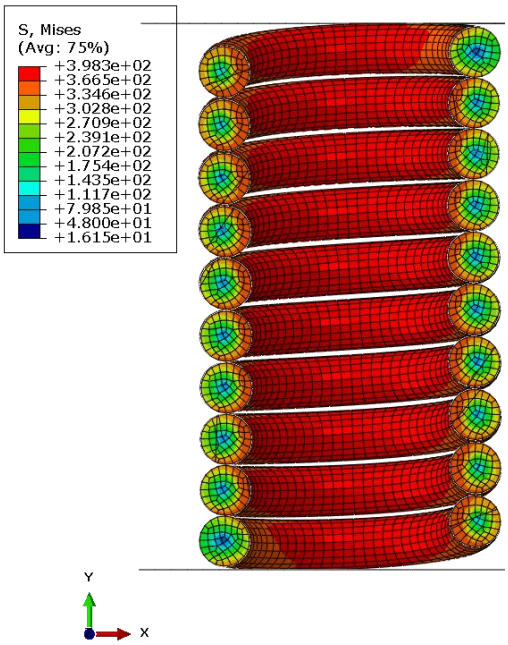


**Figure 3-23 - Field stress of von Mises for displacement of 209.8 mm.**

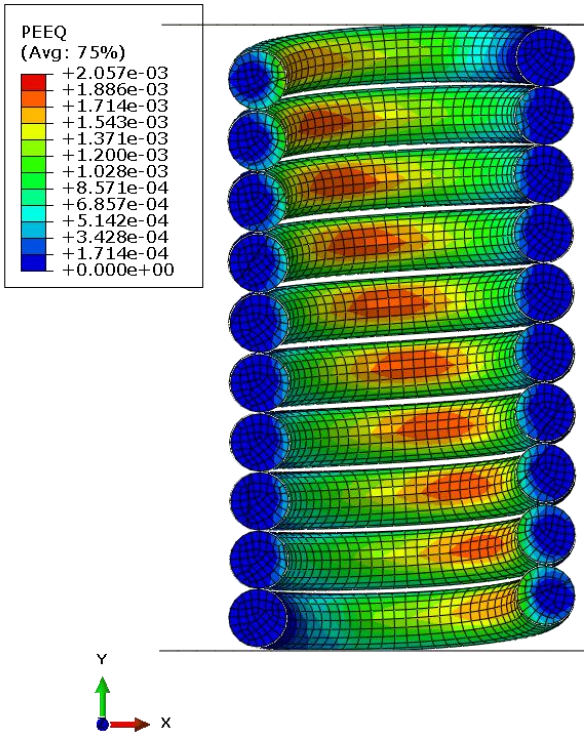


**Figure 3-24 - Field stress of equivalent plastic strain for displacement of 209.8 mm.**

To correlate the FEA numerical results with both optimal and suboptimal spring, end-stop system designs, the direct relation between the numerically modelled spring and its analytical counterpart can be compared. This definitive relation shows the extent to which the analytical assessments are estimated conservatively, which concatenates upon an already conservative hydrodynamic numerical result for maximum end-stop force; although, with a high degree of uncertainty.

## 3.5 Dimensional analysis – parameterization

Identification of important system parameters is a matter of strategy and problem contextualization. The representative, dynamical models, established in the previous sections, provide a base of standard parameter variables that are physically and explicitly descriptive, but still limited to the context of some standard dimensionality. The models spread a large scale of phenomenology, and this presents certain challenges. To achieve a meaningful comparison and assist in definitive design selection, a relation between the systems must be established. For this reason, a comparative, dimensionless description of the models' dynamics is desired.

The problems arise in attempting to assess different spatial-scaled phenomena against one another, i.e. micro ($\mu m$) and nanoscopic friction laws and tribology against macro or 'normative' ($m$) size-scale, classical mechanics and hydrodynamics for the WEC machinery under investigation. For a reliable physical comparison, the parameters need to be acceptable and tolerable between comparable models.

The limitations of the dynamical models can be characterized by simple laws of nature. For one, the "square-cube law," first addressed by Galileo, explains that the ratio between 2 volumes is greater than that of their surfaces, and is observable and proven by simple geometry. With the square-cube law it may be observed that a geometric parameterization could play an important function in the system's physical phenomena.

Looking to these, the design problem framework, both with respect to the kinematics and the phase-interfacial models, the square-cube law is both appropriate and an important consideration for the design strategy comparison under investigation.

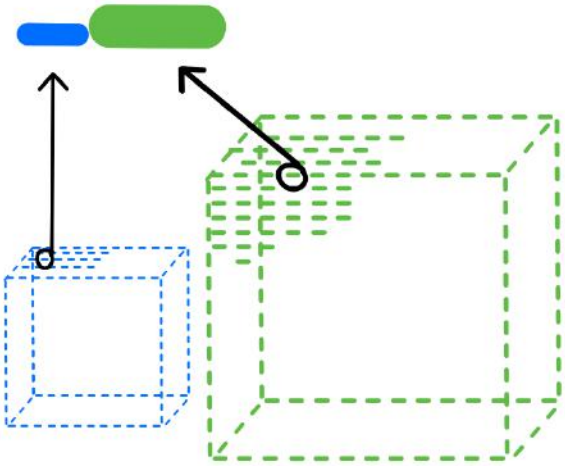

**Figure 3-25 – "Square cube law" from arbitrary, dimensional perspective. With the green and blue differential units defined at any scale in 3-dimensional space (represented by both cube structures), this spatial, law of nature is apparent at any size scale, from macro, to micro, to nano.**

The steps to meaningful parameterization are iterative, creative, and enlightening. The parameters established are intended to provide the means for a more well-educated, comparative design choice selection. Recall, the preliminary design criteria: reliability, robustness, integrability, and efficiency/economics.

The following tables present a holistic list of possible parameters involved in an end-stop allision, separated categorically, as primarily kinematic, interface, or dynamical response phenomena. Dimensionless parameters are highlighted in blue.

**Table 3-8 - Tabulated parameters of importance relative to end-stop and heaving mass kinematics. Pitch angle $\theta$ is highlighted as the dimensionless kinematic parameter determining relative stiffness and possible response of surface asperities, upon tangential contact.**

| | |
|---|---|
| $v_z$ | Relative velocity along the z-axis |
| $v_x$ | Relative movement along the x-axis |
| $z$ | Position along the z-axis |
| $\theta$ | Pitch angle of anisotropic asperities, ordered along the z-axis of a friction end-stop |
| $m/L$ | Micro-asperity masses per arbitrary, unit length of contact surface interface (from "virtual work" configuration friction model) |

**Table 3-9 - Tabulated parameters relevant to end-stop-heaving mass interfaces. The Froude number $Fr$ is highlighted as the dimensionless parameter distinguishing whether inertial or viscous forces will dominate once a contact interface is established.**

| | |
|---|---|
| $k$ | Contact stiffness |
| $Fr$ | Froud number, designating the dominance of inertial vs. viscous forces in the collision interaction |
| $\gamma$ | Surface tension |
| $R_{ES}, R_M$ | Roughness factor, of solid contact surfaces, corresponding to the end-stop and heaving mass respectively |
| $T$ | Period (time) of established contact |

**Tabulated parameters of importance for end-stop-heaving mass dynamical response. The coefficient of restitution $e$ is highlighted as a dimensionless parameter of the collision.**

| | |
|---|---|
| $e$ | Collision or allision coefficient of restitution |
| $M$ | Buoy mass + hydrodynamic added mass applied to buoy |
| $m$ | Mass of end-stop component, for both micro-asperity models and spring-mass models |
| $C$ | Linear, spring coefficient of simplified hydromechanical coupling between incident wave and floating buoy |

These parameters are now regarded with respect to their immediate and definitive usability in a preliminary design strategy comparison. Because of the nature of the multiple size scales and resulting physics involved, dimensionless parameters are prioritized; they provide a more universal outlook and categorical comparison potential. In aim to relate and equate the model parameters, meticulous, dimensional analysis is performed. Further, descriptive, dimensionless formulations are sought to provide more detail and clarity in the design choice assessment.

Buckingham Π Theorem is the method chosen to establish and assess nondimensional quantities. Significant parameters under investigation are isolated methodologically.

As a first pass, a dimensionless group to relate and compare damping mechanics of large, spring-mass systems with the modeled behavior of micro-structured friction surfaces, was desired. Attempts to isolate the pitch angle of the scales as a determinant in movement damping capability proved fruitless for two reasons. It must first be observed that angle is a dimensionless parameter to begin with. The fact that angle is dimensionless is physically significant, and will be explained in the next section. Second, incorporating the fundamental length quantities separately, as $L_x$ and $L_z$ from the two-dimensional models, in attempt to isolate the pitch angle $\theta$, of the micro-asperities in the anisotropic (snakeskin) friction model, the angle could not be disjoined from its arctan function to properly serve as It was postulated to obtain a numerical approximation of this arctan function, but this route was not taken. Instead, the pitch angle is omitted, and a new parameter is introduced, mechanical impedance, i.e. resistance to motion. The mechanical impedance wears the

same units as the damping coefficient of a 'dashpot' (viscous) damper in dynamical system models' equations of motion, $kg/s$. However, the simplistic, dynamical models presented in this work, merely consist of spring elements of stiffness $k$ and 2 distinct masses of mass $M$ (mass + hydrodynamic added mass, for a heaving buoy) and $m$ (mass of the end-stop component, or micro-component) with rigid bodies, respectively, in collision.

Mechanical impedance can be described by the following relation:

$$F(\omega) = Z(\omega)v(\omega) \qquad (3.9)$$

$F(\omega)$ is the force vector,

$v(\omega)$ is the velocity vector,

$Z(\omega)$ is the impedance matrix,

And $(\omega)$ is the rotational velocity.

Since, impedance is represented as a matrix and is considered to rely on rotational velocity (analog to cyclic or circuit flow), according to equation 3.9, the virtual work model may be assumed, and considered to either have a large $r$ in the space of collision action, virtually connected to a large imaginary wheel or gear; or similarly, the Earth can be taken as the acting body (which it is, in the case of ideal rigid bodies and ideal, rigid connections), and since it has its own rotational velocity, as well as the relative rotational influence of other celestial bodies like the Sun and the Moon affecting every plane of three-dimensional space, these quantities physically exist. It should be noted that this simplistic mechanical impedance formulation, to correspond to the assumptions made in the dynamical models, omits key nonlinearities such as viscosity, which are disregarded for this preliminary design investigation. This formulation of mechanical impedance is an attempt to isolate and assess signature, linear parameters in the models. Consequentially, Buckingham Π Theorem dimensional analysis is performed, as a means to demystify and debar the different size scale phenomena between the micro and macro physicality, outlined in Table 3-10 and equation 3.10 below.

**Table 3-10 - Buckingham Π Theorem chart of parameters to determine corresponding, impedance, $Z_z$ parameters in the heave direction. Parameters highlighted in blue are shown next to the column on the left that they are chosen to represent to determine $\pi_{1,\,Z_z}$.**

| | | | | | ↓ | | |
|---|---|---|---|---|---|---|---|
| | | $m$ | $k$ | $g$ | $Z_z$ | $v_z$ | $v_x$ |
| $k$ | $T$ | 0 | -2 | -2 | -1 | -1 | -1 |
| $M$ | $M$ | 1 | 1 | 0 | 1 | 0 | 0 |
| $v_x$ | $L_x$ | 0 | 0 | 0 | 0 | 0 | 1 |
| $g$ | $L_z$ | 0 | 0 | 1 | 0 | 1 | 0 |

$\pi_{1,\,Z_z} \rightarrow \quad Z_z k^a m^b {v_x}^c g^d$

$$[1]^0 = [T^{-1}M][T^{-2}M^1]^a[M]^b[L_x T^{-1}]^c[T^{-2}L_z]^d \qquad (3.10)$$

$$T\colon\ 0 = -2a - c - 2d - 1$$
$$M\colon 0 = a + b + 1$$
$$L_x\colon 0 = c$$
$$L_z\colon 0 = d$$

$\pi_{1,\,Z_z} \rightarrow \quad Z_z k^{-1/2} m^{-1/2}$ (3.11)

Buckingham Π method is a simply algebraic means of eliminating standard units. [56] explains, "The principal use of dimensional analysis is to deduce from a study of the dimensions of the variables in any physical system certain limitations on the form of any possible relationship

between those variables" [54]. Thus, the physical meaning from the results of the analysis must be interpreted by the investigators themselves. Buckingham Π Theorem, mechanical impedance in heave ($z$) for all, spring-mass, end-stop models, when assumed to have a coupled virtual rotational velocity $\omega$ (as in the "virtual work," friction model) can be taken as $\sqrt{km}$. This formulation of mechanical impedance will be referred to as Mode I mechanical impedance. This parameter has an interesting correlation with the natural frequency $\sqrt{k/m}$ derived in each of the collision models separately, and inherent to any mass and stiffness, but also related to shape as is apparent in certain systems, like that of the heaving buoy natural response, optimized by [5] and those of other naval vessels and civil structures alike, which are contrariwise, often engineered to mitigate potential resonance response occurrences.

The next parameter of interest is that which defines the shape or pattern, that which relates the number of anisotropic friction asperities, snake scales, bristles, spines etc., or mechanical gear teeth to the impedance quantity. Pitch angle, $\theta$, of the micro-asperities, or scales, is already dimensionless, and cannot be isolated as an independent variable for Buckingham Π Theorem due to its appearance within an $arctan$ function of $L_x$ and $L_z$, the interesting parameter to uncover to define Mode II mechanical impedance for the dynamical models shifts to a mass per length quantity. The fact that the $L_x$ and $L_z$ parameters dropped out of this first dimensional assessment of mechanical impedance (or damping)

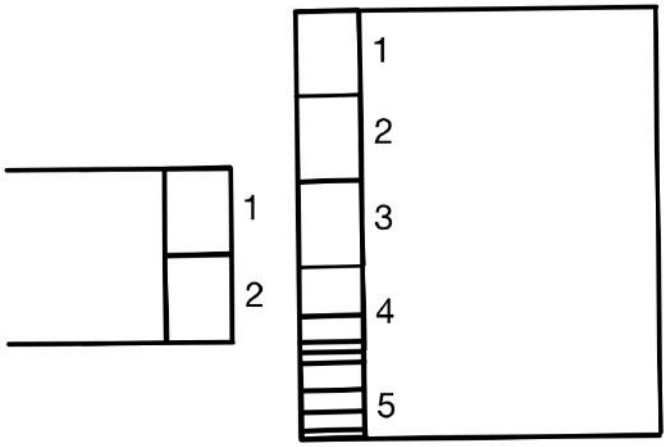


**Figure 3-26 - Schematic representation of 2 dimensionless surfaces with arbitrary units per length. These units could indicate micro-asperities; patches of differential *roughness*; the teeth of a gearwheel, unrolled, and laid oud flat; or any other pattern of objects of mass, ordered in a row of frequency $\omega$.**

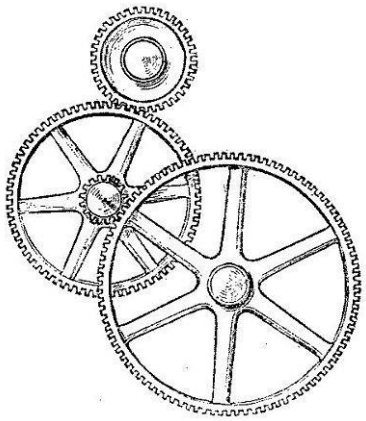

**Figure 3-27 - Transmission of motion and force by gear wheels, compound train [46]**

The teeth on a gear wheel can be imagined as friction asperities or anisotropic scales, and can be further imagined to be unrolled and laid out flat (similar to the virtual work model). Since the parameter of importance in a gear train is the number of teeth per $2\pi$, it is apparently a dimensionless quantity; moreover, the value represents a certain spatial density. In the case of the frictional surface under design, this density is considered $m/L$. In the case of snakeskin this unit can be further described by its fractal nature. Isolating this m/L term, Buckingham pi is performed to seek out the corresponding impedance, or in the snake's case *mobility* (the inverse of impedance), parameter:

**Table 3-11 - Buckingham Π Theorem chart of dynamical collision models' parameters to determine mechanical impedance Mode II with m/L anisotropy spacing (surface density) parameter relative to velocity, stiffness, and mass. Parameters highlighted in blue are shown next to the column on the left that they are chosen to represent to determine $\pi_{2,\frac{m}{L}}$.**

| | | $m/L$ | $k$ | $v$ | $m$ |
|---|---|---|---|---|---|
| $k$ | $T$ | 0 | -2 | -1 | 0 |
| $m$ | $M$ | 1 | 1 | 1 | 1 |
| $v$ | $L$ | -1 | 0 | 0 | 0 |

$$\pi_{2,\frac{m}{L}} \rightarrow \qquad [m/L]m^a v^b k^c$$

$$[1]^0 = [ML^{-1}][M]^a[LT^{-1}]^b[MT^{-2}]^c \qquad (3.12)$$

$$T\colon\ 0 = -b - 2c$$
$$M\colon 0 = 1 + a + c$$
$$L\colon 0 = -1 + b$$

From here, a general form is established:

$$\frac{\sqrt{mk}}{(\frac{m}{L})(\frac{L}{T})} \qquad (3.13)$$

The formulation above is truly remarkable.

Note that it is not an equation; it is a dimensionless formulation that describes the behavior of motion impedance. Dimensional relationships like this are not equal to anything; they define similitude. It tells how microscopic behavior could be similar to a macro based on the formulation parameters. This is dimensionless mechanical impedance, or tendency to dampen velocity directly, via waveforms that manifest in the interface. There is no equals sign in the formulation because you have to observe the physical world and see which term dominates for a particular interaction, like Re and Fr. It is relative to the interface, to a collision, of any magnitude. Unitless, there is no specific scale or range of magnitudes that constrains it.

It is intuitive that contact interfaces are already impeders of motion; this dimensionless relation defines the type and magnitude to which they impede different expressions of different interactive pairs. In this research problem, friction and direct compression *collisions* are both interface responses and can be classified by this formulation. With this, it should be possible to *tune* the dimensions of what is intended to be used as the 'damper/impeder/impediment' (whether

tangential or direct contact) according to what the predicted energy/velocity/momentum of the incoming *collider* will look like, to better attenuate its motion (kinetic energy expression/expression **between** matter and space and time), responsively yet passively.

Applied to the end-stop problem, with a hybrid solution, for the total mechanical impedance, we can sum both modes, from the numerator and denominator of the dimensionless function:

$$I_{total} = I_I(\omega) \pm I_{II}(\omega)$$

$$I_{total} = \sqrt{mk} \pm (\frac{m}{L})(\frac{L}{T}) \tag{3.14}$$

Incorporating mechanical impedance in the model is a way to account for both friction and compressive contact forces in one fell swoop.

These distinct modes of mechanical impedance are designated in the following table:

**Table 3-12 - The two modes of mechanical impedance, discovered through Buckingham Π dimensional analysis.**

| | |
|---|---|
| Mode I Mechanical Impedance | $\sqrt{mk}$ |
| Mode II Mechanical Impedance | $(\frac{m}{L})(\frac{L}{T})$ |

To effectuate preliminary design comparison via these new parameters, a representative mechanical impedance model is developed that corresponds to the collision contact interfaces. To develop this model, several conclusions are drawn pertaining to the nature of mechanical impedance:

1. The contact interface between two colliding surfaces can be modeled as a wave.
2. This waveform can be representatively modeled in 1, 2, or 3-dimensions.

3. Mechanical impedance phenomena occur within the contact interface of a collision.

**The model can be found in Appendix A**

A mechanical impedance model can be strategically applied to the end-stop problem in the following ways:

1. Task 1: impose necessary impedance to effectively constrain
2. Task 2: Fine tune impedance, gradual zones

Through mechanical impedance,

$\sqrt{mk}$ defines the inertial and stiffness properties of a collision

$(\frac{m}{L})(\frac{L}{T})$ defines spatial (arrangement) properties of a collision

### 3.5.1 Dynamical comparison

To practically apply this new model, the generalized end-stop formulation by [22], introduced in equation 1.1, can be reinterpreted as a function of interfacial, mechanical impedance ($I_{ES}$) for the acting motion constraint coefficient at the end-stop contact interfaces, as follows:

$$z_S = 2 \times z_{ES} \tag{3.15}$$

$$F_{ES} = \begin{cases} -I_{ES}(\dot{z})\ if\ \ z > z_{ES} \\ -I_{ES}(\dot{z})\ \ if\ \ z < -z_{ES} \\ 0 \qquad\qquad else \end{cases} \tag{3 .16}$$

Recall that $z_S$ is the stroke length designated for the heaving buoy, $z_{ES}$ is the vertical location where the end-stop contact interfaces engage, and z is the vertical position of the buoy.

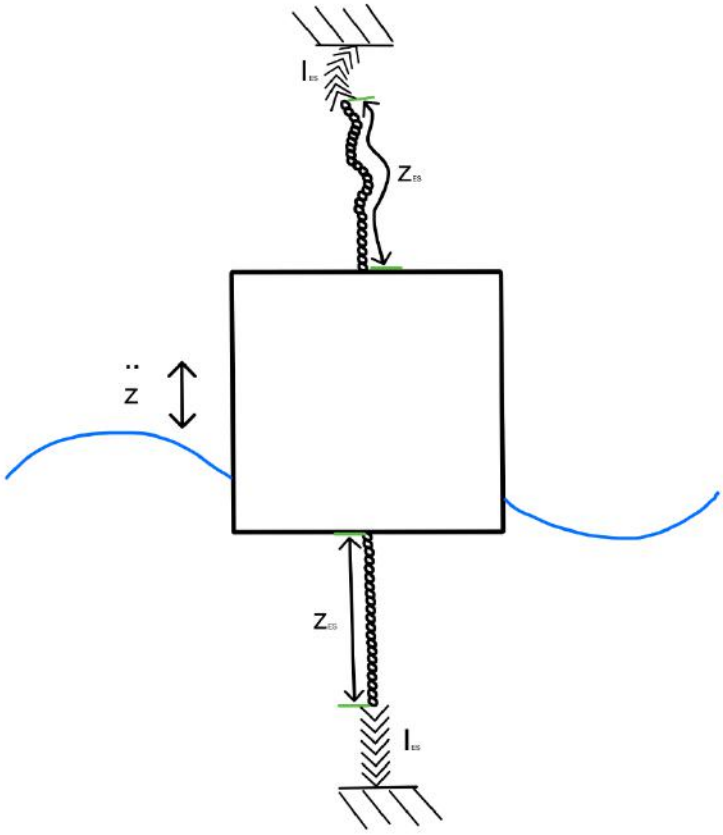


**Figure 3-28 - Schematic representation of the isolated, end-stop system, incorporating an equivalent, mechanical impedance parameter for each end-stop, adapted from figure 1-7. Mechanical impedance elements are represented by a succession of aligned arrowheads, pointing in the direction of preferred mobility (theory developed in Appendix A).**

This model portrays the nonlinear dynamics of the [22] model, presented in chapter 1, or to kinematic parameters, wherein interfacial mechanical impedance takes the form of a force acting on a velocity, much like the ubiquitous dashpot damper. This new, generalized model for a point absorber WEC end-stop system readily portrays intrinsic properties inherent to the requirements of both design tasks, regardless of constraint strategy. For a more robust practical design analysis, a detailed elaboration of the mechanical impedance element action within tangential and direct contact interfaces is portrayed in Appendix A.

This model serves two purposes:

1. It describes the nonlinear impact dynamics of end-stop collisions using kinematic parameters, allowing representative simplification of complex phenomena. Dynamically distinct impact phenomena, like tensile jerk, contact deformation, and friction can be addressed within a linear parametric formulation
2. It accounts for previously disregarded *damping* phenomena, important for any mechanical system

A theoretical representative framework to illustrate the mechanical impedance action in the interfaces can be found in appendix A.

The representative schematic intends to interpret the responses to the action of 2-surface-collision at the interface level, disregarding fluid-solid interface (traditionally called surfaces) interactions that would occur in water or air. Noting the distinct collision contact types (tangential and direct) in the mechanical impedance theoretical framework in appendix A, the difference is in the onset of collision contact, just as sea states are initiated by tangential wind *colliding* with its free surface, in a similar way to wave action propagating in response to a direct collision with the water. This is a phenomenon of scale, as capillary waves are functionally different than mature ocean waves with a gravitational restoring force.

The term *collision* is used broadly in this text, and can be attributed to the onset of surface 'contact' (the creation of a contact interface) between matter in some phase (solid, liquid, gas), resulting in some exchange or dissipation of motion (kinetic energy) to any magnitude (regardless of scale).

**Appendix B-3 contains representations of impedance response on select dynamical models of previous sections**

Mode II Impedance: (the impedance is a property of the collision, and a tangential collision all the action of the collision occurs along the interfacial line between colliding surfaces.

The fractal dimension $FD$ is how a geometrically complex form occupies its space. [45] A higher fractal dimension correlates to a higher surface roughness

$$m/L = FD \tag{3.17}$$

$$1.000 \leq \text{FD} \leq 3.000 \tag{3.18}$$

Ventral snakeskin has been shown to possess a fractal dimension of $2.75 \pm 0.05$ [45], across species.

$$L/T = Lf \tag{3.19}$$

Where L is the length of the collision interface and $f$ is the frequency of a particular collision as a function of the masses and stiffnesses involved. The natural collision frequency versus the size of contact interface space presents a very complex, but informative dynamic. Referring to the dynamical models in chapter 5, the collision frequency can be extracted for corresponding friction end-stop models, as a function of the mass ratio, and various frequencies relative to the masses and stiffnesses involved. This would require that the differential equation for each model of interest be manipulated and solved separately to obtain the detailed system collision frequency. Instead, the range of potential magnitudes can be assessed and included in a broader, inclusive comparison approach. The $L/T$ term depends on how the interface size is defined. For the most explicit comparison between end-stop types, tangential/friction or direct/spring-mass, the full interface length can be defined at the $t_b$, body separation moment, for both strategies. This is the moment when the buoy + added mass momentum is finally halted by the end-stop, and the velocity vector of the buoy has changed to the negative heave, $z$, direction. At this moment, both the tangential, friction end-stop and the spring-mass end-stop have attained their maximum contact interface size, per collision interaction. For this preliminary design analysis, the $L$, of the $L/T$ impedance parameter, will correspond to this maximum $L$ occurrence at $t = t_b$ and the $T$ will correspond to the full period of *phase 1*, in the dynamical, collision models, where $T = t_b - t_0$. With $L/T$ defined based on the dynamical models, the distinct behavior of the interfaces for the two end-stop strategies becomes apparent. However, Mode II mechanical impedance is ignored for direct, spring-mass, end-stop models, being applied and analyzed in a traditional, classical mechanics, macroscopic scale. $L/T$ may then be understood as the full length of tangential contact between

colliding surfaces, when motion has been fully constrained, over the period of time it took to get there.

To formulate graphically, in this preliminary analysis, an array of potential end-stop $L/T$ values are suggested and mapped against possible, 3-dimensional fractal patterns. Since the frequency may be very large, and the interface space, relatively small, behavioral patterns are investigated for a large array of "possible" combinations, regardless of the dynamical model used. The potential magnitudes included are a factor of buoy + added mass, relative to end-stop or micro end-stop asperity, and collision, contact stiffness.

Recognizing that the fractal dimension of the 'snakeskin' surface is only one of the two surfaces involved in a tangential collision. The other colliding surface can be assumed to play a role in an optimal interfacial pattern for snake locomotion. This in turn can be studied in detail through experimentation, where in tangential action end-stop design, both surfaces can be optimized for designated interfacial behavior upon collision. Additionally, observed by [45] in their study of particular snake species, fractal roughness patterns can be tuned and optimized regionally along a surface, as demonstrated in nature by snakeskin adaptations per specific environmental and behavioral requirements.

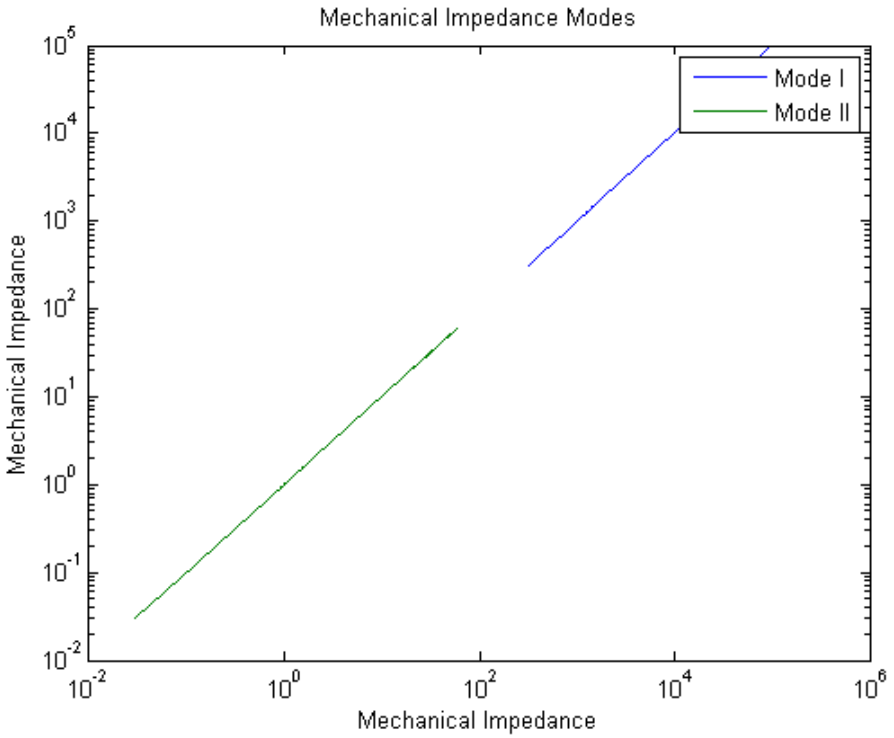


**Figure 3-29 - Linear comparison of the two mechanical impedance modes as a two-surface interaction. This graphical relationship clearly shows the distinct behavior for physical systems dominant in either mode of impedance. Mode I impedance is a brute force approach to impedance, very effective at increasing response very quickly. Mode II impedance operates more as a fine-tuning mechanism, in general, allowing much more elegance in specific design, and perhaps more dynamical controllability on the back end. The gap between the modes presents a disconnect, articulating distinct characteristics in their respective dynamical effect, that as one mode might reach for the attributes of the other, it cannot attain the characteristic response attributes alone. The explicit distinctions may be better observed in the figures to follow.**

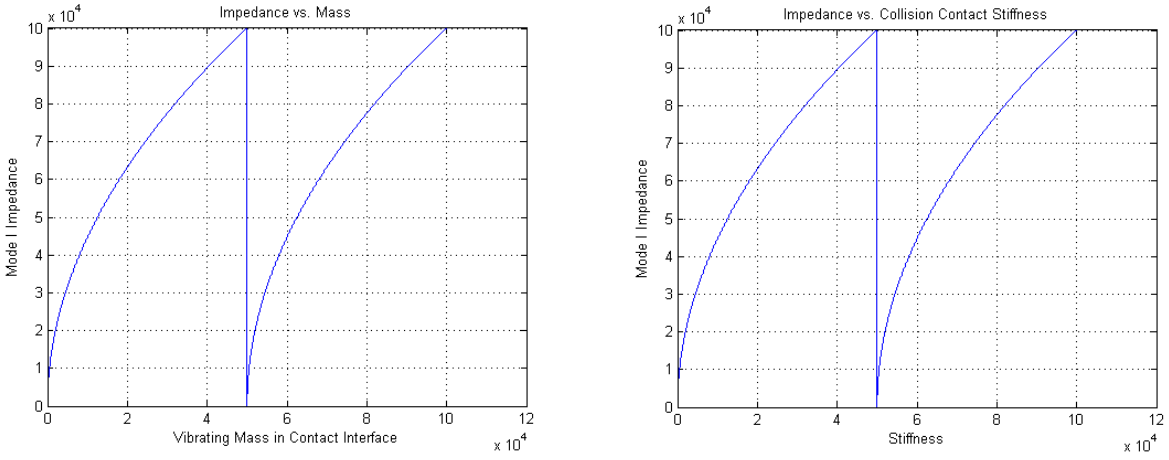


**Figure 3-30 - Mode I mechanical impedance at the interface against its component parameters, mass *m* and stiffness *k*. Notice the steep drop at about 5 units, midrange of both parameters, this likely corresponds to a natural frequency vibratory response. In application, when first adding either stiffness or mass to the end-stop, it is nearly a direct linear increase in impedance, vertical according to the graphs. This begins to taper off and hits a critical moment at the natural frequency of the collision.**

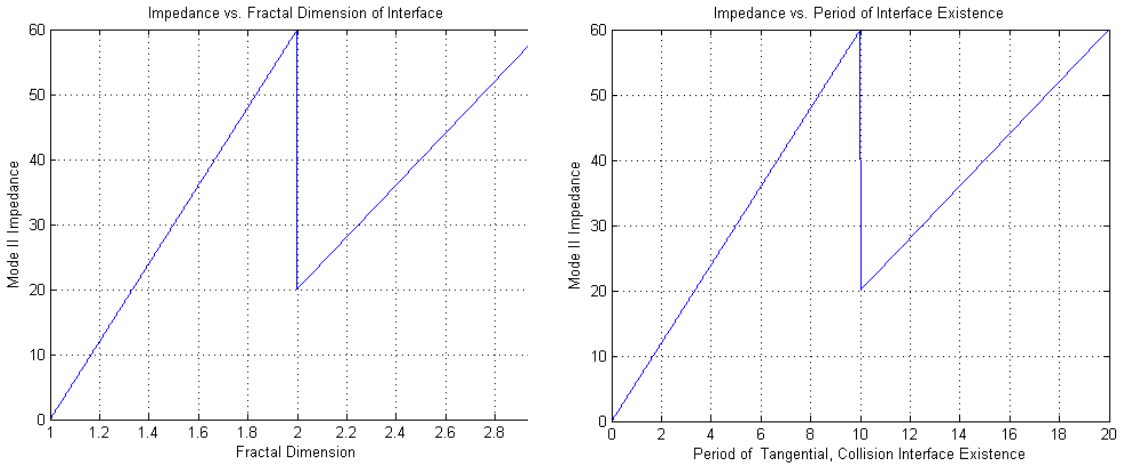


**Figure 3-31 – Mode II mechanical impedance, modeled as interfacial fractal dimension and space per time of contact interface existence, respectively. From here, a sibilance in impedance behavior is apparent; however, mode II portrays a steadier response, a gradual and continuous rise for both parameters, until a critical point is reached, expectedly the natural frequency resonance points due to collision speed, angle, and surface geometry.**

Thus, with mode II impedance, strategic arrangement of surface roughness and relative shape/engaging physiognomies of the colliding faces upon end-stop activation, provides a means to fine tune the impact dynamics. This may prove an important end-stop performance features, as mode I impedance cannot attenuate lower threshold mobility, which could result in vibrational response being fed back to the buoy-wave coupled system. Another possibility is portrayed in figure 3-32, where the number of interfaces in action is increased by magnitudes to observe functionally equivalent impedances to those characteristic of mode I.

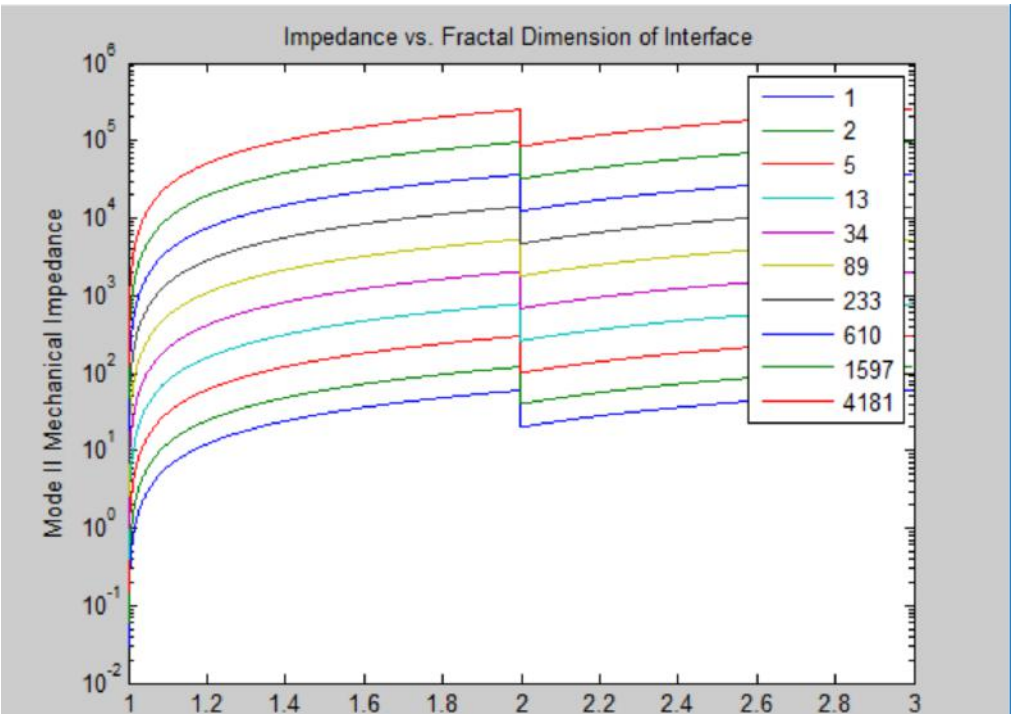


**Figure 3-32 - Mode II impedance vs fractal dimension of interface as a function of number of involved interfaces (analogous to layered sheets – of figure 2-38, but simply stacked)**

From figure 3-32, with mode II mechanical impedance it is possible to increase performance with layered stacking, as previewed previously, for a complex assembly. Notice how the number of stacked interfaces, from 1 to over 4000, increases the impedance potential. With simply stacked frictional layers, of select fractal dimension, it seems possible to attain mode I impedance values, confirmed experimentally by the interleaved phonebook experiment in [53], but further modeling and experimentation (or numerical strategies) should be made to test end-stop performance capabilities in these types of potential assemblies. By further adding kinematic constraints at angle, like the phone book model, higher impedance values may be attained for less sheets, and this may be tuned for a responsive passive motion resistance optimized for a particular WEC.

The preliminary design decision matrices evaluate general end-stop design functionality through the parameters established. Three design choices, spring-mass, friction, and hybrid have been assessed head to head in terms of projected performance. Parameters are allocated to the strategy that best presents them as an asset. Comparison scores are given on the basis win-lose-draw. Only one score of "1" (analogous to win) can be given per comparison. A "draw" can be determined for a solution with a parameter that can either help, hinder, or renders neutral depending on further application specification. This preliminary assessment rating is meant to establish a general bound for parameters of importance—strengths and weaknesses in comparative design via the established framework. Subsequently, the allocated parameters for each strategy are evaluated via design tasks and criteria to determine a winning preliminary design strategy.

**The design decision matrices can be found in Appendix C.**

# Chapter 4

# 4. Conclusions

## 4.1 Conclusions

The conclusions of this work are numerous. Initially, it is recognized that the warnings in the literature hold true, and a phase-controlled point absorber renders occasional response in excess of its actuation limits. The chosen design tasks and criteria prove to be a reliable groove informing complex decisions throughout the design process. Moreover, the kinematic representation of the problem gives key insight, presenting configuration strategy front and center as a deterministic preliminary design feature, where it could easily have been overlooked as a subtle, or inferior design parameter.

Upon establishing the initial design load, the magnitude of force present at the system limits reinforces the premise that a specialized end-stop system deserves rank in WEC initial design. All planes of potential constraint are found viable for end-stop action, but they each display unique challenges when taking a closer look at their fundamentals, namely spring and friction.

Reconstructed the idea of mechanical velocity damping, or mechanical impedance, through contact interface correlation, regardless of surface type. The formulation recognizes the waveform phenomena at an interface, composed only of fundamental dimensionless qualities, related to time, space and matter.

It took a detailed and strategic dynamical analysis and parameterization to shed light on the friction end-stop potential, but interesting and novel solutions were uncovered with anisotropic, biomimetic surface engineering and layering many friction surfaces with strategic angle.

From this research, and with contemporary materials and technology, it is clear that a hybrid strategy friction and spring solution can provide the best results for WEC end-stops, in terms of the established design criteria: reliability/effectiveness, robustness, integrability, efficiency/economics and intrinsic and explicit design tasks: mitigate effect on WEC energy conversion, constrain WEC motion to designated design limit, mitigate destructive impact dynamics during end-stop engagement.

Diverse end-stop and damper designs can be developed, scrutinized, and compared through the methodology developed in this dissertation. These include but are not limited to: hydraulic end-stops or dampers, pneumatic pressure dampers, particle impact dampers (PID), momentum

exchange impact dampers (MEID), woven net or fiber end-stops, composite fiber end-stops, lattice structure damper or end-stop assemblies, etc.

Other passive damper models (hydraulic, pneumatic, etc.) and active solutions can be scrutinized and compared by the design methodology developed in this dissertation, and not only for wave energy converters, but applications of diverse implementation.

Rao´s methodology for spring design is suggested for springs of wire diameters of less than 17 mm. In this, the numerical validation of such a design approach at significantly larger dimensions gives valuable insight into practical potential of such large springs; albeit, only under static load [38]. Similarly, friction´s empirically established AC laws, may be out of touch considering the distinct magnitude scales of the designed interactions.

However, as a preliminary design analysis, they too are a tool for establishing conceptual criteria and strategies for future investigation.

The kinematic and dynamic interplay have shown a unique light in the formulation of this problem. Establishing reactions of constraint as contact interactions, and presenting a model of impedance have given a great compare and contrast workspace regarding tangential and direct acting forces (or flows).

The principle of least action, and the logical revelation that the oscillating buoy and its inertially coupled components will take the path of least resistance, presents itself with precedence in the tangential, friction models, and even with the spring-mass. This can hamper the reliability of certain friction designs or limited action direct designs, enticing the buoy or slider parts to “jump track” and calls to question the integrability of effective solutions. However, with an elegant and rigorously modeled postliminary design, this postulation can prove obtuse, and merit again shows brightly for hybrid candidates. If nothing else, this principle should be followed in the end-stop advanced design, just as it was introduced in modeling the pure kinematics, and increasingly complex dynamics of the sincere system.

Impedance proves an ideal parameter to compare motion constraint strategies for design task 1.

A huge caveat in the assessment is the lack of consideration of mean free surface rise and fall as an effect of regular tides. This consideration alone can render drastic performance difference in

practical end-stop application. For one, a more rigidly applied end-stop as the end-stop will now become an impedance to the working state of power production that need not be impeded. The strategic parameterization has taken aim to soften the questionable reliability under unpredicted new design loads. But without including the tidal rise and fall, a steep decline in optimized robustness characteristic of the system is predicted.

And despite not affecting the 2 *practicality* design tasks (3 and 4) explicitly, the inevitable effect on the intrinsic design task renders unquestionable impracticality

This strengthens the role of the coefficient of restitution parameter in design importance.

The task of balancing WEC system constraints with power output is hinged on knowledge an implementation of all acting phenomena into the model. A more informed model for motion constraint employs safer working conditions for every component system.

This investigation clarifies and parameterizes the end-stop problem, with its growing opacity in the landscape of WEC progress, in an attempt to unveil the possibility for widespread wave energy on the horizon.

It does so by providing a first, comprehensive, preliminary analysis of end-stop parameters in general, and introducing design protocol for developing end-stop systems. It is apparent from this investigation as well as contemporary literature, that end-stop design warrants specific attention at the first stage of the WEC design process and performance estimation. Defensive WEC design will ultimately lead to higher yield as well is increased insurability potential at this crucial stage.

The theoretical, experimentally unproven, formulation of dimensionless mechanical impedance provides a heuristic approach for reducing the complex, nonlinear design strategy comparison into base, nontrivial physical parameters. Although specific systems will need to be classified and behaviorally evaluated according to the dimensionless formulation, the 2 distinct modes are accessible to be analyzed separately and compared with respect to the distinct dynamical models formulated in chapter 2.

This work intends to draw an essential line of best practice, through theory and methodology, to approach fulfillment of practical WEC motion constraint. The investigative results provide new tools and parametric means to tune and optimize particular WEC end-stop systems, allowing a

successive groove be carved through subsequent experimentation and application to deliver even more sound foundation.

The allision formulation is shown to provide distinct dynamics from a normal collision model. Although the wave may effectively operate like a MEID system, this is likely an undesirable outcome, but needs to be studied further. Allowing the wave to act as an additional damper may prove tunable/useful by some tactics, but it inevitable creates a new vibratory motion between the buoy-wave couple, and this should initially be mitigated due to the myriad of potential problems it could cause.

Tuning coefficient of restitution $e$ and mechanical impedance $I$ may be the strongest and most efficient functional parameters for end-stop design, with their included respective sub-parameters. Task 2 is most readily improved with a negative or minimized coefficient of restitution, this at the expense of task 1. Task 1 is best treated directly with impedance, but must be kept in check with task 2, luckily with the additional tool of fine tunable mode 2 impedance. The system may be designed to have variable values of these properties per length, or per time with active control, for improved performance.

## 4.2 Future works

The future work possibilities, as with any research work, are both unprecedented and boundless. Potential research routes based on this work are listed below from end-stop to infinity.

An optimal upper end-stop solution will not look like an optimal, lower end-stop. The interfaces in action for each are distinct. Using the new model of mechanical impedance, it is possible to tune both separately, with the same tool. For example, hydraulic drag can be readily to contribute to dampen downward buoy motion via submerged installations. Further work can be done on lower end-stop design and optimization, as well as the implications and differences between the two.

Furthermore, active control solutions to the end-stop problem can be analyzed in depth. It was the decision of this author to investigate specific passive elements based on specific problem

parameters and; however, specific active solutions can be included in the end-stop decision matrix to give a more complete listing for potential WEC designers. As numerical WEC and wave models evolve in intricacy, active solutions in every aspect of WEC functionality will gain more validity and may prove more responsible solutions for specific projects.

Additionally, the development of a model that includes drag can give rich insight. Perhaps the impedance formulation will prove beneficial in this analysis.

An intermediary design investigation would include in depth material analysis and selection criteria formulation, as well as comprehensive analysis of potential environmental impacts. The intermediary phase of end-stop design would focus on specific data collection and practical experimentation for considered preliminary designs.

The most insightful future works may take the form of experimentation. Due to the large cost and implementation time to test, even scaled down model WECs and their features, some simplified experimentation techniques may be sought and employed specifically for these crucial self-preservation components, in order to expedite WEC insurability and establish mature, end-stop design criteria. Particularly with friction and hybrid solutions, modified variations of the Froude pendulum may be developed to accrue and evaluate useful dynamical measurements.

**Friction end-stop, economical experimentation:**

The Froude pendulum is a simple, self-excited system with the following configuration, in figure B-2. It consists of a simple pendulum mass and rod system M rigidly attached to an external sleeve P which is in turn, fitted around a driven internal shaft S [55].

**The modified/notched Froude Pendulum model can be found in Appendix B**

A new class of experimental studies using modified, Froude pendulums may prove useful in assessing potential, WEC end-stop designs as well as other frictional components subject to driven oscillations.

Additionally, scale model or numerical experimentation to specifically study allision mechanics and dynamics would prove insightful, to measure and better understand the interplay between all

of the viscous/frictional, inertial, and contact forces involved, along with the resultant dynamics and hysteresis effects when subject to particular amplitudes and periods of incident wave action.

In the broader scope, the dimensionless, mechanical impedance formulation can be studied in depth, with nearly unlimited, potential, experimental setups between surface pairs or objects in collision, as well as static contact. This could efficiently generate rich, behavioral comparisons between classically dissimilar systems and events, with no other previous means of correlation. The more, new experimental data, together with retrofitted measurements, accrued, to be compared by dimensionless, mechanical impedance, the more general, mechanical insight will be acquired—connecting dynamical behavior amongst any size scale, from galactic to nanoscopic in their natural movement and interactions.

## 4.3 Closing remarks

This dissertation scopes from the large to the small, from research to design, from the tried and true to daring, novel outlook and formulation. The approach is one of inclusion and connection of ideas: holistic, phenomenological, and analytical, a collision of both logical and creative insights. Where empirical formulations exhibit gaps, parameterization sheds new light. Where standard practices shroud potential, nature conveys new possibility. Every problem is unique, as is every problem solver. Simplicity and efficiency are always sought, but perhaps we're looking in the wrong places.

The scientist aims to understand how the world works.
The world does not aim. It just spins and spins,
making sure the scientist never finds true bearings.

# References


[1] IPCC, 2011: Summary for Policymakers. In: IPCC Special Report on Renewable Energy Sources and Climate Change Mitigation [O. Edenhofer, R. Pichs-Madruga, Y. Sokona, K. Seyboth, P. Matschoss, S. Kadner, T. Zwickel, P. Eicke meier, G. Hansen, S. Schlömer, C. von Stechow (eds)], Cambridge University Pre ss, Cambridge, United Kingdom and New York, NY, USA.

[2] Huckerby, J., Jeffrey, H., de Andres, A. and Finlay, L., 2016. An International Vision for Ocean Energy. Version III. Published by the Ocean Energy Systems Technology Collaboration Programme. &Andrew Cornett (National Research Council, Canadian Hydraulics Centre)

[3] Krewitt W, Nienhaus K, Kleßmann C, Capone C, Stricker E, Graus W, et al. Role and potential of renewable energy and energy efficiency for global energy supply. vol. 2009,18. 2009.

[4] Mo/rk G, Barstow S, Kabuth A, Pontes MT. Assessing the global wave energy potential. ASME 2010 29th Int Conf Ocean Offshore ArctEng 2010:447–54.

[5] Shadman, M. Application of the latching control on a wave energy converter. Doctoral Thesis, Department of Ocean Engineering of the Federal University of Rio de Janeiro/COPPE, 2017.

[6] Haas K A, Fritz H M, French S P, Neary V S. Assessment of energy production potential from ocean currents along the United States coastline. Oak Ridge National Laboratory, Georgia Institute of Technology, Georgia Tech Research Corporation, U.S. Department of Energy. 2013

[7] Coe R G, Yu Y-H, Rij J v. A survey of WEC reliability, survival and design practices. Sandia national laboratories NM, National renewable energy laboratory CO. 2017

[8] Cleveland C J, Morris C. Handbook of Energy volume II: chronologies, top ten lists, and word clouds, Section 19: Ocean Energy, Chronology, p 335. Boston University, Morris books, Elsevier Science and Technology, Oxford UK. 2014

[9] Madhi F, Sinclair M E, Yeung R W. The “Berkley Wedge”: an asymmetrical energy-capturing floating breakwater of high performance. Marine Systems & Ocean Technology, Vol 9. 2014

[10] Falnes J. A review of wave-energy extraction. Dept of Physics and Centre of ships and ocean structures, Norwegian University of Science and Technology. Marine Structures 20 (2007) 185-201.

[11] Journee JMJ, Massie W W. Offshore hydromechanics 2001:570. Doi:10.1016/S0013-4686(01)00879-9.

[12] Falcao AF de O. Wave energy utilization: A review of the technologies. Renew Sustain Energy Rev 2010;14:899-918. Doi:10.1016/j.rser.2009.11.003.

[13] Estefen SF, Garcia Rosa PB, Beserra ER, Costa PR, Pinheiro M, Lourenco MI, et al. Wave energy hyperbaric converter: Small scale models, prototype and control strategies. Proc. ASME 2012 31 st Int. Conf. Ocean. Offshore Arct. Eng. Julay 1-6, 2012, Rio de Janeiro, Brazil, 2012.

[14] Khan J, Moshref A, Bhuyan G. A generic outline for dynamic modeling of ocean wave and tidal current energy conversion systems. Power Energy Soc. Gen Meet. 2009, IEEE: 2009. doi:10.1109/PES.2009.5275177.

[15] Garcia-Rosa PB, Cunha JPVS, Lizarralde F, Estefen SF, Machado IR, Watanabe EH. Wave-to-Wire model and energy storage analysis of an ocean wave energy hyperbaric converter. IEEE J Ocean Eng 2013;39:386-97. doi:10.1109/JOE.2013.2260916.

[16] Kempener R, Neumann F. Wave energy, IRENA ocean energy technology brief 4. Int Renew Energy Agency 2014.

[17] James V. Marine renewable energy: A global review of the extent of marine renewable energy developments, the developing technologies and possible conservation implications for cetaceans. whale and dolphin conservation, WDC; 2013.

[18] US DOE. Energy Efficiency and Renewable Energy Marine and Hydrokinetic Database. Energy Efficiency and Renewable Energy, US Department of Energy. Washington DC, USA; 2010.

[19] Pérez C, Iglesias G. Integration of Wave Energy Converters and Offshore Windmills. 4th Int Conf Ocean Energy 2012:1–6.

[20] The Specialist Committee on Hydrodynamics Modelling of Marine Renewable Energy Devices. Final Report and Recommendations. Proceedings of 28th ITTC – Volume II.

[21] Pecher and Kofoed, Handbook of ocean wave energy. Aalborg University Aalborg. Ocean engineering & oceanography volume 7. 2016

[22] Wright C, Pakrashi V, Murphy J. Analysis of end-stop parameters on the performance of heaving point absorber wave energy convertors. MaREI University College Cork, Dublin. 2016

[23] Evans D V. Maximum wave power absorption under motion constraint. School of mathematics, University of Bristol. Applied Ocean Research, Vol 3 No 4.1981

[24] Ringwood J V, Bacelli G, Fusco F. Energy-maximizing control of wave-energy converters, the development of control system technology to optimize their operation. IEEE control systems magazine. 2014

[25] Penalba M, Ringwood J V. A review of wave-to-wire models for wave energy converters. Centre for ocean energy research. Energies. 2016

[26] BEATTY, Scott J. et al. Experimental and numerical comparisons of self-reacting point absorber wave energy converters in regular waves. **Ocean Engineering**, [s.l.], v. 104, p.370-386, ago. 2015. Elsevier BV.

[27] Wang L, Engstrom J, Goteman M, and Isberg J. Constrained optimal control of a point absorber wave energy converter with linear generator. Journal of Renewable and Sustainable Energy. 2015

[28] Denny M, Gaylord B, Helmuth B, Daniel T. The menace of momentum: dynamic forces on flexible organisms. ASLO Limnology and Oceanography, Vol 43, No 5, pp 955-968. American society of limnology and oceanography. 1998

[29] Giorgi G, Ringwood J V. Computationally efficient nonlinear Froude-Krylov force calculations for heaving axisymmetric wave energy point absorbers. J. Ocean Eng. Mar. Energy. Springer international publishing Switzerland. 2016

[30] Cummins W. The impulse response function and ship motion. Schiffstechnik 9:101–109. 1962

[31] Falnes J. Ocean waves and oscillating systems. Cambridge University Press, Cambridge. 2002

[32] Garcia-Rosa P B, Bacelli G, Ringwood J. Control-informed geometric optimization of wave energy converters: the impact of device motion and force constraint. Energies. 2015

[33] Chen J, Schinner A, Matuttis H-G. Static friction, differential algebraic systems and numerical stability. Physics Procedia 6 (2010) 65-75.

[34] Janmey P A, Schliwa M. Rheology. National Center for Biotechnology Information, PMC, US National Library of Medicine, Bethesda MD. 2008

[35] Porteiro J L. Spring design optimization with fatigue. USF. 2010.

[36] Rao T K. Design of Machine Elements Volume II. Gandhiji Institute of Science and Technology JaggaYYapeta, Krishna Dist. I K International publishing house pvt ltd New Delhi Bangalore. Uphaar cinema market. Chapter 2 Mechanical springs pgs 63-150. 2010

[37] Pavani P N L, Prafulla B K, Rao R P, Srikiran S. Design, modeling and structural analysis of wave springs. Dept. of ME Kaushik Engineering College, Visakhapatnam. Procedia Materials Science 6. 3rd International Conference on materials processing and characterization (ICMPC). 2014

[38] Budynas R G, Nisbett J K. Shigley's Mechanical Engineering Design ninth edition. McGraw Hill series in mechanical engineering. 2011

[39] Bramfitt B L. Structure/Property Relationships in Irons and Steels. Homer research laboratories, Bethlehem steel corporation. Metals handbook desk edition, second edition J R Davis Editor, p 153-173. ASM International. 1998

[40] Hibbitt, Karlsson and Sorensen. “ABAQUS User’s and Theory Manuals, Version 6.12, Hibbitt, Karlsson and Sorensen, Inc., Providence, RI. 2013

[41] Pawar B.H., Patil A.R., Zope S.B. Design and analysis of front suspension coil spring for three wheeler vehicle. 2016.

[42] Stewart L. M.A., A computational approach for evaluating helical compression spring. 2014.

[43] Filippov A E, Gorb S N. Modelling of the frictional behaviour of the snake skin covered by anisotropic surface nanostructures. Springer Nature Scientific Reports 6. 2016

[44] Hu D L, Nirody J, Scott T, Shelley J. The mechanics of slithering locomotion. Applied Mathematics Laboratory, Courant Institute of Mathematical Sciences, New York University, New York, NY and Departments of Mechanical Engineering and Biology, Georgia Institute of Technology, Atlanta, GA. 2009

[45] Abdel-Aal H A, Mansori M El. The fractal structure of the ventral scales in legless reptiles. Department of Mechanical Engineering, Drexel university, Philadelphia, Pennsylvania and Mechanics, Surfaces and Materials Processing Laboratory (MSMP), Arts et MetiersParisTech, 2 cours des Arts et Metiers, Aix-en-Provence. 2015

[46] Illustration from Army Service Corps Training on Mechanical Transport, Fig. 112 Transmission of motion and force by gear wheels, compound train. 1911

[47] Salustri F A. Pairwise comparison. 2005

[48] Trevor Sewell/Electron Microscope Unit, University of Cape Town

[49] Leahy, S, Brennan A. Shark Skin Inspires Ship Coating. WIRED. Sharklet sharkote. University of Florida. 2005

[50] Kushida Y, Umehara H, Hara S, Yamada K. Momentum exchange impact damper design methodology for object-wall-collision problems. Journal of Vibration and Control I-13. 2017

[51] Modelling of the friction behavior of snake skin covered by anisotropic surface nanostructures

[52] Ringfeder Power Transmission. Features of RINGFEDER® Friction Springs, Technical Information. Standard Friction Springs.

[53] Alarcon H, Salez T, Poulard C, Bloch JF, Raphael E, Dalnoki-Veress K, Restagno F. Self-amplification of solid friction in interleaved assemblies.Laboratoire de Physique des Solides, CNRS &Universite Paris-Sud, Universite Paris-Saclay, Orsay Cedex; Laboratoire de Physico-ChimieTheorique, UMR CNRS Gulliver, ESPCI ParisTech, PSL Research University, Paris; Universite de Grenoble Alpes, Saint-Martin-d'Heres; Department of Physics & Astronomy, McMaster University, Hamilton, ON. 2015

[54] Sonin A A. The physical basis of dimensional analysis second edition. Dept of mechanical engineering MIT. 2001

[55] Shodhganga. Chapter 3 The Froude pendulum and its dynamics. Mahatma Gandhi University Kottayam. Beehive Digital

[56] Bridgman P W. 1969

[57] Slattery J C, Sagis L. 2.3 Structural models for interface. Interfacial Transport Phenomena. Pp. 231. Springer Science+Business Media New York. 1990

# Resources

## Information aggregators

- Researchgate
- ScienceDirect
- Wikipedia Wikimedia commons
- Physics stack exchange
- Quora
- MIT open source courses and library

## Software

- COPPE Nearshore WEC model (FORTRAN developed)
- Microsoft Excel
- MATLAB R20
- Solidworks
- Abaqus/CAE
- Notability for iPad

# Appendices

## Appendix A – Interface impedance

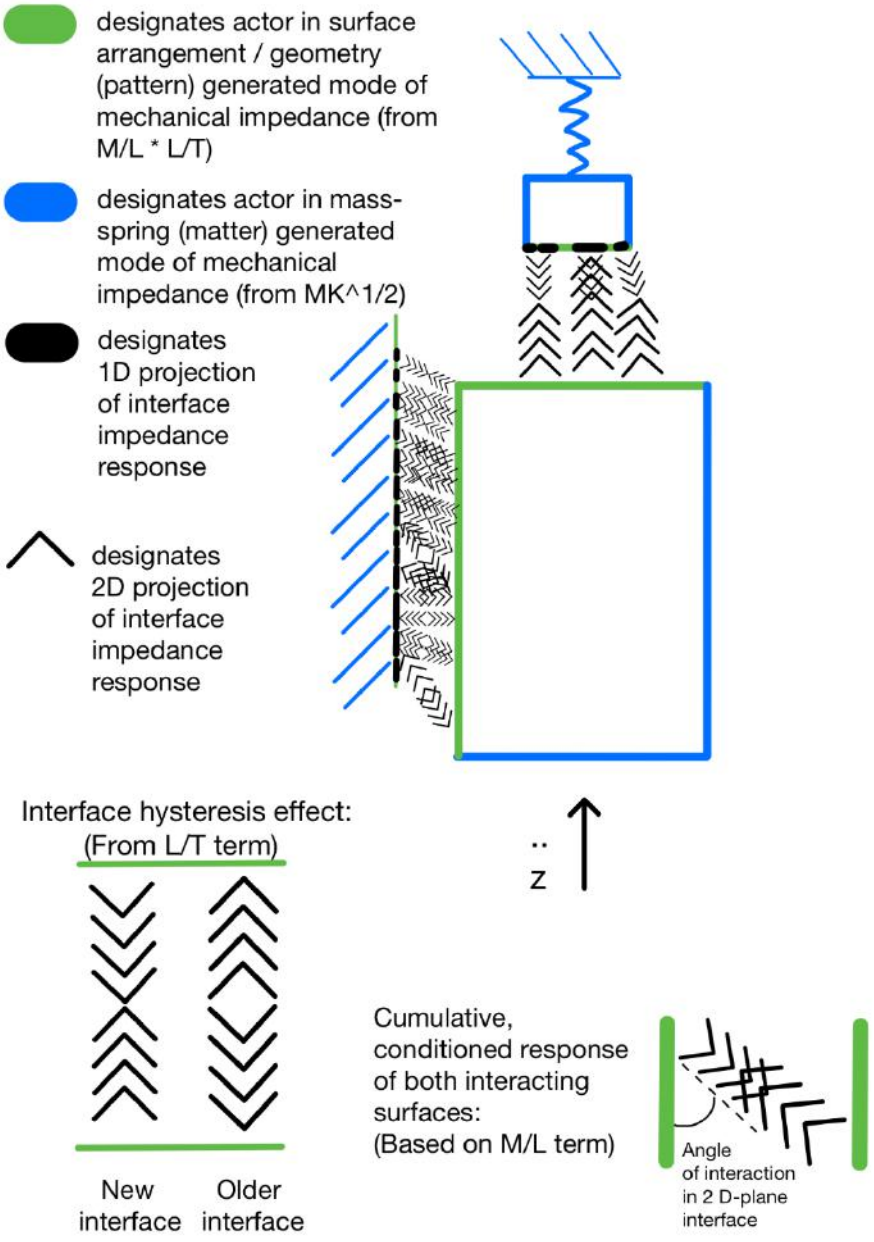


**Figure A- 1- Theoretical schematic, and system of representation for mechanical impedance interfacial phenomena, at both distinct contact interface types (direct and tangential), for a heaving mass experiencing motion constraint and energy dissipation simultaneously.**

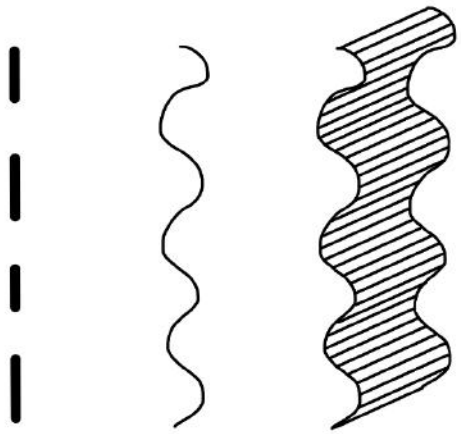

**Figure A- 2 - Simplified depiction of one-dimensional contact interface signal, two-dimensional contact interface response, and three-dimensional contact interface response, simplified to a single waveform, to introduce and demonstrate the association of the three in their respective, representative spaces.**

Each dimensional portrayal of the mechanical interface has its own merits and disadvantages in depicting the true physical phenomenon. To exhibit this interplay, the 3 graphical projections are shown relative to one another in subsequent figures.

**Figure A- 3 - Theoretical depiction of one-dimensional contact interface response embedded in two-dimensional contact interface response, to show an associative similitude.**

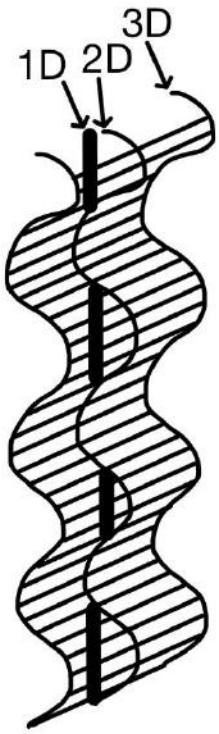


**Figure A- 4 - Depiction of one-dimensional contact interface response, embedded in two-dimensional contact interface response, embedded in three-dimensional contact interface response, to demonstrate the association of the three in their respective, representative spaces.**

The physical interface response of snake ventral scales can be illustrated by this visual characterization. This natural interface representation is shown in Figure 0-5 with a 1-dimensional signal projection depicted alongside.

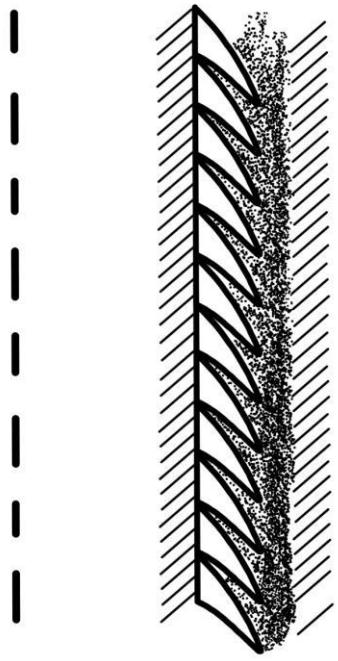

**Figure A- 5 - Application of a one-dimensional, contact interface response to represent the natural occurrence of snake ventral scales in contact with dirt (pitch angle of scales exaggerated for clarity); if the hypothetical snake were to slither forward (towards the top of this page) the 1-D response would develop a pattern of taller lines towards the tail (bottom of figure) and shorter, intermittent lines or dots near the initial contact locale.**

Vibrations are traditionally thought to reduce the friction effect. This is intuitive, imagine something stuck, the first reaction to unstick it, is to wiggle it, but cretain vibration frequencies tend to work better for certain stuck things. The snake uses an approach that is related, yet sophisticated. Simplictically, it wriggles free from the static friction state, to a more efficient kinetic friction, laterally, inducing a surface interface response that propels it forward via this wave, and possibly a dominating $(m/L)$ mode impedance at the microscopic cross-section of its progessing tangential contact with the ground. The snake has the ability to control one surface of the tangential interface collisions with the earth. Evolution can further specialize this pattern over time, for specific habitat terrain. In the end-stop design, it is possible to control nearly, every aspect of both surfaces; they can be optimized, and tested through experimentation. Relatively cheap, iterative design and experimentation may yield magnitudes of mechanical efficiency potential, applicable cross-industry, and as interfaces are modeled and categorized, quick deductive

reasoning can save laborious guess and check, or numerical modelling, within specific product ranges.

To depict the dynamical model for this interfacial phenomenon, a mechanical impedance representative element is developed for explicit depiction of mechanical impedance action during a collision, as a function of the colliding surfaces. The mechanical impedance is manifested in the waveform of the interface, but the characteristics of each surface contribute to interface properties and potential.

# Appendix B – Additional dynamical models & representations

## B – 1 - Stick-slip

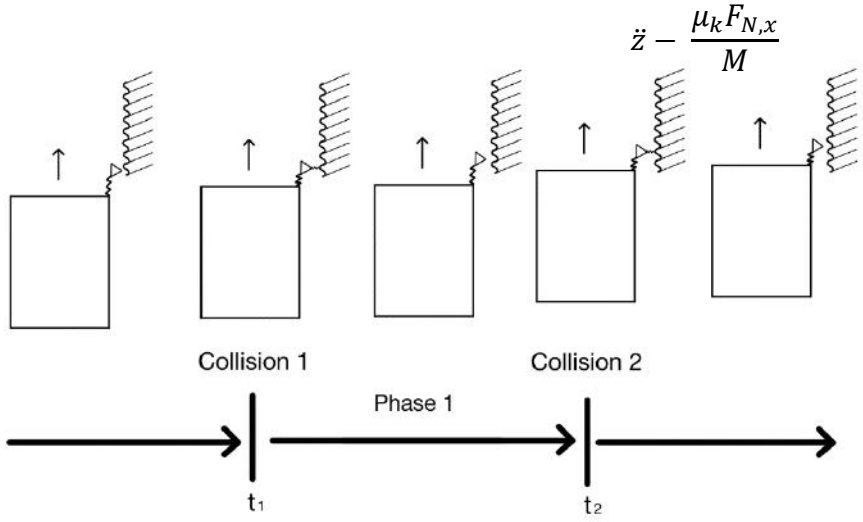


**Figure B- 1 - The stick-slip model can be conceived as an array of standing wave fixtures that come into intermediary contact with the heaving mass. It can be modeled as a Heaviside step-function between the two accelerations described by the parameters.**

# B – 2 - Modified/notched Froude Pendulum

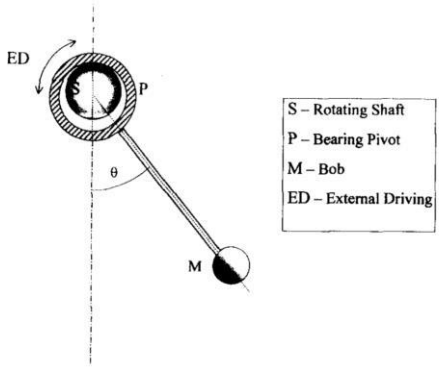


**Figure B- 2 - Froude pendulum [55]**

The pendulum displays complex nonlinear and chaotic behavior. The equation of motion can be expressed in the following form following [55]:

$$\ddot{\theta} + 2\kappa\dot{\theta} + A\theta = 0 \tag{B.1}$$

When the shaft rotates, variable friction forces occur and the motion takes the form [55]:

$$\ddot{\theta} + q_1\dot{\theta}\left(q_2\dot{\theta}^2 - 1\right) + \ Asin\theta = G\omega_0 + fsin\omega t \tag{B.2}$$

By identifying characteristic parameters of semblance, the pendulum can be modified to represent an operational point absorber equipped with friction end-stops.

The WEC equation of motion from chapter 2 can be modified to clump all non-end-stop forces into a single resultant force $F_R$ and assuming very stiff end-stops, can be formulated:

$$(M + A)\ddot{Z} = F_R - F_{ES} \tag{B.3}$$

where $F_{ES}$ is the Heaviside step function from Equation 1.1 [22].

To project this behavior in polar coordinates gives a clean formulation.

This system may serve a good representation for scaled simulation of the friction end-stop concepts presented. It may also serve for potential experimental analysis under ideal and

In an experimental setting, the $F_R$ drive force can be derived from the numerical WEC model.

The behavior of the modified, *notched* Froude pendulum model in polar coordinates is described in equation B.4.

Coefficient of restitution, $e < 0$

Derived equations of motion:

$$\ddot{r} = \begin{bmatrix} \frac{C - k_{N_0,r} - k_{f_0,r}}{M} \\ \frac{-C - k_{f_1,r} + k_{N_1,r}}{M} \end{bmatrix} \mathrm{r(t)} \qquad \ddot{\theta} = \begin{bmatrix} \frac{k_{N_0,\theta} - k_{f_0,\theta}}{M} \\ \frac{-k_{f_1,\theta} - k_{N_1,\theta}}{M} \end{bmatrix} \theta(\mathrm{t}) \tag{B.4}$$

$\theta$(t) angular position over time

r(t) radial displacement as a function of time

$C$ linear hydrostatic coefficient

# B – 3 – Impedance in dynamical models

Select dynamical models are imagined in terms of interfacial behavior:

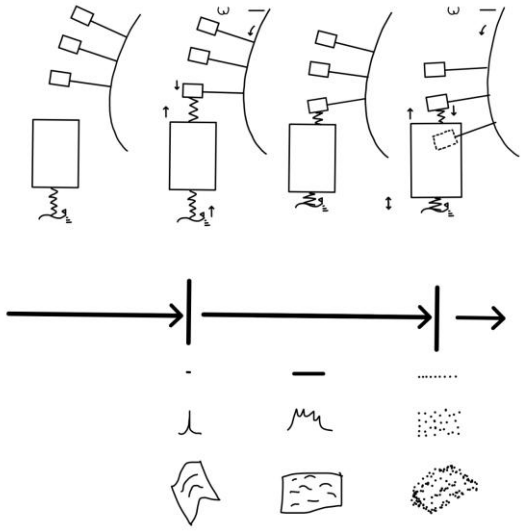

**Figure B- 3 - Virtual work friction allision, interface representation. Potential interface responses are mapped in 1, 2, and 3-dimensions below the phase moments of interest, following the format of the original allision model schematic presented in the text.**

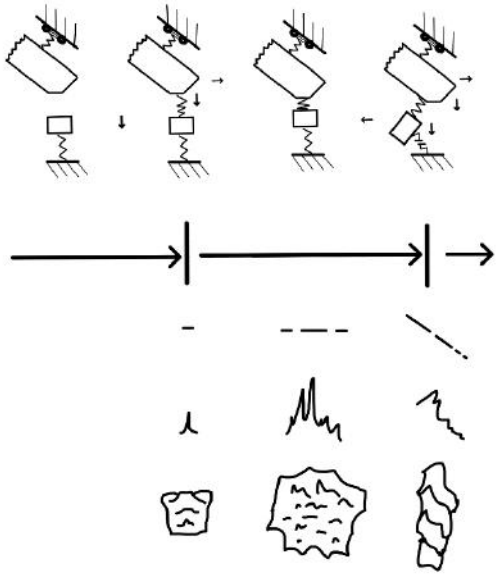

**Figure B- 4 - Anisotropic friction micro-collision, interface representation. Interface responses are mapped in 1, 2, and 3-dimensions below their corresponding, contact moments for the interface experiencing collision.**

# B – 4 – Select allision representations

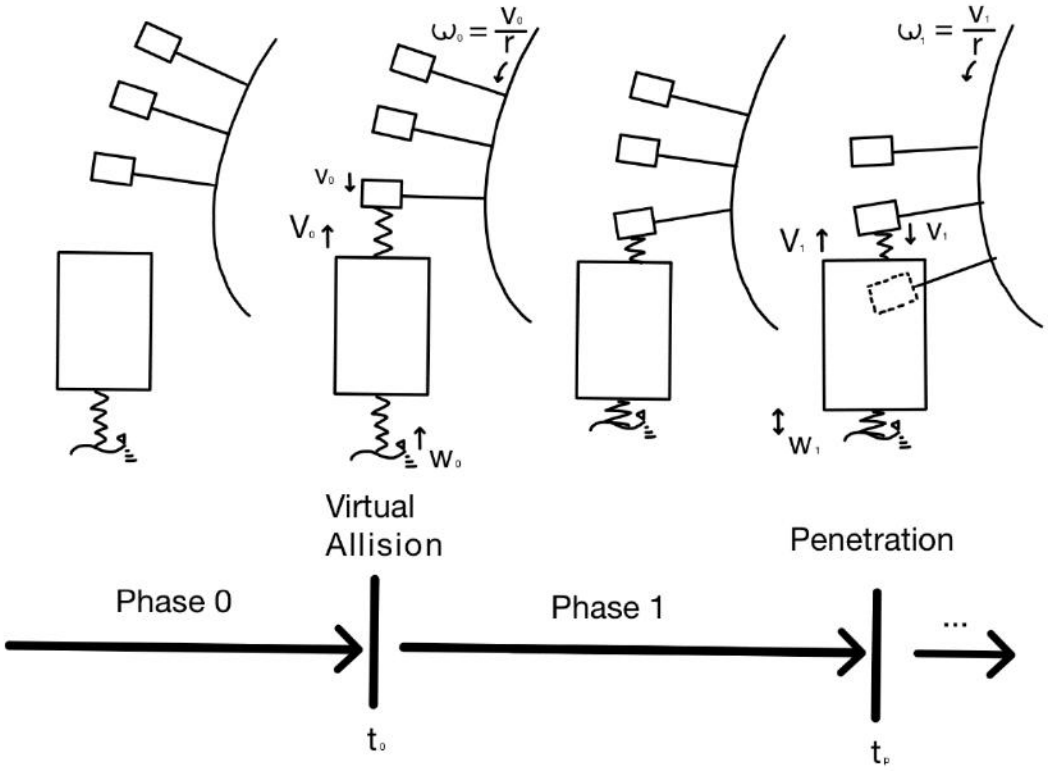


**Figure B- 5 – Schematic representation of virtual work friction allision dynamical model.**

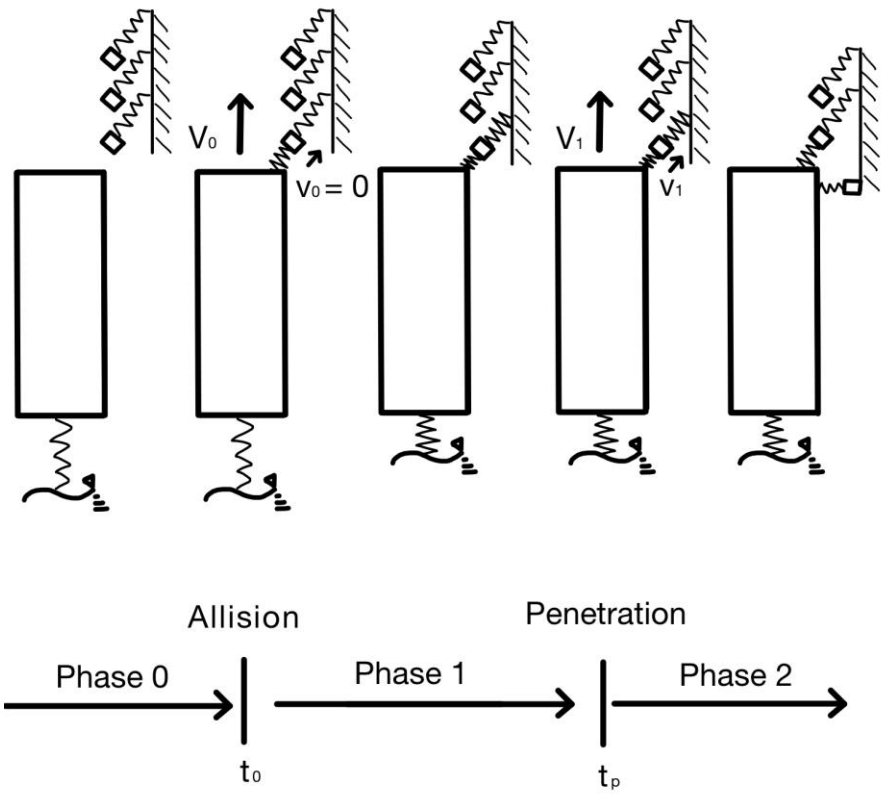


**Figure B- 6 - True orientation depiction of the anisotropic friction model representing the mechanical transitions of one-dimensional motion heaving WEC-anisotropic friction end-stop allisions, from an exaggerated macroscopic viewpoint.**

Allision $e < 0$ for anisotropic friction asperity micro-allision with penetration.

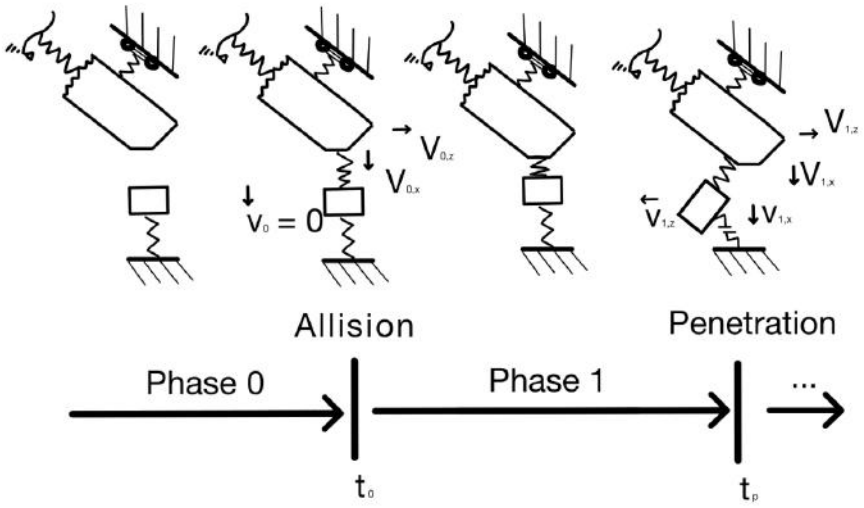


**Figure B- 7 – Rotated reference frame model schematic for anisotropic friction asperity micro-allision with penetration.**

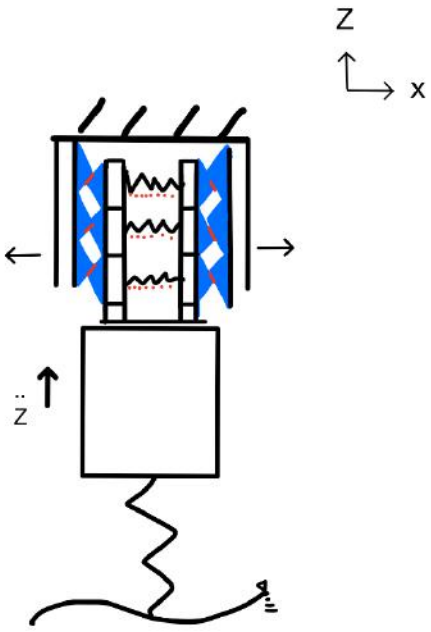


**Figure B- 8 - Schematic representation of the commercialized, "friction spring" [52] end-stop attenuating allision. Friction contact interfaces are highlighted in red, and spring contributors are colored blue.**

The friction spring is an example of a hybrid solution.

# Appendix C – Preliminary design decision matrices and selections

The premature design strategy determination will focus on design task 1 – constraining WEC motion. This first pass evaluation is based on end-stop strategy kinematics (i.e. line of constraint force application) and projected ability to complete design task 1 under the design load presented in section 3.3. Decisions are informed by the 4 design criteria presented in section 2.1.2.

The selection for line of constraint force application, based on preliminary design criteria, is presented in Table 3-3.

Methodology is developed and applied to assist in an immature, projected performance comparison between the two strategies.

Based on the magnitude of the design load, and the practicality a direct compressive resistance is as the most reliable/effective (design criteria 1) treatment of the problem. The design of a compression spring to attain this load is elaborated in chapter 4.

Tables C-1 and C-2 and the subsequent discussions elaborate on this premature determination protocol.

**Table C- 1 - Comparative evaluation rankings used to preliminarily quantify projected performance of different strategies.**

| Qualitative comparison valuation | Rankings |
|---|---|
| Better | 2 |
| Likely better | 1 |
| Indeterminable | 0 |
| Probably worse | -1 |
| Worse | -2 |

- Indeterminable implies it is truly difficult to distinguish based on given information.
- This evaluation can be given even if the other solution seems better.

This approach to evaluation is strictly qualitative, based on selection perspective and designer intuition. In general, the procedure is straightforward, with few caveats. The evaluation procedure begins from the hypothetical perspective of having selected either solution candidate. The selection is evaluated with respect to the particular criteria under analysis, against the other candidate. A qualitative comparison valuation is assigned. The perspective is then reversed, and the choice is viewed from the perspective of having selected the other choice. This process is continued in sequence for all design criteria. In the case that a valuation seems highly indeterminable from one perspective, from preliminary design knowledge and engineering intuition, a valuation of 0 is given, even if the other candidate´s valuation was determined beforehand as being better or worse. The grade is then not revoked; instead, so as not to penalize the candidate´s unknown quality, the valuation of indeterminable is given as well. The following tables, 3-4 and 3-5, effectuate this decision procedure for the WEC end-stop and present the determination for two, sequential, key, premature, design strategy decisions, for preliminary investigation.

**Table C- 2 - Premature, quantitative valuations for qualitative comparison between direct and tangential axis constraint force.**

| **Constraint force axis vs. design criteria** | Direct | Tangential | Preliminary Results |
|---|---|---|---|
| Reliability/effectiveness | 1 | -1 | Direct |
| Robustness | -1 | 1 | Tangential |
| Integrability | 1 | 0 | Direct |
| Efficiency/economics | 0 | 1 | Tangential |
| Subtotal | 1 | 1 | undetermined |

Recalling the designated design criteria weights, established in section 2.1.1,

1. reliability/effectiveness = 48%
2. robustness = 32%,
3. integrability = 16%
4. efficiency/economics = 4%

These weights are now applied to the line of constraint force application decision.

For direct constraint force application:

$$100 \times [1(0.48) - 1(0.32) + 1(0.16) + 0(0.04)] = 32$$

For tangential constraint force application

$$100 \times [-1(0.48) + 1(0.32) + 0(0.16) + 1(0.04)] = -12$$

A direct constraint force application axis is prematurely chosen for further analysis on its basis to complete design task 1.

The next design decision is based on how the end-stop will receive this direct load, in which direction along the *z* axis (colinear with heaving force vector) the primary motion constraint force will operate. In this respect, there are two options for constraining force engagement, tensile and direct compressive. The evaluation procedure is shown in Table C-3.

**Table C- 3 - Premature, quantitative valuations for qualitative comparison between compressive and tensile constraint force action**

| **Constraint force direction vs. design criteria** | Compressive | Tensile | Preliminary Results |
|---|---|---|---|
| Reliability/effectiveness | 1 | -1 | Compressive |
| Robustness | 0 | 0 | Indeterminable |
| Integrability | 2 | -2 | Compressive |
| Efficiency/economics | 1 | -1 | Compressive |
| Subtotal | 4 | -4 | Compressive |

No further calculations are necessary for this preliminary decision, as compressive choice universally overwhelms tensile in all criteria valuations. Thus, compressive direction is chosen for the direction of primary end-stop constraint force.

**Dimensionless parameters corresponding to design criteria for explicit design task 1 (kinematic constraint parameters):**

1. Angle of end-stop application $\theta$

| Spring-mass | Sliding friction | Hybrid |
|---|---|---|
| 1 | N/A | 0.5 |

2. Comparative contact stiffness potential ratio $k_s/k_f$ (spring stiffness / friction normal force stiffness)

| Spring-mass | Sliding friction | Hybrid |
|---|---|---|
| 1 | 0 | N/A |

3. Ratio of # of direct system interfaces to # of tangential interfaces (#/#)

| Spring-mass | Sliding friction | Hybrid |
|---|---|---|
| 0.5 | 0 | 1 |

4. Static friction coefficient $\mu_s$

| Spring-mass | Sliding friction | Hybrid |
|---|---|---|
| 0 | 0.5 | 1 |

5. Dimensionless impedance $I$

| Spring-mass | Sliding friction | Hybrid |
|---|---|---|
| 0.5 | 0 | 1 |

6. # of potential planes of engagement

| Spring-mass | Sliding friction | Hybrid |
|---|---|---|
| 0 | 0.5 | 1 |

- Kinematic conditions: 6,
- Forces of constraint: 4,
- Impedance: 5

**Dimensioned parameters corresponding to design criteria for explicit design task 1 (kinematic constraint parameters):**

1. Material stiffness

| Spring-mass | Sliding friction | Hybrid |
|---|---|---|
| 1 | 0 | 0.5 |

2. Mechanical impedance mode I

| Spring-mass | Sliding friction | Hybrid |
|---|---|---|
| 1 | 0 | 0.5 |

3. Mechanical impedance mode II

| Spring-mass | Sliding friction | Hybrid |
|---|---|---|
| 0.5 | 0.5 | 1 |